FACULTY OF SCIENCE
UNIVERSITY OF COPENHAGEN

Sub-gap States in Superconducting Cylinders

Mathias Nesheim

Master's Thesis in Physics

Supervisor: Prof. Jens Paaske

Niels Bohr Institute

University of Copenhagen

Date: October 18, 2018

ABSTRACT

Nanowire systems have in recent decades become a topic to receive much attention in condensed matter physics. Especially so for the possible confirmation of the existence of Majorana zero modes, proposed to be highly useful for future quantum computing.

In this thesis I study the sub-gap states found in superconducting cylinder systems in the presence of an applied magnetic field, as these systems can approximate the nanowire systems. A possible example of these sub-gap states is the Caroli-de Gennes-Matricon states, which are bound vortex states in type-II superconductors. These sub-gap features were believed to have been observed in a recent nanowire experiment. I examine the states analytically through a detailed derivation of the energy spectrum, followed by a numerical analysis. I compare the numerical result to another recent experiment and found these to be commensurate. I present the numerically determined eigenfunctions, resembling Bessel functions in the radial direction, and show how the higher energy states correspond to larger angular momentum. The supercurrents corresponding to the occupied states are plotted and discussed as well. Furthermore, I present the numerical method describing the sub-gap states of a hollow hexagonal wire system, for which I find the energy spectrum, eigenfunctions and supercurrents.

Magnetic field effects were included in the analytical derivation of the CdGM states, which resulted in an increase in the energy spacing between the states. This was verified numerically as well.

I give a thorough account of Andreev reflections and discuss how these can result in bound states in either vortices or normal metal cores of cylinders encased by a superconducting shell.

Finally, I determine the force acting on particles undergoing Andreev reflection and hypothesize how this can lead to precession of the bound states in superconducting cylinders.

FOREWORD

In the original thesis I had a sign error in Fig.(23) which I could not identify. The figure previously featured both the actual result and the expected result with the correct sign. Later I discovered the error was simply due to a confusion of convention in the definition of the electronic charge, when comparing different articles. The error has been corrected and Fig.(23) now only depicts the expected result. This was implemented on the 13. December 2018.

ACKNOWLEDGEMENTS

First of all I must give a huge thanks to my supervisor Prof. Jens Paaske. His unending patience and good humour kept me positive and hopeful even when the project seemed undefeatable. He was interested and always ready to discuss, even at the weirdest hours of the day, and I am very grateful. He made this tough journey an enjoyable one.

I must also thank those friends whom I somehow managed to convince to read and comment on parts of my thesis. Stefan Hasselgren, Ida Egholm Nielsen and Mads Kruse, your help was invaluable and you guys are awesome!

I also extend my gratitude to the entire CMT group, it has been a pleasure to study the wonders of physics in your merry company.

I give also a huge thank you to both Marieke Van Beest and Peter Røhr Beresford Tunstall. Countless evenings have I spent either working hard or watching Lord of the Rings with you, and you are the reason I have kept my sanity throughout the year. I am lucky to have friends like you!

And finally, another thank you to Peter is in order. This entire project would never have been possible had you not been there to help and fight alongside me. You are the one that got me into physics and for that I cannot thank you enough!

CONTENTS

1

INTRODUCTION

Since the discovery of superconductivity in condensed matter systems, much research has been invested to understand the underlying physics. It was first discovered experimentally by H. K. Onnes in 1911 and later described theoretically with the BCS theory in 1957 [1]. In recent decades there has been a lot of focus on superconductivity and one especially vibrant topic is novel phenomena of nanowire systems. As explained for example in an article by R. M. Lutchyn et al.[2], these nanowire systems are strong contenders for realizing Majorana zero modes, believed to be crucial for the realization of quantum computing. The article presents the nanowires as superconducting cylinders in the presence of an axial magnetic field, i.e. along the length of the cylinder. The work presented in this thesis revolve around the possible sub-gap states observed in these superconducting cylinder systems.

The article by S. Vaitiekenas et al.[3] presents an experiment using hexagonal nanowires consisting of an indium arsenide semiconductor core with an aluminium shell wrapped around the core. They identify (tentatively) the sub-gap features of the cylinder as the Caroli-de Gennes-Matricon (CdGM) states, which are bound states in Abrikosov vortices in type-II superconductors. The main topic of this thesis is the understanding of these CdGM states, through both analytical and numerical work. Interestingly, the existence of these states has recently (March 2018) been observed experientially by M. Chen et al.[4], further solidifying the importance of understanding the CdGM states.

Superconducting cylinders in axial magnetic fields also exhibit Little-Parks effect, see again [3]. A discussion of this effect is therefore included in this work, so that one can investigate the effect of the magnetic flux through the cylinder. This is done in section (2), where the physics of the Little-Parks effect in a superconducting cylinder is studied. Section (3) presents the main topic of the thesis; a thorough study of the sub-gap states in superconducting cylinder system. This includes both an analytical derivation of the energies of the CdGM states, followed by a numerical analysis for comparison based on the experiment presented in [4]. In the numerical work the vortex line is imagined as a solid superconducting cylinder, of course with the magnetic field along the vortex line. Afterwards, the numerical method is applied to a hexagonal shell (hollow hexagonal structure), as an example of a typical nanowire system, in order to find sub-gap states here.

Afterwards, in section (4), the magnetic field effects are included in the analysis, as these were neglected throughout the previous section. The energies are determined analytically and the theoretical prediction is verified numerically. Next, in section (5) Andreev reflection is studied and its relation to the bound states of these cylindrical system is discussed. Following the work of [5], Andreev reflection is studied for several different cases. Section (6) presents the forces acting on particles undergoing Andreev reflection and discusses how

these affect our bound states.
A few important features and phenomena is presented in the following paragraph, among these the Abrikosov vortex, to keep in mind throughout the thesis.

1.1 THE ABRIKOSOV VORTEX

It is assumed the reader is familiar with the basics of superconductivity, such as how it emerges, the concept of Cooper-pairs, energy gap, critical temperature, the Meissner effect and so on. A brief discussion of the two different types of superconductors and afterwards the Abrikosov vortex is given.
As stated, superconductors can be split into two categories depending on their material properties. The categories are labelled using the Ginzburg-Landau parameter $\kappa = \frac{\lambda}{\xi}$, where λ is the magnetic field penetration depth and ξ is the coherence length. λ measures how far into superconductor the magnetic field penetrates, before it is reduced by a value e^{-1}. ξ relates to the "size" of the Cooper-pair. As explained in [6] Sec.(1.8), the properties of a superconductor cannot change substantially on a scale much smaller than ξ. The two types of superconductors are determined as follows: For values of $0 < \kappa < \frac{1}{\sqrt{2}}$, it is a type-I superconductor, whereas for $\kappa > \frac{1}{\sqrt{2}}$ it is a type-II.
An important difference between the two types is presented in Fig.(1). Type-I superconductors exhibit the usual Meissner effect, where the magnetic field lines are expelled from the superconductor for temperatures below T_C, until some critical field H_C. Type-II superconductors on the other hand enters another state between the critical fields H_{C1} and H_{C2}. This state is called the Abrikosov vortex state and is characterised by a "reduced" Meissner effect. For this state the magnetic field penetrates the superconductor in some places in the form of magnetic field lines. These lines are screened from the rest of the superconductor by an induced supercurrent circulating the line, and this is the creation of an Abrikosov vortex. The vortices were presented by A. A. Abrikosov in 1957 [7]. The upper critical field corresponds to having created so many vortices that these begin to overlap.

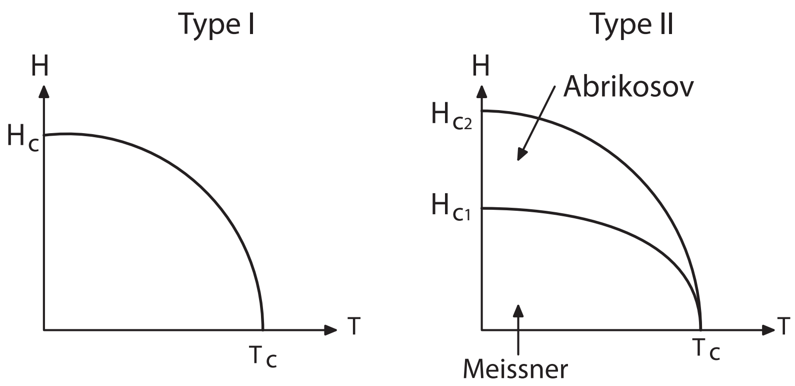

Figure 1: The different types of superconductors. The figure is taken directly from [8], Fig.(1.9). The regions from 0 to T_C and 0 to H_C or H_{C1} represent the superconducting phase. If either the temperature or the applied magnetic field increases beyond these values, the system exits the superconducting state. In type-I metals superconductivity is destroyed as the magnetic field reaches the critical field. For type-II superconductors however, the system can enter the Abrikosov vortex phase. Here the system exhibits a reduced Meissner effect and the creation of vortices around magnetic field lines penetrating the superconductor in certain places.

These vortices are characterized by having a normal core, i.e the superconducting order parameter Δ becomes zero in the center of the vortex. As mentioned earlier, the screening current circulates this normal region core, decaying on a distance λ away from the center. The radius of the vortex is approximately equal to the coherence length of the superconductor [8], Sec.(1.9). Due to the magnetic field, each vortex carries one quantum of magnetic flux, labelled Φ_0. This is a result of the single-valuedness of the superconducting order parameter, when taking a closed loop around in the superconductor. Essentially, the phase difference depends on the magnetic flux and the phase can vary only with values $2\pi n$, with n being an integer, when completing a loop. Thus the flux must be quantized as well. This argument is displayed nicely in Sec.(17.5) of [9].
These vortices will be of major importance to our work going forward. One main focus is the Caroli-de Gennes-Matricon states, which are exactly excitations confined in such a vortex. But first, a study of another novel feature, occurring in a superconductor in a magnetic field, is presented.

2 LITTLE-PARKS EFFECT

2.1 OSCILLATION OF T_C

The first topic will be the examination of the Little-Parks effect, as seen in the article by S. Vaitiekenas et al. [3], Fig.(1). They present resistance as a function of the temperature and the magnetic field and present data showing the "destructive regime" of the Little-Parks effect. This concept is investigated in order to understand the effect of applying a magnetic field to a superconducting cylinder.
The gap parameter is dependent on the critical temperature (T_C) through the BCS-ratio: $\Delta_0 = 1.76 k_B T_C$, with k_B being the Boltzmann constant, and that the resistance changes heavily for temperatures near T_C. Thus, a closer look into the critical temperature as a function of the magnetic field is in order.

To understand the physics happening behind the scenes, the concept Little-Parks (LP) effect is examined, named from W. Little and R. Parks; the first to present an experiment in which this effect was observed. They present their work in the article [10] from 1962, showing the periodic oscillation of the critical temperature, through measurements of the resistance as a function of the magnetic field. This is the heart of the LP effect. This section will present a detailed description of the effect, the system in which it occurs, and an analytical derivation of the actual dependence.
Fig.(2) presents the system to keep in mind throughout this section. W. A. Little and R. D. Parks examined a thin-walled cylinder with thickness d, in the presence of an axial magnetic field, i.e. along the length of the cylinder. One can derive an expression for the critical temperature as a function of the magnetic field and subsequently compare with their experimental findings.

Figure 2: Sketch of a superconducting cylinder in the presence of an axial magnetic field. The thickness d was small in the experiment of Little and Parks [10]. The authors examined the oscillation of the critical temperature as a function of the magnetic flux through the cylinder.

The Ginzburg-Landau theory presents a description of the free energy Ω_s of the superconducting state as a function of the order parameter. This work will not go into the details of this theory, but simply use it as a framework for the current topic. Suffice to say that the theory describes the microscopic behaviour of a superconductor in the presence of a magnetic field H, for temperatures near T_C [11].

Look first at the free energy form as presented in Sec.(17.5) of the book [9] by A. A. Abrikosov, upon which the following derivation is based. Here the electron mass and charge have been rewritten as twice the value presented in [11], as the following deals with Cooper-pairs.

Eq.(17.5) of [9] writes an integral of the free energy (renamed Ω_s) expanded in terms of the order parameter in the presence of the external magnetic field, H:

$$\int \Omega_s \, dV = \int \Omega_N^{(0)} \, dV + \int \left[\alpha \, \tau |\psi|^2 + \frac{\beta}{2} |\psi|^4 + \frac{1}{4m} \left| \left(-i\hbar \boldsymbol{\nabla} - \frac{2e}{c} \mathbf{A} \right) \psi \right|^2 + \frac{\mathbf{H}^2}{8\pi} \right] dV, \tag{2.1}$$

where α and β are positive constants, $\tau = \frac{T - T_C}{T_C}$, $\mathbf{A}$ is the vector potential and ψ is a complex field, proposed by Ginzburg and Landau in 1950 as the superconducting order parameter.

The terms involving α and β represent the condensation energy; the amount of energy the system can save by entering a superconducting phase. The gradient term describes the kinetic energy of the electrons and finally the last term is simply the energy of the applied

magnetic field. The assumed superconducting order parameter ψ was later found to be the gap parameter Δ. Note that everything will be written in SI-units and therefore $c = 1$ is used, while the magnetic field is rewritten as $\mathbf{B}$.
Writing out the order parameter as $\psi = |\psi|e^{i\chi}$, one can write the integrand of Eq.(2.1) as

$$\Omega_s - \Omega_N^{(0)} = \alpha\ \tau|\psi|^2 + \frac{b}{2}|\psi|^4 + \frac{\hbar^2}{4m}|\psi|^2 \left(\boldsymbol{\nabla}\chi - \frac{2e}{\hbar}\mathbf{A}\right)^2 + \frac{\mathbf{B}^2}{8\pi}, \tag{2.2}$$

The bracketed expression can be written as an average, using the fact that $\mathbf{A}$ and $\boldsymbol{\nabla}\chi$ are constant around the superconducting cylinder:

$$\boldsymbol{\nabla}\chi - \frac{2e}{\hbar}\mathbf{A} = \frac{1}{2\pi R}\oint \left(\boldsymbol{\nabla}\chi - \frac{2e}{\hbar}\mathbf{A}\right)\ dl, \tag{2.3}$$

where R is the radius of the cylinder. Thus the term is now expressed as an integral along a closed path taking one revolution in the cylinder, divided by the circumference. The integral of each term is taken separately and for $\boldsymbol{\nabla}\chi$ one uses now that ψ must remain single-valued. This is satisfied if the phase varies by $2\pi n$ after one complete turn around the cylinder, where n represents the winding number which is an integer. Therefore

$$\oint \boldsymbol{\nabla}\chi\ dl = 2\pi n. \tag{2.4}$$

The second term of Eq.(2.3) is rewritten using Stokes theorem and the definition of the vector potential:

$$\oint \mathbf{A}\ dl = \int \boldsymbol{\nabla}\times\mathbf{A}\ ds = \int \mathbf{B}\ ds = \Phi, \tag{2.5}$$

where Φ is the flux through the surface area ds. Now Eq.(2.3) can be written as

$$\boldsymbol{\nabla}\chi - \frac{2e}{\hbar}\mathbf{A} = \frac{1}{2\pi R}\left(2\pi n - \frac{2e}{\hbar}\Phi\right) = \frac{1}{R}\left(n - \frac{\Phi}{\Phi_0}\right), \tag{2.6}$$

where the definition of a flux-quantum, $\Phi_0 = \frac{h}{2e}$, was used. Plugging this back into Eq.(2.2) yields:

$$\Omega_s - \Omega_N^{(0)} = \alpha\tau|\psi|^2 + \frac{b}{2}|\psi|^4 + \frac{\hbar^2}{4m}|\psi|^2 \left(\frac{1}{R}\left(n - \frac{\Phi}{\Phi_0}\right)\right)^2 + \frac{\mathbf{B}^2}{8\pi}. \tag{2.7}$$

Collecting now the $|\psi|^2$ terms:

$$\Omega_s - \Omega_N^{(0)} = \alpha\tau'|\psi|^2 + \frac{b}{2}|\psi|^4 + \frac{\mathbf{B}^2}{8\pi}, \tag{2.8}$$

where the notation $\tau' = \tau + \frac{\hbar^2}{4mR^2\alpha}\left(n - \frac{\Phi}{\Phi_0}\right)^2$ was introduced. Now, the phase transition happens as the sign changes on the term with the order parameter squared. Thus one can set $\tau' = 0$:

$$0 = \frac{T - T_C}{T_C} + \frac{\hbar^2}{4mR^2\alpha}\left(n - \frac{\Phi}{\Phi_0}\right)^2, \tag{2.9}$$

and obtain the expression for the critical temperature as a function of the magnetic field:

$$\boxed{-\frac{T - T_C}{T_C} \cdot \frac{4mR^2\alpha}{\hbar^2} = \left(n - \frac{\Phi}{\Phi_0}\right)^2.} \tag{2.10}$$

Thus the critical temperature depends on the applied magnetic field through the magnetic flux. This dependence is plotted and discussed later, but first the kinetic term of Eq.(2.1) is studied. Using the following relation (as for example presented in the book by M. Tinkham [12], Eq.(4.9), with χ instead of θ):

$$\mathbf{v}_s = \frac{\hbar}{2m}\left(\boldsymbol{\nabla}\chi - \frac{2e\mathbf{A}}{\hbar}\right), \tag{2.11}$$

one can write the supercurrent velocity in the cylinder as a function of the applied field as well. This was expected as the velocity is proportional to the critical temperature, as can be seen from Eq.(2.2).

Performing once again a contour integral, quite like in Eq.(2.6), one gets

$$2\pi R v_s = \frac{\hbar}{2m}\left(2\pi n - \frac{2e}{\hbar}\Phi\right) \tag{2.12}$$

which one can rewrite as to have the supercurrent depending on the magnetic field:

$$\boxed{v_s \frac{2mR}{\hbar} = \left(n - \frac{\Phi}{\Phi_0}\right),} \tag{2.13}$$

where again $\Phi_0 = \frac{h}{2e}$. One sees that v_s depends linearly on Φ, where T_C depends on Φ quadratically. Fig.(3) shows this, in terms of $\frac{\Phi}{\Phi_0}$. Note that the integer n changes in the plot. From $\frac{\Phi}{\Phi_0}$ between 0 and $\frac{1}{2}$, one has $n = 0$, from $\frac{\Phi}{\Phi_0}$ between $\frac{1}{2}$ and $\frac{3}{2}$ one has $n = 1$ and so on. This occurs since it becomes more energetically favourable to increase the winding instead of increasing the supercurrent in the cylinder. This in turn will flip the direction of the supercurrent, see Eq.(2.13). Recall that the supercurrent is generated to counter the applied magnetic field.

Notice further that it is the negative change in critical temperature, so that in the valleys where $\frac{\Phi}{\Phi_0}$ is equal to an integer one has the highest T_C possible, as the change is 0. This can also be seen directly from Eq.(2.10). Oppositely, $\frac{\Phi}{\Phi_0}$ equal to half odd-integers corresponds to the lowest T_C possible, as the velocity is at its peak. Thus a lot of energy is spent on the supercurrent, meaning that lower temperatures would be able to destroy superconductivity. These results agree with the finding of Little and Parks, [10] Fig.(1), as well as Abrikosov [9], Fig.(112). It is also presented in Tinkham [12], Fig.(4.5), although with a sign difference on v_s.

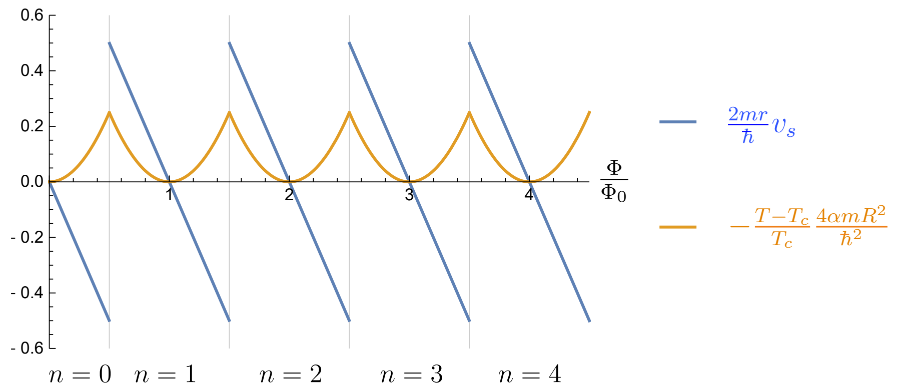

Figure 3: Supercurrent velocity and change in critical temperature as a function of $\frac{\Phi}{\Phi_0}$. The vertical lines represent change in the integer winding number, n, which is 0 for $\frac{\Phi}{\Phi_0}$ between 0 and $\frac{1}{2}$, 1 for $\frac{\Phi}{\Phi_0}$ between $\frac{1}{2}$ and $\frac{3}{2}$, and so on. When $\frac{\Phi}{\Phi_0}$ assumes integer values there is no reduction in T_C and no current running in the cylinder, while for $\frac{\Phi}{\Phi_0}$ equal to half integers there is maximum current and the corresponding maximum reduction of T_C.

This is the essence of the LP effect; a slight suppression of the critical temperature as a function of the magnetic field. The reasoning set forth by Little and Parks [10] for the existence of this effect is as follows. Exactly at the transition temperature, the free energy of normal- and superconducting electrons is exactly the same, as both states are equally energetically favourable. The free energy of the superconducting electrons depends on the magnetic flux, while that of the normal electrons does not. The flux induces a current that counters and cancels the field in the SC, which in turn means the kinetic energy of the electrons can be increased with the magnetic field. Thus, if the energy of the superconducting electrons depend on the magnetic flux, then so must the transition temperature.

Another interesting point to discuss concerns the thickness of the cylinder, d. Abrikosov [9] notes that this thickness in the original LP experiment was so small that no quantization of magnetic flux occurred. Recall that the argument for the quantization demands the phase to be equal to an integer times 2π upon making a complete closed loop around the cylinder, as explained in Sec.(1.1). What I failed to note, however, was that this path must be made

deep in the superconductor, so that no screening currents can interfere. These screening currents lie exactly within λ, the magnetic field penetration depth, from the surface, so in the LP experiment where the thickness was actually smaller than λ, this can not be satisfied! The result is that the flux may assume quanta different from the value Φ_0.
Thus, for a superconducting cylinder in an axial magnetic field, an increase in the magnetic field can increase the winding n through the cylinder. The case of $n = -1$ is studied in Sec.(3.2.3).

2.2 DESTRUCTIVE REGIME OF LITTLE-PARKS EFFECT

Before concluding this topic, a final note is discussed. Inspired by the "islands" of superconductivity seen in the article S. Vaitiekenas et al.[3], I look closer into the so-called destructive regime of LP effect. Their Fig.(1D) is presented in Fig.(4) for easy reference to this neat example.
The phenomenon is well-studied and the references presented below are only some of many. A clear and concise explanation is found in the article [13] by Sternfeld et al., describing a system of a superconducting shell of diameter D which is smaller than the zero-temperature coherence length $\xi(0)$. At odd half-quanta Φ_0 values for the flux, superconductivity will be completely destroyed. As presented in Fig.(3), it is at these points the reduction of T_C is at its largest, and the "islands" emerge simply because the critical temperature is reduced to 0. Thus even at $T = 0$ the kinetic energy of the current exceeds the condensation energy. Both [13] and for example Schwiete & Oreg [14] report the reduction in T_C to depend on the ratio $\frac{D}{\xi(0)}$, where for values $\frac{D}{\xi(0)} \leq 1.2$ the critical temperature will be reduced to 0 for flux close to half-integer flux quantum.
This is exactly as seen in Fig.(4). The temperature is very close to 0, and for this very thin metal one indeed sees these destructive regimes, in which superconductivity is lost. The mean diameter of the wire used in [3] was presented as $D \approx 160$ nm, whereas the coherence length is found on page 8 as $\xi_S = 180$ nm, and thus $\frac{D}{\xi(0)} < 1.2$ is satisfied. Superconductivity is regained and lost as the magnetic field increases, meaning one can actually observe a flux-tuned quantum phase transition [13][14] (phase transition happening at zero temperature). This holds of course only until the critical field is reached, beyond which superconductivity remains impossible, which is also the explanation for the decreasing "height" of the islands in Fig.(4).

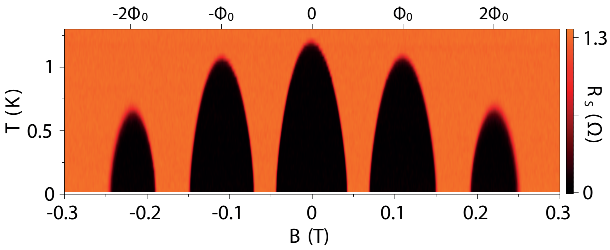

Figure 4: This picture is taken directly from [3], Fig.(1D). Temperature evolution of the resistance as a function of the magnetic field B. The destructive regime of the LP effect refers to the reduction of T_C to 0 at Φ around odd half-integer Φ_0. The system can enter, exit, and re-enter the superconducting state at $T = 0$ depending on the magnetic field, and thus the phenomenon is a quantum phase transition.

3 BOUND EXCITATIONS IN A VORTEX

3.1 THE CDGM STATES

Now for the main topic of this thesis, the states known as Caroli-de Gennes-Matricon (CdGM) states. Proposed first in the article [15] by C. Caroli, P. G. De Gennes and J. Matricon in 1964, these states are described as low energy excitations that exist near an Abrikosov vortex line in a pure type-II superconductor. As mentioned earlier, the sub-gap features seen in [3] could turn out to be exactly these CdGM states. Furthermore, these states are believed to have been found experimentally in the work of M. Chen et al. [4]. Therefore I believe that a closer look into the nature of CdGM states could be more than worthwhile.

This section will deal with the reproduction of the results of [15], i.e. finding the eigenvalues of these low-energy excited vortex states analytically. Afterwards, a method in Mathematica is designed in order to find these states numerically and compare these with the theory. In this case, one imagines a solid superconducting cylinder with a magnetic field passing through along the length of the magnetic field line. A disk region will be defined and the CdGM states are found within, and thus these states are energy states of a superconducting cylinder, as possibly seen in [3].
Furthermore, in Sec.(4), the magnetic field effects are included in the system, following the work of [16] and the system is solved analytically, followed again by a numerical procedure. The sketch of a vortex in which the CdGM states may live is shown in Fig.(5), in Cartesian coordinates. The gap profile is shown as starting from 0 in the center (thus a normal region), and growing to its value in the superconductor over a distance equal to the coherence length of the superconductor. One may assume the gap increases linearly for x, y close to zero. The supercurrent induced by the magnetic field encircles the vortex line and screens the magnetic field in the center from the rest of the superconductor.

Determine the energy of the vortex states is done using the Bogoliubov-de-Gennes (BdG) equation, presented for example in [11], chapter 5. The BdG equation is a two-component Schrödinger equation that describes electron- and hole-like excitations in a superconducting system. These excitations are called Bogoliubov quasiparticles; superpositions of both electrons and holes, [6] page 36.

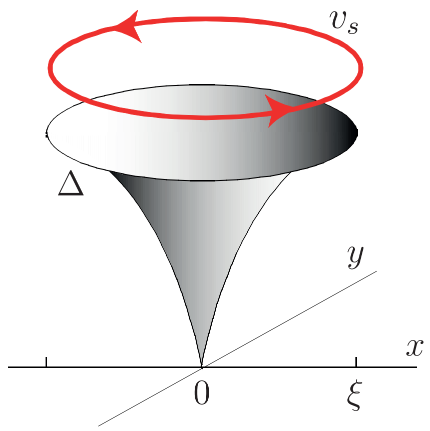

Figure 5: The spatial dependence of the gap in the vortex. The picture is taken from [6], Fig.(4.11a). The radius of the vortex is labelled ξ, which was justified in the Sec.(1.1). The gap is assumed to increase linearly close to the center. The supercurrent v_s is generated to screen the magnetic field from the rest of the superconductor.

The relevant energies are the low energy excitations, i.e. states with energy much smaller than the gap, $\epsilon < \Delta_0$. Cylindrical coordinates will be used going forward.
A slight rewriting of [15] Eq.(1) yields the starting point with the BdG equation:

$$-\frac{\hbar^2}{2m}\left(\boldsymbol{\nabla} - \frac{ie}{\hbar}\mathbf{A}\right)^2 u(r,\theta,z) - E_F u(r,\theta,z) + W(r)v(r,\theta,z) = \epsilon\, u(r,\theta,z), \tag{3.1a}$$

$$\frac{\hbar^2}{2m}\left(\boldsymbol{\nabla} + \frac{ie}{\hbar}\mathbf{A}\right)^2 v(r,\theta,z) + E_F v(r,\theta,z) + W^*(r)u(r,\theta,z) = \epsilon\, v(r,\theta,z), \tag{3.1b}$$

where $\hbar$ is the reduced Planck's constant, m is the electron mass, e is the electronic charge, $\mathbf{A}$ is the vector potential, E_F is the Fermi energy, ϵ are the eigenenergies and u, v are the wavefunctions. These are the amplitudes presented earlier, describing the quasiparticles as superpositions of electrons and holes. Going forward, I write only the radial dependence explicitly, i.e. $u(r)$, $v(r)$, as this will be the most relevant component. Finally, $W(r) = \Delta(r)\mathrm{e}^{-in\theta}$ is the gap function as presented in [15], with an exception of an added n. This represents the winding, where for the current case $n = 1$ is used throughout, as the Abrikosov vortex has a single flux quantum penetrating the superconductor, corresponding to a winding number $n = 1$. This number, n, will become much more relevant in Sec.(3.2.3), where one can introduce greater (and negative) winding numbers. However, for now n remains 1 and

is subsequently no longer written out explicitly.
Define first the overall wavefunction:

$$\begin{pmatrix} u(r) \\ v(r) \end{pmatrix} = e^{ik_F \cos(\alpha) z} e^{i\mu\theta} \begin{pmatrix} e^{-\frac{1}{2}i\theta} f_+(r) \\ e^{\frac{1}{2}i\theta} f_-(r) \end{pmatrix}, \tag{3.2}$$

where α is some arbitrary angle, μ is the azimuthal quantum number and k_F is the Fermi wavevector. The first exponential function represents the infinite longitudinal direction (parallel to the flux tubes), which is of little importance here, as one simply expects standing waves. The second exponential function represents the azimuthal direction and finally $f_\pm$ represent the radial part of the wavefunction. The lecture notes by V. B. Eltsov [6] also finds these CdGM states analytically (but without much in-depth explanation) and their expression for Eq.(3.2) can be seen on their page 99. Note that [6] uses a different sign convention compared to the work of Caroli et al. and therefore also this thesis. However, where Caroli et al. state that μ in Eq.(3.2) should be an integer, both [6] and another article [16], which is used later on, introduce μ as a half-integer. The same goes for [4]; even though they do not write up the wavefunctions, they do write the same equation for the eigenvalues as Caroli et al., in which μ is presented as a half-integer.
The external non-magnetic potential that is otherwise present in the BdG equations has been set to 0. In accordance with [15], one can now further neglect all magnetic field effects and so $\mathbf{A}$ is set to 0 as well. In Sec.(4) I reintroduce the magnetic field and investigate its effect. To begin the search for the energy, one should first write out the Laplace operator acting on $u(r)$ and $v(r)$ in cylindrical coordinates. Note that the radial dependence of $f_\pm$ W and u, v will be suppressed for notational convenience going forward. Specifically for $\boldsymbol{\nabla}^2 u$:

$$\begin{aligned} \boldsymbol{\nabla}^2 u &= \frac{1}{r}\frac{\partial}{\partial r}\left(r\frac{\partial u}{\partial r}\right) + \frac{1}{r^2}\frac{\partial^2 u}{\partial \theta^2} + \frac{\partial^2 u}{\partial z^2} \\ &= \frac{\partial^2 u}{\partial r^2} + \frac{1}{r}\frac{\partial u}{\partial r} + \frac{1}{r^2}\frac{\partial^2 u}{\partial \theta^2} + \frac{\partial^2 u}{\partial z^2}. \end{aligned} \tag{3.3}$$

Writing out the above and inserting this into the Eqs.(3.1a) and (3.1b) yields

$$\begin{aligned} &-\frac{\hbar^2}{2m} e^{ik_F\cos(\alpha)z} e^{i\mu\theta} e^{-\frac{1}{2}i\theta}\left[\frac{\partial^2 f_+}{\partial r^2} + \frac{1}{r}\frac{\partial f_+}{\partial r} - \frac{1}{r^2}\left(\mu - \frac{1}{2}\right)^2 f_+ - k_F^2\cos^2(\alpha) f_+\right] \\ &- E_F u + W\ v = \epsilon u, \end{aligned} \tag{3.4a}$$

$$\begin{aligned} &\frac{\hbar^2}{2m} e^{ik_F\cos(\alpha)z} e^{i\mu\theta} e^{\frac{1}{2}i\theta}\left[\frac{\partial^2 f_-}{\partial r^2} + \frac{1}{r}\frac{\partial f_-}{\partial r} - \frac{1}{r^2}\left(\mu + \frac{1}{2}\right)^2 f_- - k_F^2\cos^2(\alpha) f_-\right] \\ &+ E_F v + W^*\ u = \epsilon v. \end{aligned} \tag{3.4b}$$

μ is discussed in [15], presented as $0 < \mu (k_F)^{-1} \ll \xi$, and this is the range in which I will solve the Eqs.(3.4a) and (3.4b).

Dividing out the exponential functions in front of the square brackets in both equations will result in a phase appearing on both the W terms:

$$-\frac{\hbar^2}{2m}\left[\frac{\partial^2 f_+}{\partial r^2}+\frac{1}{r}\frac{\partial f_+}{\partial r}-\frac{1}{r^2}\left(\mu-\frac{1}{2}\right)^2 f_+ - k_F^2\cos^2(\alpha)f_+\right]$$
$$-E_F f_+ + W\ e^{i\theta} f_- = \epsilon f_+, \tag{3.5a}$$
$$\frac{\hbar^2}{2m}\left[\frac{\partial^2 f_-}{\partial r^2}+\frac{1}{r}\frac{\partial f_-}{\partial r}-\frac{1}{r^2}\left(\mu+\frac{1}{2}\right)^2 f_- - k_F^2\cos^2(\alpha)f_-\right]$$
$$+E_F f_- + W^*\ e^{-i\theta} f_+ = \epsilon f_-. \tag{3.5b}$$

The gap function W is written out as $W(r) = \Delta(r)e^{-i\theta}$, meaning the phases will drop out. Further, using the following relation (having omitted $f_\pm$)

$$\mp\frac{\hbar^2}{2m}\left[-k_F^2\cos^2(\alpha)\right]\mp E_F = \mp\frac{\hbar^2}{2m}\left[-k_F^2(\cos^2(\alpha)-1)\right] = \mp\frac{\hbar^2}{2m}\left[k_F^2(\sin^2(\alpha))\right], \tag{3.6}$$

allows one to obtain the following form for the BdG equations:

$$-\frac{\hbar^2}{2m}\left[\frac{\partial^2 f_+}{\partial r^2}+\frac{1}{r}\frac{\partial f_+}{\partial r}-\frac{1}{r^2}\left(\mu-\frac{1}{2}\right)^2 f_+ + k_F^2\sin^2(\alpha)f_+\right]$$
$$+\Delta(r)f_- = \epsilon f_+, \tag{3.7a}$$
$$\frac{\hbar^2}{2m}\left[\frac{\partial^2 f_-}{\partial r^2}+\frac{1}{r}\frac{\partial f_-}{\partial r}-\frac{1}{r^2}\left(\mu+\frac{1}{2}\right)^2 f_- + k_F^2\sin^2(\alpha)f_-\right]$$
$$+\Delta(r)f_+ = \epsilon f_-. \tag{3.7b}$$

Collecting these into spinor notation (electron-hole space) one obtains

$$\boxed{\sigma_z\frac{\hbar^2}{2m}\left[-\frac{d^2\hat{f}}{dr^2}-\frac{1}{r}\frac{d\hat{f}}{dr}+\left(\mu-\frac{1}{2}\sigma_z\right)^2\frac{\hat{f}}{r^2}-k_F^2\sin^2(\alpha)\hat{f}\right]+\sigma_x\Delta(r)\hat{f}=\epsilon\hat{f} \qquad (3.8)}$$

Thus, an expression for the Bogoliubov-de Gennes equations for the system is achieved, which one can solve for the energy ϵ.

In practise one can obtain solutions for the radial part of the wavefunction, $\hat{f} = \begin{pmatrix} f_+ \\ f_- \end{pmatrix}$, in the high-$r$ and low-r limits, and then compare them at some in-between "critical" r_c, from which one can extract an expression for ϵ. This r_c is chosen so that for $r < r_c$ the gap

strength is assumed neglectable, while still satisfying $r_c < \xi$.
First the case $r < r_c$ is examined, for which one can set $\Delta = 0$ in Eq.(3.8):

$$\sigma_z \frac{\hbar^2}{2m}\left[-\frac{d^2\hat{f}}{dr^2} - \frac{1}{r}\frac{d\hat{f}}{dr} + \left(\mu - \frac{1}{2}\sigma_z\right)^2 \frac{\hat{f}}{r^2} - k_F^2 \sin^2(\alpha)\hat{f}\right] = \epsilon\hat{f}. \tag{3.9}$$

Rewriting this to Bessel's differential equation by first multiplying $-r^2$ on both sides and collecting everything on the left hand side yields:

$$\sigma_z \frac{\hbar^2}{2m}\left[r^2\frac{d^2\hat{f}}{dr^2} + r\frac{d\hat{f}}{dr} + \left(\left(k_F^2 \sin^2(\alpha) + \epsilon\sigma_z \frac{2m}{\hbar^2}\right) r^2 - \left(\mu - \frac{1}{2}\sigma_z\right)^2\right)\hat{f}\right] = 0. \tag{3.10}$$

Note the relation $\sigma_z\sigma_z = 1$ has been employed. The definition of Bessel's differential equation can be found in the book by K. Riley & M. Hobson, Eq.(9.70) [17].
Rescale now Eq.(3.10) by introducing the notation $s = \left(k_F^2 \sin^2(\alpha) + \epsilon\sigma_z \frac{2m}{\hbar^2}\right)^{1/2} r$ so that

$$\frac{d\hat{f}}{dr} = \frac{d\hat{f}}{ds}\frac{ds}{dr}, \qquad \frac{ds}{dr} = \left(k_F^2 \sin^2(\alpha) + \epsilon\sigma_z \frac{2m}{\hbar^2}\right)^{1/2}, \tag{3.11}$$

allowing one to write:

$$\sigma_z \frac{\hbar^2}{2m}\left[s^2\frac{d^2\hat{f}}{ds^2} + s\frac{d\hat{f}}{ds} + \left(s^2 - \left(\mu - \frac{1}{2}\sigma_z\right)^2\right)\hat{f}\right] = 0. \tag{3.12}$$

The expression in the square brackets is now on the form of Bessel' differential equation for which the solutions $\hat{f}$ are Bessel functions. Thus one can write

$$f_\pm \propto J_{\mu \mp \frac{1}{2}}\left[s\right]. \tag{3.13}$$

Note here that the order of the Bessel function indicates that μ most likely is a half-integer, not an integer as [15] states.
One can further rewrite the expression s as follows:

$$s = k_F \sin(\alpha)\sqrt{1 + \epsilon\sigma_z \frac{2m}{\hbar^2 k_F^2 \sin^2(\alpha)}}\, r. \tag{3.14}$$

Using $E_F = \frac{k_F^2\hbar^2}{2m}$ and the fact that the eigenvalues are smaller than the Fermi energy, $\epsilon < E_F$ (since the states in question have energy smaller than the gap), one can make the approximation

$$s \approx k_F \sin(\alpha)\left(1 + \frac{1}{2}\epsilon\sigma_z \frac{2m}{\hbar^2 k_F^2 \sin^2(\alpha)}\right) r = \left(k_F \sin(\alpha) + \sigma_z \frac{\epsilon \cdot m}{\hbar^2 k_F \sin(\alpha)}\right) r. \tag{3.15}$$

Introduce the notation $q = \frac{\epsilon}{\hbar v_F \sin(\alpha)}$, where $v_F = \frac{\hbar k_F}{m}$, and write

$$s \approx (k_F \sin(\alpha) + \sigma_z q)\, r. \tag{3.16}$$

The solutions to Eq.(3.9) become

$$\boxed{f_{\pm} = A_{\pm} J_{\mu \mp \frac{1}{2}} \left[(k_F \sin(\alpha) \pm q)\, r \right], \tag{3.17}}$$

in accordance with Eq.(4) of Caroli et al [15]. Here $A_{\pm}$ are arbitrary coefficients.
Now, for the case $r > r_c$ one cannot neglect the pair potential Δ in Eq.(3.8), and so one seeks solutions of the very general form:

$$\hat{f} = \hat{g}(r) H_n \left[k_F \sin(\alpha) r \right] + c.c, \tag{3.18}$$

where c.c represents the complex conjugate and H_n represents a Hankel function of the first kind and of the order $n = \sqrt{\mu^2 + \frac{1}{4}}$. Note that the Hankel function of the first kind is given by $H_n(x) = J_n(x) + iY_n(x)$, where Y_n represents Bessel functions of the second kind.
The functions $\hat{g}(r) = \begin{pmatrix} g_+(r) \\ g_-(r) \end{pmatrix}$ are slowly varying envelope functions and vary at distances of the order of ξ, as explained in [6], page 100. One can analyze this solution further by looking into the form of $\hat{g}(r)$.
One may obtain an equation for $\hat{g}(r)$ by inserting the above solutions into Eq.(3.8). The variable dependencies on both $\hat{g}(r)$ and $H_n \left[k_F \sin(\alpha) r \right]$ in the calculations to follow are suppressed for notational convenience.

$$\begin{aligned}
\sigma_z \frac{\hbar^2}{2m} \Bigg(&- \left[2 \frac{d\hat{g}}{dr} \frac{dH_n}{dr} + \hat{g} \frac{d^2 H_n}{dr^2} + H_n \frac{d^2 \hat{g}}{dr^2} + 2 \frac{d\hat{g}^*}{dr} \frac{dH_n^*}{dr} + \hat{g}^* \frac{d^2 H_n^*}{dr^2} + H_n^* \frac{d^2 \hat{g}^*}{dr^2} \right] \\
&- \frac{1}{r} \left[H_n \frac{d\hat{g}}{dr} + \hat{g} \frac{dH_n}{dr} + H_n^* \frac{d\hat{g}^*}{dr} + \hat{g}^* \frac{dH_n^*}{dr} \right] \\
&+ \left[-(k_F \sin(\alpha))^2 + \frac{1}{r^2} (\mu - \frac{1}{2} \sigma_z)^2 \right] \left[\hat{g} H_n + \hat{g}^* H_n^* \right] \Bigg) \\
+ \sigma_x \Delta(r) \left[\hat{g} H_n + \hat{g}^* H_n^* \right] &= \epsilon \left[\hat{g} H_n + \hat{g}^* H_n^* \right].
\end{aligned} \tag{3.19}$$

The complex conjugate of the Hankel function of the first kind is called a Hankel function of the second kind; $H_n^*(x) = H_n^{(2)}(x) = J_n(x) - iY_n(x)$.
Rewriting the term $(\mu - \frac{1}{2}\sigma_z)^2$ yields

$$(\mu - \frac{1}{2} \sigma_z)^2 = \mu^2 + \frac{1}{4} - \sigma_z \mu. \tag{3.20}$$

Move now the σ_z part of Eq.(3.20) to the right hand side (RHS) of Eq.(3.19) and look only at the first term of $\hat{f}$, meaning one disregards $\hat{g}^* H_n^*$, allowed because the two terms are separable. Thus one may write

$$\begin{aligned}\sigma_z \frac{\hbar^2}{2m}\Bigg(&- \left[2\frac{d\hat{g}}{dr}\frac{dH_n}{dr} + \hat{g}\frac{d^2 H_n}{dr^2} + H_n \frac{d^2\hat{g}}{dr^2}\right] - \frac{1}{r}\left[H_n \frac{d\hat{g}}{dr} + \hat{g}\frac{dH_n}{dr}\right] \\ &+ \left[-(k_F \sin(\alpha))^2 + \frac{1}{r^2}\left(\mu^2 + \frac{1}{4}\right)\right]\hat{g}H_n\Bigg) \\ + \sigma_x \Delta(r)\hat{g}H_n &= \left(\epsilon + \sigma_z \frac{\hbar^2 \sigma_z \mu}{2mr^2}\right)\hat{g}H_n. \end{aligned} \tag{3.21}$$

By reformulating above equation one can show that certain terms make up another Bessel differential equation:

$$\begin{aligned}&\sigma_z \frac{\hbar^2}{2m}\cdot\hat{g}\left(-\frac{d^2 H_n}{dr^2} - \frac{1}{r}\frac{dH_n}{dr} + \left[-(k_F\sin(\alpha))^2 + \frac{1}{r^2}\left(\mu^2+\frac{1}{4}\right)\right]H_n\right) \\ &+ \sigma_z \frac{\hbar^2}{2m}\left(-2\frac{d\hat{g}}{dr}\frac{dH_n}{dr} - \frac{1}{r}H_n\frac{d\hat{g}}{dr} - H_n\frac{d^2\hat{g}}{dr^2}\right) + \sigma_x\Delta(r)\hat{g}H_n = \left(\epsilon + \frac{\hbar^2\mu}{2mr^2}\right)\hat{g}H_n. \end{aligned}\tag{3.22}$$

Once again $\sigma_z\sigma_z = 1$ was used on the RHS. The top line of Eq.(3.22) can be rescaled to be on the form of Bessel' differential equation, as in Eq.(3.12), to which the Hankel functions are solutions. This also determines the order of the Hankel function as $n = \sqrt{\mu^2 + \frac{1}{4}}$. Thus one can now set the top line of Eq.(3.22) equal to 0, again because Hankel functions are solution to the differential equation, resulting in the equation

$$\sigma_z \frac{\hbar^2}{2m}\left(-2\frac{d\hat{g}}{dr}\frac{dH_n}{dr} - \frac{1}{r}H_n\frac{d\hat{g}}{dr} - H_n\frac{d^2\hat{g}}{dr^2}\right) + \sigma_x\Delta(r)\hat{g}H_n = \left(\epsilon + \frac{\hbar^2\mu}{2mr^2}\right)\hat{g}H_n. \tag{3.23}$$

One can evaluate the derivative of the Hankel functions using $\frac{dH_n(k\cdot x)}{dx} = i\,kH_n(k\cdot x)$, where k is a constant and i is of course the imaginary unit. Furthermore, for the current case of $r > r_c$, the term $\frac{1}{r}H_n\frac{d\hat{g}}{dr}$ is small and can be neglected:

$$\sigma_z \frac{\hbar^2}{2m}\left(-2\frac{d\hat{g}}{dr}(ik_F\sin(\alpha))H_n - H_n\frac{d^2\hat{g}}{dr^2}\right) + \sigma_x\Delta(r)\hat{g}H_n = \left(\epsilon + \frac{\hbar^2\mu}{2mr^2}\right)\hat{g}H_n. \tag{3.24}$$

Dividing through by H_n yields the following differential equation for $\hat{g}$ (where the radial dependence is restored):

$$\boxed{-\sigma_z\frac{\hbar^2}{2m}\frac{d^2\hat{g}(r)}{dr^2} - i\sigma_z\hbar v_F\sin(\alpha)\frac{d\hat{g}(r)}{dr} + \sigma_x\Delta(r)\hat{g}(r) = \left(\epsilon + \frac{\hbar^2\mu}{2mr^2}\right)\hat{g}(r),} \tag{3.25}$$

where $v_F = \frac{k_F\hbar}{m}$ was used.
Regarding the second order derivative on $\hat{g}(r)$, one can reasonably disregard this, as $g(r)$ is a slowly varying function, allowing for the neglecting of higher order terms. In Appendix

(A.4) I show and compare the order of the different terms in Eq.(3.23).
Eq.(3.25) will now allow one to find an expression for $\hat{g}(r)$. Proceeding now with the ansatz that $\hat{g}(r)$ can be written as

$$\hat{g}(r) = \begin{pmatrix} g_+(r) \\ g_-(r) \end{pmatrix} = c \begin{pmatrix} e^{\frac{i}{2}\psi(r)} \\ -ie^{-\frac{i}{2}\psi(r)} \end{pmatrix} e^{-K(r)} e^{i\frac{\pi}{4}}, \tag{3.26}$$

leaves one to find expressions for the introduced $\psi(r)$ and $K(r)$. Note that the ansatz here differs from that of [15], Eq.(7) by the extra term $e^{i\frac{\pi}{4}}$. The usefulness of this term will become evident later on.
The c in Eq.(3.26) is a constant and is neglected subsequently, as it can be divided out in all calculations. The same holds for the extra phase term $e^{i\frac{\pi}{4}}$. Recall that one seeks a description for Eq.(3.18) so that Eq.(3.17) and Eq.(3.18) can be compared at the critical radius r_c, which in turn yields an expression for the energy, ϵ.
One can now insert Eq.(3.26) into Eq.(3.25). I show the derivation for the upper part of Eq.(3.25), that is, for g_+. Neglecting the second order derivative on g_+ as explained earlier, one can get the following differential equation for g_+:

$$\begin{aligned} &- i\hbar v_F \sin(\alpha) \frac{d}{dr}\left(e^{\frac{i}{2}\psi(r)} e^{-K(r)}\right) + \Delta(r)\left(-ie^{\frac{-i}{2}\psi(r)} e^{-K(r)}\right) \\ &= \left(\epsilon + \frac{\hbar^2\mu}{2mr^2}\right) e^{\frac{i}{2}\psi(r)} e^{-K(r)}. \end{aligned} \tag{3.27}$$

As $e^{i\frac{\pi}{4}}$ is r-independent, it has been divided out from all terms.
Perform the derivatives, divide by $e^{-K(r)}$ and introduce the shorthand notation $a = \hbar v_F \sin(\alpha)$ to get:

$$-ia\left(\frac{i}{2}\frac{d\psi(r)}{dr} - \frac{dK(r)}{dr}\right) e^{\frac{i}{2}\psi(r)} - i\Delta(r) e^{\frac{-i}{2}\psi(r)} = \left(\epsilon + \frac{\hbar^2\mu}{2mr^2}\right) e^{\frac{i}{2}\psi(r)}. \tag{3.28}$$

Multiplying by $e^{\frac{-i}{2}\psi(r)}$ yields

$$\frac{a}{2}\frac{d\psi(r)}{dr} + ia\frac{dK(r)}{dr} = \left(\epsilon + \frac{\hbar^2\mu}{2mr^2}\right) + i\Delta(r) e^{-i\psi(r)}. \tag{3.29}$$

The exponential function on the RHS is written out in terms of sine and cosine and following the same procedure for g_- one obtains the equations

$$\frac{a}{2}\frac{d\psi(r)}{dr} + ia\frac{dK(r)}{dr} = \left(\epsilon + \frac{\hbar^2\mu}{2mr^2}\right) + i\Delta(r)\left[\cos(\psi(r)) - i\sin(\psi(r))\right] \tag{3.30a}$$

&

$$\frac{a}{2}\frac{d\psi(r)}{dr} - ia\frac{dK(r)}{dr} = \left(\epsilon + \frac{\hbar^2\mu}{2mr^2}\right) - i\Delta(r)\left[\cos(\psi(r)) + i\sin(\psi(r))\right]. \tag{3.30b}$$

Subtracting the second from the first yields

$$2ia\frac{dK(r)}{dr} = 2i\Delta(r)\cos(\psi(r)), \tag{3.31}$$

while adding the two equations yields

$$a\frac{d\psi(r)}{dr} = 2\left(\epsilon + \frac{\hbar^2\mu}{2mr^2}\right) + 2\Delta(r)\sin(\psi(r)). \tag{3.32}$$

Isolate the derivatives and one gets the wanted expressions:

$$\frac{dK(r)}{dr} = (a)^{-1}\Delta(r)\cos(\psi(r)) \tag{3.33}$$

&

$$\frac{d\psi(r)}{dr} = 2(a)^{-1}\left[\left(\epsilon + \frac{\hbar^2\mu}{2mr^2}\right) + \Delta(r)\sin(\psi(r))\right]. \tag{3.34}$$

One may now guess expressions for $\psi(r)$ and $K(r)$ satisfying Eqs.(3.33) and (3.34), allowing one to formulate $\hat{g}$ completely. Using now that $\mu(k_F)^{-1} \ll \xi$, from which one can assume $\psi(r)$ is small, which I will show later, one may write

$$K(r) = (a)^{-1}\int_0^r \Delta(r')dr', \tag{3.35}$$

$$\psi(r) = -\int_r^\infty \exp\{2K(r) - 2K(r')\}\left(2q + \frac{\mu}{k_F\sin(\alpha)r'^2}\right)dr', \tag{3.36}$$

where again $a = \hbar v_F\sin(\alpha)$ and $q = \frac{\epsilon}{a}$ was introduced. Shown in the Appendix (A.1) is that Eqs.(3.35) and (3.36) indeed satisfy Eqs.(3.33) and (3.34) for small $\psi(r)$.
Also shown, in Appendix (A.2), is that $\hat{g}$ given in Eq.(3.26), using the expressions (3.35) and (3.36), is a solution to the differential equation (3.25), given that one can neglect the second order derivative. This should be the case trivially, as 3.33 and 3.34 were determined from the equation for $\hat{g}(r)$, so if Eqs.(3.35) and (3.36) satisfy Eqs.(3.33) and (3.34), then $\hat{g}(r)$ with these will be satisfied. Thus it is merely a sanity check to ensure nothing went wrong under way.
Now, having described $\hat{g}(r)$, one has obtained an expression for Eq.(3.18), representing the radial part of our wavefunction in the case $r > r_c$. Finally one can compare the two radial solutions Eqs.(3.17) and (3.18) in the limit where they "meet", r_c!
Evaluating Eq.(3.36) in $r = r_c$ by rewriting the integral using the notation $\Gamma(r') = \exp\{2K(r_c) - 2K(r')\}\left(2q + \frac{\mu}{k_F\sin(\alpha)r'^2}\right)$, one finds:

$$-\int_{r_c}^\infty \Gamma(r')\,dr' = -\int_0^\infty \Gamma(r')\,dr' + \int_0^{r_c}\Gamma(r')\,dr', \tag{3.37}$$

where subsequently the integration variable r' will be renamed back to r. Performing the last integral on the RHS yields

$$\int_0^{r_c} \exp\{2K(r_c) - 2K(r)\} \left(2q + \frac{\mu}{k_F \sin(\alpha) r^2}\right) dr \approx \int_0^{r_c} \left(2q + \frac{\mu}{k_F \sin(\alpha) r^2}\right) dr, \quad (3.38)$$

where it is assumed that $\mathrm{e}^{K(r_c)-K(r)} \approx 1$. This holds as Δ is neglected for $r < r_c$, resulting in the integral $\int_0^{r_c} \Delta(r) dr$ in $K(r_c)$ becoming zero, and similarly for $K(r)$. The resulting integral is evaluated as:

$$\int_0^{r_c} \left(2q + \frac{\mu}{k_F \sin(\alpha) r^2}\right) dr = 2qr_c - \left[\frac{\mu}{k_F \sin(\alpha) r}\right]_0^{r_c}. \quad (3.39)$$

The $r = 0$ term of Eq.(3.39) will be shown to cancel with another term later, so the division by zero will not ruin the day.

Directing ones attention to the first integral on the RHS of Eq.(3.37), while once again neglecting $\mathrm{e}^{K(r_c)}$, one finds:

$$\int_0^{\infty} \mathrm{e}^{-2K(r)} \left(2q + \frac{\mu}{k_F \sin(\alpha) r^2}\right) dr. \quad (3.40)$$

Look first at the second term, which one can rewrite using partial integration. Specifically, $\int_0^\infty jh' \; dr = \int_0^\infty (jh)' \; dr - \int_0^\infty j'h \; dr$, with the notation $j = \exp\{-2K(r)\}$ and $h' = \frac{\mu}{k_F \sin(\alpha) r^2}$, so that $h = \frac{-\mu}{k_F \sin(\alpha) r}$. Thus

$$\begin{aligned}
&\int_0^{\infty} \mathrm{e}^{-2K(r)} \frac{\mu}{k_F \sin(\alpha) r^2} dr \\
&= \int_0^{\infty} \left(\mathrm{e}^{-2K(r)} \frac{-\mu}{k_F \sin(\alpha) r}\right)' dr - \int_0^{\infty} \left(-2K'(r)\right) \mathrm{e}^{-2K(r)} \frac{-\mu}{k_F \sin(\alpha) r} dr \\
&= \left[\mathrm{e}^{-2K(r)} \frac{-\mu}{k_F \sin(\alpha) r}\right]_0^{\infty} - \int_0^{\infty} 2 \left(\frac{\Delta(r)}{\hbar v_F \sin(\alpha)}\right) \mathrm{e}^{-2K(r)} \frac{\mu}{k_F \sin(\alpha) r} dr. \quad (3.41)
\end{aligned}$$

In the final equality the definition for the derivative of $K(r)$ in Eq.(3.33) with $\cos(\psi(r)) \approx 1$ was used. The first term in the final equality becomes 0 for the ∞ limit, as both parts tend to zero, while the 0 limit becomes $+\frac{\mu}{k_F \sin(\alpha) r}\big|_{r=0}$, which exactly cancels the unwanted term from Eq.(3.39)! Removing this term, the final equality of Eq.(3.41) becomes

$$\int_0^{\infty} \mathrm{e}^{-2K(r)} \frac{\mu}{k_F \sin(\alpha) r^2} dr = -\int_0^{\infty} 2\mathrm{e}^{-2K(r)} \frac{\mu \Delta(r)}{k_F v_F \hbar \sin^2(\alpha) r} dr. \quad (3.42)$$

Including the first term of Eq.(3.40) and the surviving terms of Eq.(3.39), one finally obtains the following expression for $\psi(r = r_c)$:

$$\boxed{\psi(r_c) = 2qr_c - \frac{\mu}{k_F \sin(\alpha) r_c} - 2\int_0^\infty \mathrm{e}^{-2K(r)} \left(q - \frac{\mu\Delta(r)}{k_F v_F \hbar \sin^2(\alpha) r} \right) dr. \qquad (3.43)}$$

This is in agreement with the result of [15] Eq.(8), with the exception of a missing $\frac{1}{r}$ in their final term (this is later restored in the article).
Finally the solutions for the radial parts of the wavefunction can be matched. Recall that Eq.(3.17) was the solution for $r < r_c$ while Eq.(3.18) held for $r > r_c$. Matching these at $r = r_c$ will yield another expression for $\psi(r_c)$, which I stress is *not* a wavefunction, but rather a value introduced in Eq.(3.26) and determined in Eq.(3.36). One may obtain another expression for $\psi(r_c)$, shown in the calculations below, which can be compared with Eq.(3.43) in order to obtain an expression for ϵ.
Writing Eq.(3.17) equal to Eq.(3.18) at $r = r_c$ yields:

$$A_{\pm} J_{\mu \mp \frac{1}{2}} \left[k_F \sin(\alpha) r_c \pm q r_c \right] = \hat{g}(r_c) H_n \left[k_F \sin(\alpha) r_c \right] + c.c, \tag{3.44}$$

where again $n = \sqrt{\mu^2 + \frac{1}{4}}$ and $c.c$ is the complex conjugate. First and foremost one should introduce the asymptotic forms of the Bessel function of the first kind and the Hankel functions, viable for the argument z being much larger than the order σ. These are used in both [15] and in [6] page 101. The following form is adopted, using z to represent the argument and σ the order:

$$J_\sigma [z] = \sqrt{\frac{2}{\pi}}\, z^{-\frac{1}{2}} \cos \left[z + \frac{\sigma^2}{2z} - \frac{\pi}{2}\sigma - \frac{\pi}{4} \right], \tag{3.45a}$$

$$H_\sigma [z] = \sqrt{\frac{2}{\pi}}\, z^{-\frac{1}{2}} \exp \left[i \left(z + \frac{\sigma^2}{2z} - \frac{\pi}{2}\sigma - \frac{\pi}{4} \right) \right], \tag{3.45b}$$

$$H_\sigma^{(2)} [z] = \sqrt{\frac{2}{\pi}}\, z^{-\frac{1}{2}} \exp \left[-i \left(z + \frac{\sigma^2}{2z} - \frac{\pi}{2}\sigma - \frac{\pi}{4} \right) \right]. \tag{3.45c}$$

Shown below are the calculations for $g_+(r_c)$ while the $g_-(r_c)$ part can be found in the Appendix (A.3). Using the asymptotic forms to rewrite Eq.(3.44), while using the shorthand notation $\gamma = k_F \sin(\alpha) r_c$ for notational convenience, one finds:

$$\begin{aligned} &A_+ \sqrt{\frac{2}{\pi}}\, (\gamma + q r_c)^{-\frac{1}{2}} \cos \left[\gamma + q r_c + \frac{\left(\mu - \frac{1}{2}\right)^2}{2\left(\gamma + q r_c\right)} - \frac{\pi}{2}\left(\mu - \frac{1}{2}\right) - \frac{\pi}{4} \right] \\ &= \sqrt{\frac{2}{\pi}}\, \gamma^{-\frac{1}{2}} \Bigg(g_+(r_c) \exp \left[i \left(\gamma + \frac{n^2}{2\gamma} - \frac{\pi}{2} n - \frac{\pi}{4} \right) \right] \\ &+ g_+^*(r_c) \exp \left[-i \left(\gamma + \frac{n^2}{2\gamma} - \frac{\pi}{2} n - \frac{\pi}{4} \right) \right] \Bigg). \end{aligned} \tag{3.46}$$

Recall the definition of $\hat{g}$ from Eq.(3.26), which one can rewrite as $\begin{pmatrix} g_+(r_c) \\ g_-(r_c) \end{pmatrix} = \begin{pmatrix} e^{\frac{i}{2}\psi(r_c)+i\frac{\pi}{4}} \\ -ie^{-\frac{i}{2}\psi(r_c)+i\frac{\pi}{4}} \end{pmatrix}$, where the constant c has been neglected and once more the assumption $\mathrm{e}^{K(r_c)} \approx 1$ was made. Now one will appreciate the extra term $e^{i\frac{\pi}{4}}$. Insert $g_+(r_c)$ in Eq.(3.46), collect the exponential functions and thus reduce the RHS as follows:

$$\begin{aligned} RHS = \sqrt{\frac{2}{\pi}}\,\gamma^{-\frac{1}{2}}\Bigg(&\exp\left[i\left(\gamma+\frac{n^2}{2\gamma}-\frac{\pi}{2}n-\frac{\pi}{4}+\frac{\psi(r_c)}{2}+\frac{\pi}{4}\right)\right] \\ &+\exp\left[-i\left(\gamma+\frac{n^2}{2\gamma}-\frac{\pi}{2}n-\frac{\pi}{4}+\frac{\psi(r_c)}{2}+\frac{\pi}{4}\right)\right]\Bigg) \\ &= 2\sqrt{\frac{2}{\pi}}\,\gamma^{-\frac{1}{2}}\cos\left[\gamma+\frac{n^2}{2\gamma}-\frac{\pi}{2}n-\cancel{\frac{\pi}{4}}+\frac{\psi(r_c)}{2}+\cancel{\frac{\pi}{4}}\right]. \end{aligned} \tag{3.47}$$

Eq.(3.46) becomes $\Big($having cancelled the $\sqrt{\frac{2}{\pi}}$ and the other constants by choosing A_+ appropriately$\Big)$:

$$\begin{aligned} (\gamma+qr_c)^{-\frac{1}{2}}\cos\left[\gamma+qr_c+\frac{\left(\mu-\frac{1}{2}\right)^2}{2\left(\gamma+qr_c\right)}-\frac{\pi}{2}\left(\mu-\frac{1}{2}\right)-\frac{\pi}{4}\right] \\ = \gamma^{-\frac{1}{2}}\cos\left(\gamma+\frac{n^2}{2\gamma}-\frac{\pi}{2}n+\frac{\psi(r_c)}{2}\right). \end{aligned} \tag{3.48}$$

Use now $\gamma \gg qr_c$, which follows from $\frac{q}{k_F\sin(\alpha)} = \frac{\epsilon}{\hbar k_F v_F \sin^2(\alpha)} = \frac{\epsilon}{2E_F\sin^2(\alpha)} \ll 1$, since the eigenenergies should be much lower than the Fermi energy, $\epsilon \ll E_F$. Therefore $\frac{q}{k_F\sin(\alpha)} \ll 1 \Leftrightarrow q \ll k_F\sin(\alpha)$. One can then approximate $(\gamma+qr_c)^{-\frac{1}{2}} \approx \gamma^{-\frac{1}{2}}$ and neglect qr_c in the denominator on the LHS:

$$\gamma^{-\frac{1}{2}}\cos\left[\gamma+qr_c+\frac{\left(\mu-\frac{1}{2}\right)^2}{2\gamma}-\frac{\pi}{2}\left(\mu-\frac{1}{2}\right)-\frac{\pi}{4}\right] = \gamma^{-\frac{1}{2}}\cos\left[\gamma+\frac{n^2}{2\gamma}-\frac{\pi}{2}n+\frac{\psi(r_c)}{2}\right]. \tag{3.49}$$

Finally one can match the arguments, write out $n = \sqrt{\mu^2+\frac{1}{4}}$ and reduce

$$\begin{aligned} &\gamma+qr_c+\frac{\left(\mu-\frac{1}{2}\right)^2}{2\gamma}-\frac{\pi}{2}\left(\mu-\frac{1}{2}\right)-\frac{\pi}{4} = \gamma+\frac{\mu^2+\frac{1}{4}}{2\gamma}-\frac{\pi}{2}\sqrt{\mu^2+\frac{1}{4}}+\frac{\psi(r_c)}{2} \\ &\Updownarrow \\ &qr_c-\frac{\mu}{2\gamma}-\frac{\pi}{2}\mu = -\frac{\pi}{2}\sqrt{\mu^2+\frac{1}{4}}+\frac{\psi(r_c)}{2}. \end{aligned} \tag{3.50}$$

Now one can, in the $\mu \gg 1$ limit, set $\sqrt{\mu^2+\frac{1}{4}} \approx \mu$ and so obtain the following expression for $\psi(r_c)$:

$$\boxed{\psi(r_c) = 2qr_c - \frac{\mu}{k_F \sin(\alpha) r_c}.} \tag{3.51}$$

The newly found $\psi(r_c)$ is now matched with the previously found expression in Eq.(3.43). It is seen immediately that the r_c dependent terms cancel and one is left with

$$0 = 2\int_0^\infty \mathrm{e}^{-2K(r)} \left(q - \frac{\mu\Delta(r)}{k_F v_F \hbar \sin^2(\alpha) r} \right) dr, \tag{3.52}$$

once again recalling the definition $q = \frac{\epsilon}{\hbar v_F \sin(\alpha)}$. Thus, the eigenenergy ϵ can finally be found as follows

$$\boxed{\begin{aligned} &\int_0^\infty \mathrm{e}^{-2K(r)}\ \epsilon\ dr = \cancel{\hbar v_F \sin(\alpha)} \int_0^\infty \mathrm{e}^{-2K(r)} \frac{\mu\Delta(r)}{k_F \cancel{v_F \hbar} \sin^{\cancel{2}}(\alpha) r} dr \\ &\Updownarrow \\ &\epsilon = \frac{\mu}{k_F \sin(\alpha)} \cdot \frac{\int_0^\infty \frac{\Delta(r)}{r} \mathrm{e}^{-2K(r)} dr}{\int_0^\infty \mathrm{e}^{-2K(r)} dr}. \end{aligned}} \tag{3.53}$$

Finally the eigenenergies are found! These are indeed in agreement with the result of Caroli et al. as seen in their Eq.(10) [15]. But the expression Eq.(3.53) can be analysed further by looking at the fraction with the integrals.

The value of this fraction is not immediately apparent, so further investigation is in order. One can assume that Δ is linear for small r, as argued in Fig.(5), leading to the entire fraction becoming 1. For large r the exponential functions will diverge, and thus one would expect the value of the fraction to lie somewhere between 0 and 1, depending on the constants and the exact form of $\Delta(r)$.

I present a numerical example of a calculation of this fraction using Mathematica; Δ is chosen to have the form $\Delta_0 \tanh(r)$ over the range $0 \leq r < \infty$, which represent starting from the very centre of the vortex core and moving away radially in an infinitely long superconductor. The function $\tanh(r)$ indeed has an approximately linear form for small r, so one can approximate

$$\exp(-2K(r)) = \exp\left(-c_1 \int_0^r \Delta(r')dr'\right) \approx \exp\left(-c_1 \int_0^r c_2 r' dr'\right) = \exp\left(-cr^2\right), \tag{3.54}$$

where c_1 and c_2 are constants and $c = \frac{c_1 c_2}{2}$. The constant c_2 depends on the slope of the gap function $\Delta(r)$ for r close to zero.
The quantity

$$\frac{\int_\eta^\infty \frac{\tanh(r)}{r} \mathrm{e}^{-cr^2} dr}{\int_\eta^\infty \mathrm{e}^{-cr^2} dr}, \tag{3.55}$$

can now be evaluated, where the very small number η is introduced in order to avoid the divergence due to $r^{-1}|_{r=0}$. The value Δ_0 was also pulled out, as the focus is presently only on the order of the above expression. Let now $\eta \to 0$ and evaluate the above for different values of c, which is some positive value. The result is shown in Fig.(6), indeed revealing the fraction being between 0 and 1.

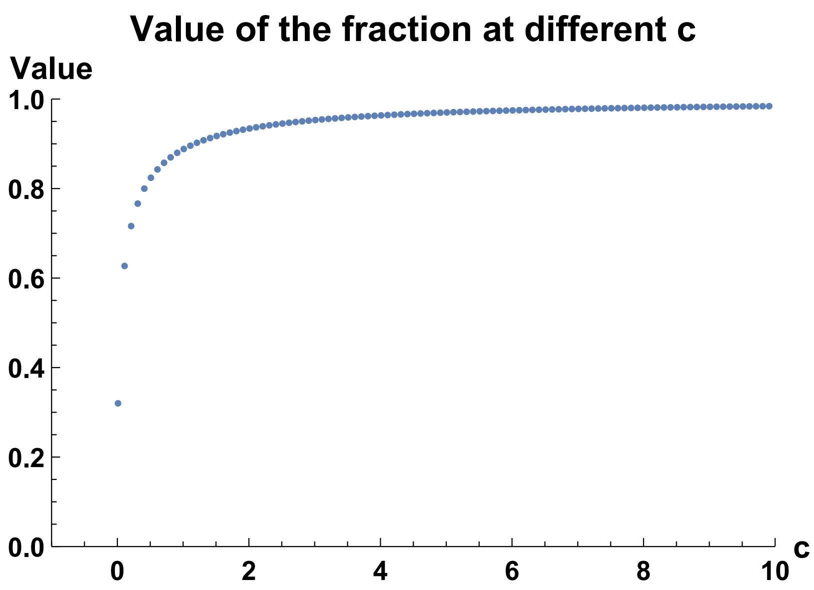

Figure 6: Eq.(3.55) is plotted with $\eta = 10^{-10}$. The fraction is between 0 and 1 and goes to zero for $c \to 0$. The constant c depends on material properties through the dependence of v_F.

Thus the fraction present in Eq.(3.53) is always between 0 and 1 and therefore does not seem to be of any great significance. Consequently one can safely get rid of this rather unsightly expression in Eq.(3.53).
One can then write $\Delta(r) = r\frac{d\Delta(r)}{dr}\Big|_{r=0}$, i.e. as approximately linear near $r = 0$ with the

slope defined as $\left.\frac{d\Delta(r)}{dr}\right|_{r=0}$. The $\frac{r}{r}$ in the upper integral of Eq.(3.53) cancel and one can pull the "slope" outside the integral, thus also cancelling the integrals at the same time:

$$\epsilon = \frac{\mu}{k_F \sin(\alpha)} \left.\frac{d\Delta(r)}{dr}\right|_{r=0}. \tag{3.56}$$

Since the radius of the vortex is approximately equal to the coherence length ξ and the value of $\Delta(r)$ in $r = \infty$ is labelled Δ_0, one may rewrite the slope as approximately equal to $\frac{\Delta_0}{\xi}$. Furthermore, assuming that $\alpha = \frac{\pi}{2}$ allows one to focus on just the order of the eigenvalues.

$$\epsilon = \frac{\mu}{k_F \sin(\alpha)} \left.\frac{d\Delta(r)}{dr}\right|_{r=0} \approx \frac{\mu}{k_F}\frac{\Delta_0}{\xi}. \tag{3.57}$$

Lastly, using $\xi \approx \frac{\hbar v_F}{\Delta_0}$ and $\hbar k_F v_F = 2E_F$, one obtains the final result

$$\boxed{\epsilon \approx \frac{\mu \Delta_0^2}{2E_F}.} \tag{3.58}$$

This is exactly as found in [15], and thus an approximate energy has been determined for the CdGM states in the vortex core. Recall that the vortex system represents a superconducting cylinder, where the direction along the length of the cylinder is mostly ignored. In Sec.(3.2.2) I attempt to find these states numerically, comparing with the experimentally found values in the article [4]. But first I must validate the numerical method. This is done by solving a very general problem analytically and testing the numerical method on this problem.

3.2 NUMERICAL APPROACH

3.2.1 *Laplace on a Unit Disk*

The well known problem of solving the Laplace operator on a unit disk is presented in this section. Just as before, I seek to describe the system and find the eigenvalues analytically. The main goal of this section is to show that the constructed numerical method in Mathematica can reproduce the eigenvalues obtained analytically, so that one can place confidence in the method. Thereafter I will apply the method to the original problem of low energy excited states in the vortex.

The Laplace eigenvalue equation on a 2-dimensional disk of radius unity is most easily handled in plane polar coordinates, (r, θ), and thus one can begin by writing

$$\nabla^2 u(r, \theta) = -\lambda\, u(r, \theta), \tag{3.59}$$

where u is the wavefunction and λ is the eigenvalue. The following is inspired by the method of [17], Sec.(11.3.1), though the procedure proceeds slightly differently.
One can find the eigenvalues using the boundary conditions of the problem; $u(1,\theta)=0$ and $u(r,\theta)=u(r,\theta+2\pi)$. These of course represent respectively the wavefunction being zero everywhere on the boundary and being phase periodic in 2π.
Using separation of variables, the solution may be written as

$$u(r,\theta) = R(r)\Theta(\theta), \tag{3.60}$$

so that $u(r,\theta)$ is a product of a function depending only on the radius, r, and another depending only on the angle, θ. The Laplacian is now written in plane polar coordinates, as found in [17] Eq.(11.23), and using this form for $u(r,\theta)$, one finds

$$\begin{aligned}
&\Theta(\theta)\frac{\partial^2 R(r)}{\partial r^2} + \frac{\Theta(\theta)}{r}\frac{\partial R(r)}{\partial r} + \frac{R(r)}{r^2}\frac{\partial^2\Theta(\theta)}{\partial\theta^2} = -\lambda R(r)\Theta(\theta)\\
&\Updownarrow\\
&\frac{1}{R(r)}\frac{\partial^2 R(r)}{\partial r^2} + \frac{1}{rR(r)}\frac{\partial R(r)}{\partial r} + \frac{1}{r^2\Theta(\theta)}\frac{\partial^2\Theta(\theta)}{\partial\theta^2} = -\lambda\\
&\Updownarrow\\
&\frac{r^2}{R(r)}\frac{\partial^2 R(r)}{\partial r^2} + \frac{r}{R(r)}\frac{\partial R(r)}{\partial r} + \lambda r^2 = -\frac{1}{\Theta(\theta)}\frac{\partial^2\Theta(\theta)}{\partial\theta^2}.
\end{aligned} \tag{3.61}$$

Having separated the variables, one may conclude that both sides of Eq.(3.61) must equal a constant, that is

$$\frac{r^2}{R(r)}\frac{\partial^2 R(r)}{\partial r^2} + \frac{r}{R(r)}\frac{\partial R(r)}{\partial r} + \lambda r^2 = n^2 \tag{3.62}$$

&

$$-\frac{1}{\Theta(\theta)}\frac{\partial^2\Theta(\theta)}{\partial\theta^2} = n^2. \tag{3.63}$$

The second order differential equation dealing with the angular part has the well known solution

$$A\cos(n\theta) + B\sin(n\theta), \tag{3.64}$$

where A and B are constants. Due to the condition of periodicity, the equation above restricts the values of n to integers only. The remaining equation can be recast on the form

$$r^2\frac{\partial^2 R(r)}{\partial r^2} + r\frac{\partial R(r)}{\partial r} + (\lambda r^2 - n^2)R(r) = 0. \tag{3.65}$$

One should now get rid of the λ in the last term, so one must rescale the variable with $\sqrt{\lambda}$ and thus introduce a new function $P(\sqrt{\lambda}r)$, so that:

$$R(r) = P(\sqrt{\lambda}r), \qquad R'(r) = \sqrt{\lambda}P'(\sqrt{\lambda}r), \qquad R''(r) = \lambda P''(\sqrt{\lambda}r). \tag{3.66}$$

Substituting this into Eq.(3.65) yields

$$\lambda r^2 P''(\sqrt{\lambda}r) + \sqrt{\lambda}rP'(\sqrt{\lambda}r) + (\lambda r^2 - n^2)P(\sqrt{\lambda}r) = 0. \tag{3.67}$$

Finally, introduce the variable $\rho = \sqrt{\lambda}\, r$, so that the equation becomes

$$\rho^2 P''(\rho) + \rho P'(\rho) + (\rho^2 - n^2)P(\rho) = 0, \tag{3.68}$$

which is exactly Bessels equation! Thus the solution will be a linear combination of Bessel functions of the first kind, $J_n(\rho)$, and the second kind, $Y_n(\rho)$:

$$P(\rho) = C \cdot J_n(\rho) + D \cdot Y_n(\rho), \tag{3.69}$$

where the integer n labels the order of the Bessel functions, and C and D are constants. Fig.(7) shows the Bessel functions of the first and second kind for the zeroth and first order. A linear combination of these constitutes the radial solution of the Laplace eigenvalue equation. This is interesting as Bessel and Hankel function were solutions to the radial part of the wavefunction in the vortex core system as well, in the limits $r < r_c$ and $r > r_c$ respectively. Thus one might expect the wavefunction of the low-lying excited state in the vortex to have an oscillatory behaviour around 0 in the radial direction, just as seen in the Fig.(7)!

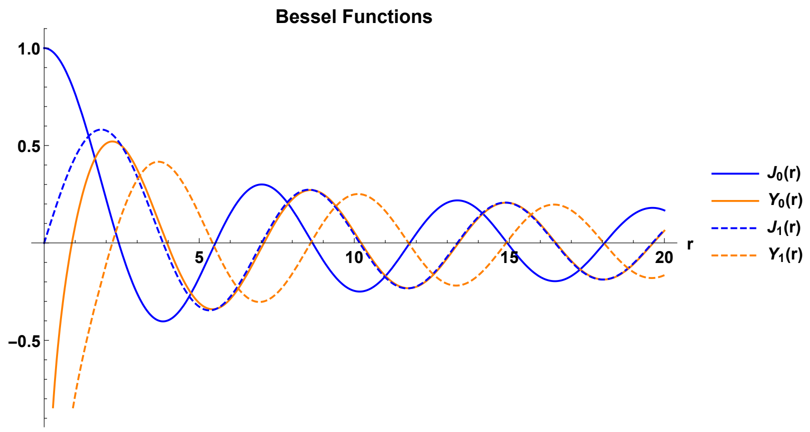

Figure 7: Bessel functions of the first and second kind of order 0 and 1. The blue lines are of the first kind while the orange represent Bessel functions of the second kind. The full lines show the order $n = 0$ while dashed lines are for order 1. The functions oscillate around 0 and are dampened as the radius increases.

Note that the Bessel functions of the second kind all blow up at $\rho = 0$, and since this point is indeed included, one must demand that $D = 0$ in Eq.(3.69). Thus the solution for the Laplace eigenvalue equation on a unit disk is

$$u(r, \theta) = [A\cos(n\theta) + B\sin(n\theta)]\left[CJ_n(\sqrt{\lambda}r)\right]. \tag{3.70}$$

One can now find the eigenvalues of the purely radial solution, $n = 0$, using the boundary condition $u(1, \theta) = 0$. Setting the constants $A = C = 1$ reduces Eq.(3.70) to

$$0 = J_0(\sqrt{\lambda} \cdot 1). \tag{3.71}$$

The eigenvalues λ are then to be found from the roots, which are given as $\sqrt{\lambda}$, of the Bessel function of the first kind with order 0. Thus one must find the roots and square these to obtain the eigenvalues.
In Fig.(8) the zeroth order Bessel function of the first kind is plotted and its roots are identified. The first few are presented in the figure.

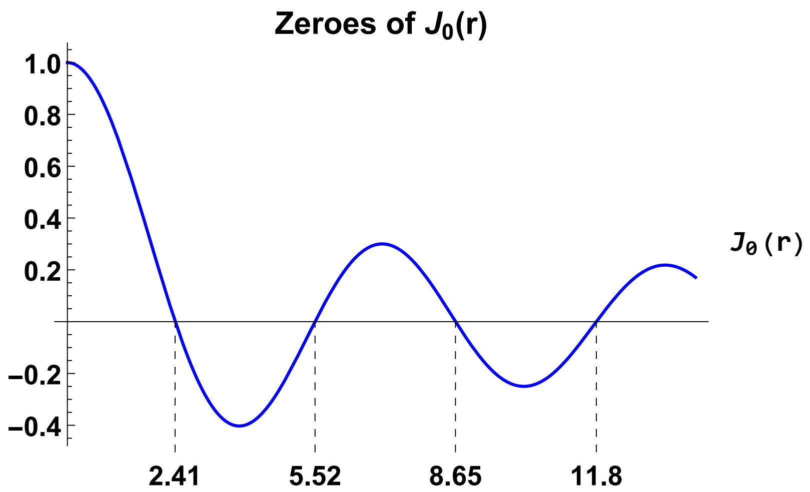

Figure 8: The roots of the zero order Bessel function of the first kind is shown. The eigenvalues are given as the square of these roots, as seen in Eq.(3.71)

The eigenvalues of this purely radial solution are then found as

$$\lambda = \{5.78319, \quad 30.4713, \quad 74.887, \quad 139.04\}. \tag{3.72}$$

Note that the values presented in Eq.(3.72) are calculated using the "BesselJZero" function in Mathematica, which of course finds the roots of a given Bessel function. Thus one has something with which one can compare a result from a numerical calculation, which follows below.

The function NDEigensystem solves, as the name suggests, (coupled) differential equations numerically, yielding both the eigenvalues and eigenfunctions. For completeness sake I present now the function as it is written in Mathematica:

$$\begin{aligned}\{\lambda, u\} = &\text{NDEigensystem}\left[\{-\text{Laplacian}\left[u\left[x,y\right],\{x,y\}\right],\right.\\ &\text{DirichletCondition}\left[u\left[x,y\right]==0,\text{True}\right]\},u\left[x,y\right],\{x,y\}\in\text{Reg}, m,\\ &\text{Method}\rightarrow\{\text{"SpatialDiscretization"}\rightarrow\{\text{"FiniteElement"},\text{"MeshOptions"}\rightarrow\\ &\left.\{\text{"MaxCellMeasure"}\rightarrow MCM\}\}\}\right],\end{aligned} \tag{3.73}$$

where m is the number of solutions found and MCM is a measure for how finely the region is discretized. The smaller this number, the more precise our solution is. In this case $MCM = 0.001$ was used, which I found to be more than sufficient. The Dirichlet condition is simply the boundary condition and "Reg" is a discretized region, which in this case is a disk of radius 1.

Note that the function is written using Cartesian coordinates, and so a transformation is necessary. For the case of the Laplacian on a unit disk this is trivial, but less so when one returns to the excited states in the vortex.

Shown in Fig.(9) is a contour plot of the eigenfunctions of the Laplace operator on a unit disk as found from the NDEigensystem method. The contour shows changes around 0, so a change in colour represents a change from positive to negative values, or oppositely. Above each contour plot is displayed the associated eigenvalue for the given eigenfunction. Note further that there are duplicates of certain energies, but the corresponding solutions are clearly the same (n is the same for solutions with same energy).

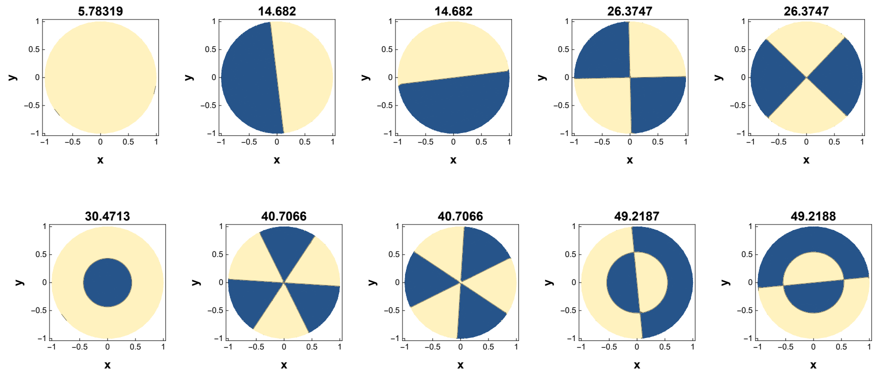

Figure 9: Contours around 0 for the lowest energy solutions for the problem of Laplace on a unit ($r = 1$) disk. The value above each plot is the eigenvalue associated with the shown eigenfunction. The increase to number of "regions" seen in a plot corresponds to an increase in n. Plots with a θ dependence are the $n \neq 0$ solutions.

First of all, one sees some familiar eigenvalues! These correspond to the plots with $n = 0$, as expected. The other eigenvalues in Fig.(9) of course represent $n \neq 0$ solutions. This is expected, as these are dependent on the angle θ and so exhibit some circulation of the eigenfunctions.

Looking only at the purely radial solutions found by NDEigensystem in Fig.(10), one finds the same eigenvalues as was found analytically!

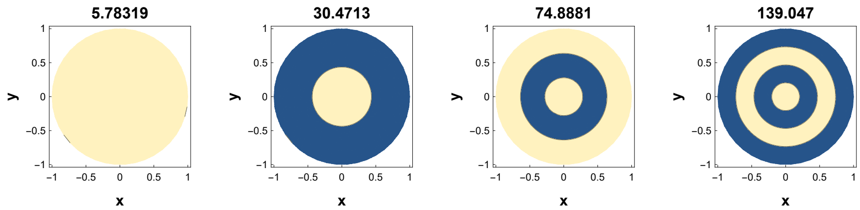

Figure 10: Purely radial solutions of the Laplace on a unit disk problem. Thus $n = 0$ for these solutions. Above each contour plot is shown the corresponding eigenvalue, and these match exactly with those found analytically. One sees an increase in the energy as the solutions increase in oscillations around 0.

The eigenvalues found by the numerical method, as seen in Fig.(10), exactly match those of the analytical procedure from Eq.(3.72), and so the numerical method is a success, at least so far.

3.2.2 *Numerical Analysis of the CdGM States*

Armed with some trust in our numerical method, one may turn to the problem of the CdGM states again. The NDEigensystem function in Mathematica should now be able to find the eigenvalues and -functions describing the low-lying excited states near the center of a vortex in a pure type-II superconductor numerically!
Thus one can now design a system of a single vortex in an infinite superconductor and attempt to find the energy of the states living in the vortex. Before looking into possible materials to house the vortex, one must first prepare the numerical method for the task at hand. This is done by rendering the BdG Hamiltonian onto a dimensionless form.
Start first all the way back to Eq.(3.1a) and Eq.(3.1b), which without the magnetic field can be written as

$$-\frac{\hbar^2}{2m}\boldsymbol{\nabla}^2 u(r) - E_F u(r) + \Delta(r)\mathrm{e}^{-i\theta} v(r) = \epsilon u(r), \tag{3.74a}$$

$$\frac{\hbar^2}{2m}\boldsymbol{\nabla}^2 v(r) + E_F v(r) + \Delta(r)\mathrm{e}^{i\theta} u(r) = \epsilon v(r), \tag{3.74b}$$

where $W(r) = \Delta(r)\mathrm{e}^{-i\cdot 1\cdot\theta}$. The above equations must further be transformed into Cartesian coordinates and subsequently made dimensionless. Using the standard transformations $r = \sqrt{x^2+y^2}$ and $\theta = \arctan\left(\frac{y}{x}\right)$, one finds:

$$-\frac{\hbar^2}{2m}\left(\frac{d^2u(x,y)}{dx^2}+\frac{d^2u(x,y)}{dy^2}\right) - E_F u(x,y) + \Delta(x,y)\mathrm{e}^{-i\arctan\left(\frac{y}{x}\right)}v(x,y) = \epsilon u(x,y), \tag{3.75a}$$

$$\frac{\hbar^2}{2m}\left(\frac{d^2v(x,y)}{dx^2}+\frac{d^2v(x,y)}{dy^2}\right) + E_F v(x,y) + \Delta(x,y)\mathrm{e}^{i\arctan\left(\frac{y}{x}\right)}u(x,y) = \epsilon v(x,y). \tag{3.75b}$$

Now one can write the above to a dimensionless form by using the substitutions $x = \frac{\alpha}{k_F}$ and $y = \frac{\beta}{k_F}$, so that $\frac{d^2u(x,y)}{dx^2} = k_F^2 \cdot \frac{d^2u(\alpha,\beta)}{d\alpha^2}$ and likewise for y. This also means that one should scale the parameters with respect to k_F in the code, which will be addressed later. For now:

$$-\frac{\hbar^2k_F^2}{2m}\left(\frac{d^2u(\alpha,\beta)}{d\alpha^2}+\frac{d^2u(\alpha,\beta)}{d\beta^2}\right) - E_F u(\alpha,\beta) + \Delta(\alpha,\beta)\mathrm{e}^{-i\arctan\left(\frac{\beta}{\alpha}\right)}v(\alpha,\beta) = \epsilon u(\alpha,\beta), \tag{3.76a}$$

$$\frac{\hbar^2k_F^2}{2m}\left(\frac{d^2v(\alpha,\beta)}{d\alpha^2}+\frac{d^2v(\alpha,\beta)}{d\beta^2}\right) + E_F v(\alpha,\beta) + \Delta(\alpha,\beta)\mathrm{e}^{i\arctan\left(\frac{\beta}{\alpha}\right)}u(\alpha,\beta) = \epsilon v(\alpha,\beta). \tag{3.76b}$$

Dividing through by $E_F = \frac{\hbar^2k_F^2}{2m}$ will leave every term dimensionless:

$$-\frac{d^2u(\alpha,\beta)}{d\alpha^2}-\frac{d^2u(\alpha,\beta)}{d\beta^2} - u(\alpha,\beta) + \frac{\Delta(\alpha,\beta)}{E_F}\mathrm{e}^{-i\arctan\left(\frac{\beta}{\alpha}\right)}v(\alpha,\beta) = \frac{\epsilon}{E_F}u(\alpha,\beta), \tag{3.77}$$

$$\frac{d^2v(\alpha,\beta)}{d\alpha^2}+\frac{d^2v(\alpha,\beta)}{d\beta^2} + v(\alpha,\beta) + \frac{\Delta(\alpha,\beta)}{E_F}\mathrm{e}^{i\arctan\left(\frac{\beta}{\alpha}\right)}u(\alpha,\beta) = \frac{\epsilon}{E_F}v(\alpha,\beta). \tag{3.78}$$

Eqs.(3.77) and (3.78) are now entirely dimensionless and one can finally find the eigenvalues, ϵ, using the NDEigensystem method! One only needs values for the energy gap and the Fermi energy.

When choosing values for Δ_0, E_F and the radius of the vortex, I found inspiration from the paper [4], in which these CdGM states are believed to have been found experimentally. The experiment involved the iron-based superconductor $FeTe_{0.55}Se_{0.45}$. First of all, the energy gap function is again chosen to be represented by a hyperbolic tangent multiplied by the gap size at $r \to \infty$, labelled Δ_0, as this nicely depicts the change in the gap from the normal region (the vortex core) to the superconducting region. Thus

$$\Delta(r) = \Delta_0 \tanh\left(\frac{\sqrt{x^2+y^2}}{3}\right)\mathrm{e}^{i\arg(x+iy)}, \tag{3.79}$$

where the number 3 determines how quickly $\Delta(r)$ reaches Δ_0, which should match the radius of the vortex, $\approx \xi$. This was decided looking at Fig(2a) of [4], where an approximate number for the radius of the vortex is set as 3 nm. One must also define the region on which the states can exist. This region will be a disk, just as in Sec.(3.2.1), with the radius R. The vortex of course extends all the way through the superconductor, but this direction does not play a big role, so it is left out. As the vortex itself is 3 nm in radius, one should choose some $R > 3$. Ideally one would want to write $R \to \infty$, so that the entire superconductor is included. This would prove computationally inefficient. Luckily, this seems not to be necessary, as $\Delta(r)$ changes only until the edge of the vortex ($R \approx \xi$) and remains constant from $r > \xi$ until infinity, meaning the most important features happen in the first 3 nm. Recall that the parameters used in the code are scaled with respect to k_F. For example, if one have $x = \frac{\alpha}{k_F}$, then one must know k_F to determine α, the size used in the code. Fortunately, from [4] one finds $k_F \approx 0.1\text{Å}^{-1}$, so that $k_F^{-1} \approx 10\text{Å} = 1\text{nm}$, meaning conversion is trivial.

Thus one can calculate the eigenenergies for different values of the radius R of the disk itself, while keeping the vortex radius constant at $\xi = 3$, and see if the energies converge. This is shown in Fig.(11), where the negative ϵ are calculated for R running from 3 nm to 14 nm. The eigenvalues themselves and how these were obtained will be discussed shortly.

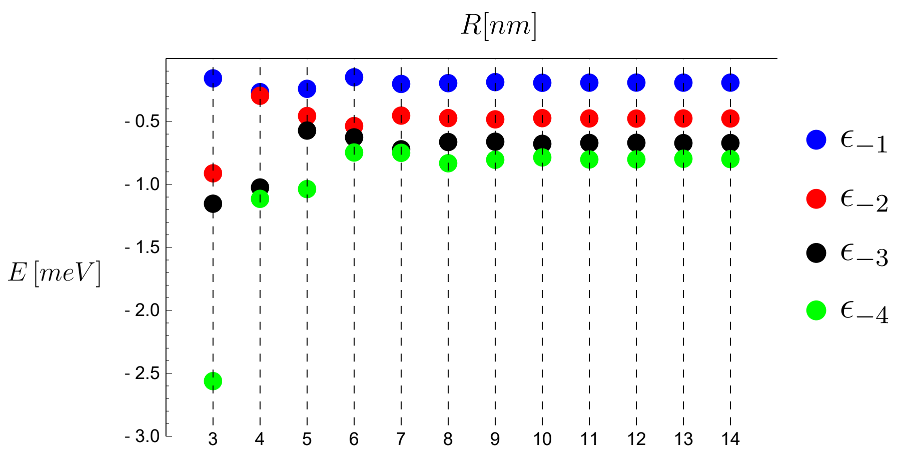

Figure 11: The first 4 negative eigenvalues are calculated for different radii, R, of the region (the disk). The radius of the vortex was set constant at 3 nm, a value obtained from [4] Fig.(2a). The subscripts of ϵ refer to the order of the energies, with higher numbers representing higher order excitation.

Notice that the eigenvalues indeed converge as the radius of the entire region is increased, and I choose $R = 10$ nm for subsequent calculations. With this, one can finally find the eigenvalues!

As mentioned before, [4] was used for inspiration for our values of gap strength and Fermi energy. They present the following ranges of values: $\Delta_0 = [1.1,\ 2.1]\,\text{meV}$ and $E_F =$

[1.3, 4.9] meV. The Fermi energy was found from the relation Eq.(3.58) using the stated range of Δ_0 and the experimentally observed eigenvalues. Using $\Delta_0 = 1.1$ meV and $E_F = 1.3$ meV in the numerical method, Fig.(12) presents the 8 eigenvalues closest to 0, with $R = 10$ nm

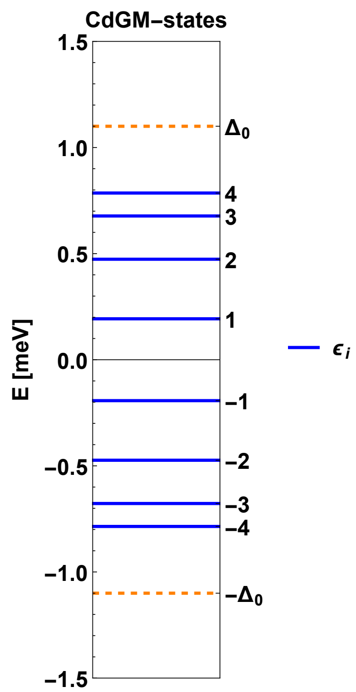

Figure 12: The energies for radius $R = 10$ are presented in units of meV. Also plotted is the gap strength, $\Delta_0 = 1.1$ meV. The energies come in pairs of $\pm\epsilon$. Several bound states are observed in the vortex. The energies seem *not* to be equidistant.

These states come in pairs of $\pm\epsilon_1 = \epsilon_{\pm 1}$, where a notation of higher numbers in the subscript to represent higher excitations was adopted. The energies are paired up due to particle-hole symmetry. Fig.(12) shows several bound states in the vortex, as also presented in [6], Fig.(4.12-left). Here the states are also shown to increase in energy with the quantum number μ, which is essentially the angular momentum. Furthermore the states close to the core are shown to be equidistant, which is something Fig.(12) does not reproduce. However, the energies do match the behaviour further away from the core, see again Fig.(4.12-left) of [6]; the spacing becomes smaller until the energies seem to join the continuum. The 10 lowest positive eigenvalues are shown in Fig.(13) and one sees that they indeed approach Δ_0!

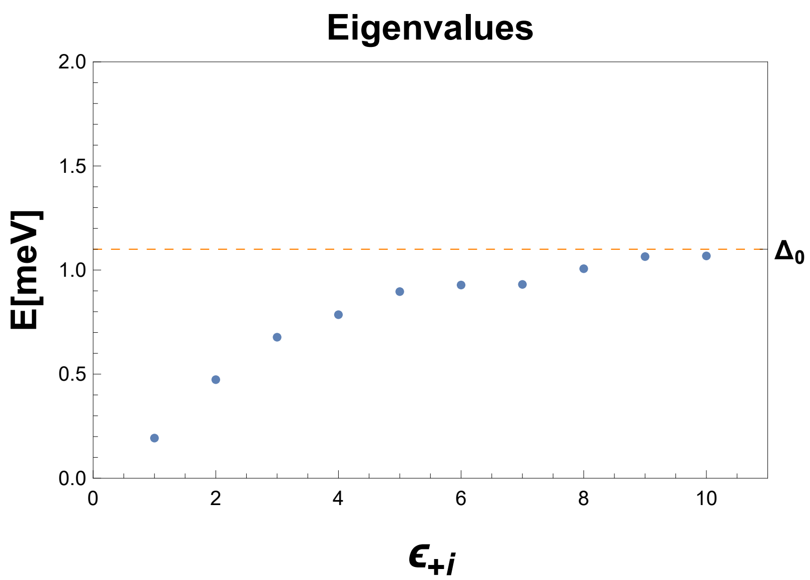

Figure 13: The positive eigenenergies of the first 10 CdGM states, calculated for $R = 10$ nm. They approach Δ_0 for higher excitations, as predicted in [6], Fig.(4.12-left). The numbers on the x-axis represent the index i, i.e. the first point corresponds to ϵ_{+1}, the next to ϵ_{+2} and so on. The higher order states seem to join the continuum.

Take now a closer look into the actual values of these eigenvalues. Specifically, the very first eigenvalues obtained are

$$\epsilon_{num.} = \pm 0.19 \text{ meV}, \tag{3.80}$$

which is most easily seen in Fig.(13). The analytical result yields

$$\epsilon_{an} = 0.45\text{meV}. \tag{3.81}$$

To be perfectly clear; the analytical result above is from the article [4], found experimentally. From the values $\Delta_0 = 1.1$ meV, $\epsilon = 0.45$ meV and then using Eq.(3.58) they find $E_F = 1.34$ meV. Using these values for Δ_0 and E_F I obtained the numerical result presented in Eq.(3.80). Thus the numerical method can successfully find the eigenenergies at least to the correct order.

The NDEigensystem method also finds the eigenfunctions, which to be discussed presently. Recalling the Eqs.(3.17) and (3.18) one expects the "radial behaviour" to look like Bessel functions. Having plotted plenty of these in Sec.(3.2.1), one should be able to recognize the form! Fig.(14) show the eigenfunctions for the lowest positive eigenvalue of the vortex states. Recall that the wavefunction is a superposition of u and v.

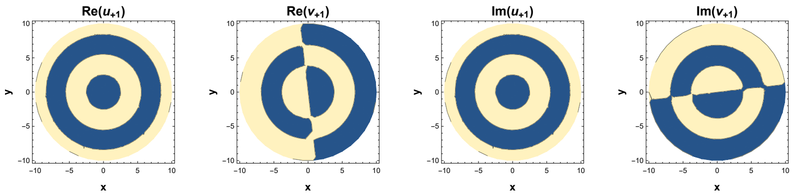

Figure 14: Contour plots of the eigenfunctions of the lowest positive eigenvalue. The real part and the imaginary part are plotted for both the electron-like part and the hole-like part of the eigenfunction. They are seen to behave like Bessel functions in the radial direction, as expected. They have some angular momentum as well, from the quantum number μ.

One indeed sees Bessel function like behaviour in the radial direction, in the form of an oscillatory behaviour around 0. As a sanity check, Fig.(15) shows an example of an actual wavefunction given by $\Psi(x, y) = \begin{pmatrix} u(x, y) \\ v(x, y) \end{pmatrix}$, where the probability plotted is found as $|\Psi(x, y)|^2$, with eigenfunctions corresponding to the lowest positive eigenvalue. Note that integrating the squared modulus from 0 to infinity equals 1 and thus it is indeed normalized. The figure shows that this state is localized around the center of the vortex and does not exhibit any significant azimuthal dependence.

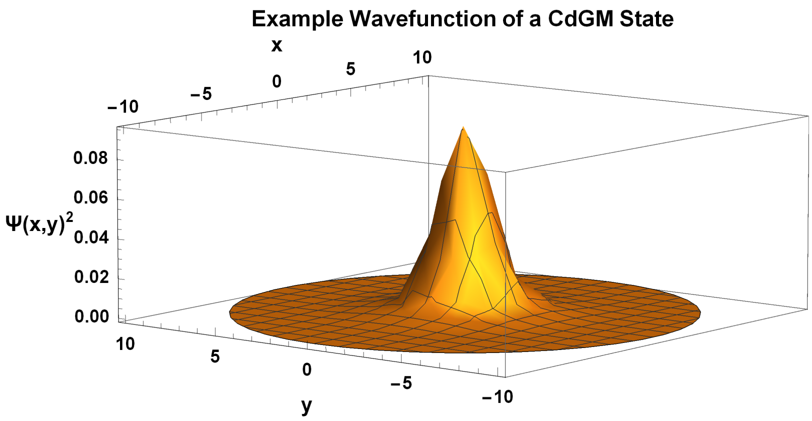

Figure 15: Plot of the wavefunction of the lowest positive energy state. The wavefunction squared is presented in the plot as $|\Psi(x, y)|^2$. Integration of $|\Psi(x, y)|^2$ from 0 to infinity reveals that the wavefunction is indeed normalized.

One can now plot contours around 0 for the other energy excitations in the vortex. Looking exclusively at the positive eigenvalues, Fig.(16) shows the real part of their associated eigenfunctions.

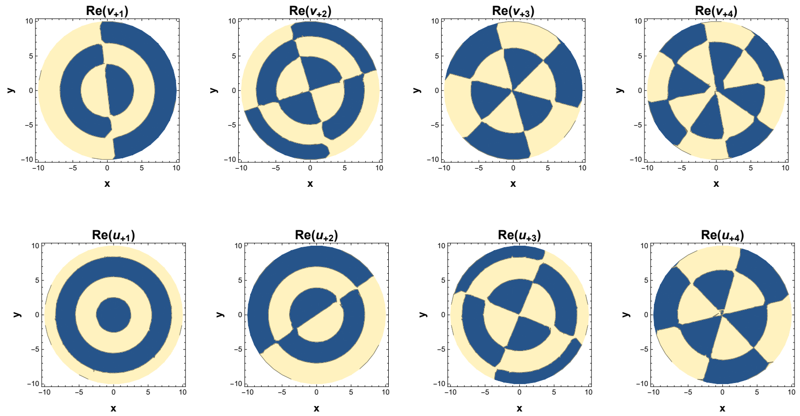

Figure 16: Eigenfunctions of the energy excitations. Contour plots of the real part of u and v for the lowest 4 positive eigenvalues. The v_{+1} and u_{+1} are also presented in Fig.(14). An increase to the energy is associated with a higher angular momentum, labelled with the quantum number μ. Note that $Re(v_{+1})$ starts at $\mu = 1$ while $Re(u_{+1})$ has $\mu = 0$. For the negative eigenvalues (v_{-1}, v_{-2} and so on) this is reversed, so that $Re(v_{-1})$ would show $\mu = 0$ and $Re(u_{-1})$ would have $\mu = 1$.

The eigenfunctions are seen to increase in energy with the azimuthal quantum number μ, representing angular momentum. Where the positive eigenvalues results in the hole part having $\mu = 1$ for the lowest energy and the electron part having $u = 0$ for the lowest energy, the opposite holds for the negative eigenvalues.

The supercurrents are shown as well, for some of the first 8 negative eigenvalues in Fig.(17). These are calculated using

$$\mathbf{j} \propto \mathrm{Im}\left[\Psi^* \boldsymbol{\nabla} \Psi\right], \tag{3.82}$$

where one should only use the eigenfunctions related to negative eigenvalues, as these represent the occupied states and thus the ones contributing to the current. One indeed sees currents circulating the vortex core. The currents calculated for each state should, when summed together, converge to a specific direction around the core, either clockwise or anti-clockwise.

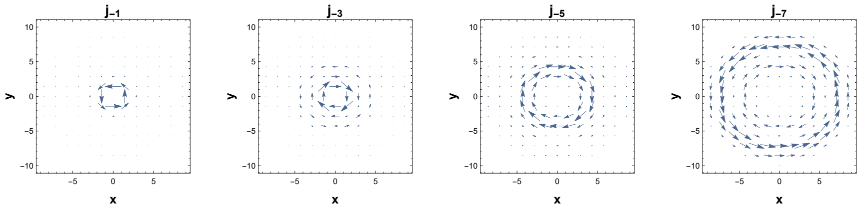

Figure 17: Supercurrents for the first, third, fifth and seventh eigenfunction corresponding to a negative energy. These eigenfunctions are the ones contributing to the supercurrent, as they denote occupied states in the vortex. The summation of the supercurrents should converge when including every single state, which reflects the actual current seen in the physical system.

Note also that the supercurrents reduce to zero if one removes the phase factor, as expected. This corresponds to having set $n = 0$ in $W(r)$, i.e. no winding is present.

As a final note, I discuss the Fermi energy obtained in the experiment [4]. This Fermi energy is very small, and so one would expect the electron concentration to be small as well. This is investigated and compared with other often used superconductors, from Fig.(6) of [18], reprinted in Fig.(18). Here the Fermi temperature and the critical temperature for several superconductors is shown, and an estimate for the superconductor examined in this section, $FeTe_{0.55}Se_{0.45}$, is included in the form of a black vortex.

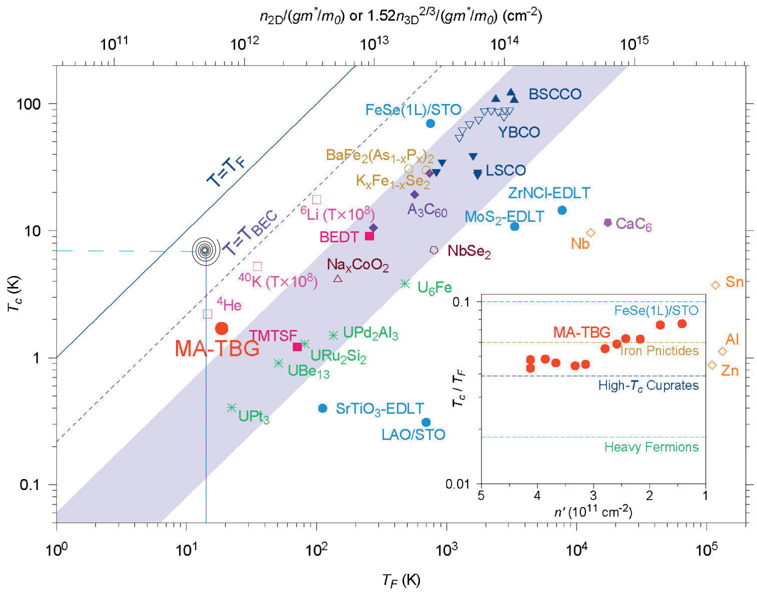

Figure 18: Figure taken directly from [18], Fig.(6). Shown above are the Fermi temperature, critical temperature and carrier density of many superconducting compounds. Having seen a rather low Fermi energy for the iron based superconductor $FeTe_{0.55}Se_{0.45}$, I investigated the density of electrons by adding it to the figure. It was found that $T_F = 15.1K$ and $T_C \approx 7.24K$, placing the superconductor in question near the $T = T_F$ line, labelled by a black vortex.

The Fermi temperature was found as $T_F = \frac{E_F}{k_B} = \frac{0.0013\ eV}{8.617{\cdot}10^{-5}\ eV{\cdot}K^{-1}} = 15.1K$ and the critical temperature as $T_C \approx \frac{\Delta_0}{1.764 k_B} = \frac{0.0011\ eV}{1.764{\cdot}8.617{\cdot}10^{-5}\ eV{\cdot}K^{-1}} \approx 7.24K$.
Thus the iron-based superconductor used here was placed close to the $T = T_F$ line, indeed revealing a rather low density. As expected, the Fermi temperature is smaller compared to most of the presented compounds, while the critical temperature is around average, if not a bit below average.

This concludes the analysis of the CdGM states in a vortex for now. I have found the states analytically and subsequently numerically in a specific case inspired by the experiment [4], using the iron-based superconductor $FeTe_{0.55}Se_{0.45}$. The energies found from the numerical method were comparable with the analytical result Eq.(3.58) and the experimental result. In Sec.(4) I investigate how the magnetic field, which was neglected throughout this section, could affect the energy of the vortex states. Later, in Sec.(5), I investigate a more phenomenological claim about these CdGM states, namely that they in [6] Fig.(4.11) were described as Andreev states. This claim and the concept of Andreev reflection will be studied.

But first, the numerical method is applied a system with a region different from a disk. Specifically, the model is applied to a hollow hexagonal structure as used in the article [3] and the energy spectrum of whatever states are present in such a system is found.

3.2.3 *Hexagonal Superconductor*

The numerical method can now be applied to a cylindrical superconductor in the presence of a magnetic field pointing along the length of the cylinder. However, the cylindrical structure is replaced with a hexagonal structure, as experiments such as [3] use hexagonal wires. It is assumed the two regions are approximately similar.

Ideally I would analyze the hexagonal wire presented in [3], consisting of an indium arsenide core with an outer aluminium shell that is used to proximitize the InAs. Unfortunately this was not feasible due to computational constraints arising from the material properties of aluminium. Using the Fermi wavevector for aluminium, $k_F = 17.5$ nm^{-1}, the dimensionless parameters used in the numerical method would have to be far too large for the computer to handle. Instead, to showcase the concept, I investigate a hexagonal wire of the material used in the prior section, $FeTe_{0.55}Se_{0.45}$. For this wire, the center is not included. This is due to the fact that the proximity effect of the superconducting aluminium does not reach the core, and so the system reduces to a hexagonal shell, as seen in Fig.(19). The inner radius is set to $R_1 = 10$ nm while the outer radius is $R_2 = 14$ nm. The Fermi energy and the energy gap is kept at the same values as the prior section. However, the gap profile is set to be constant over the entire region.

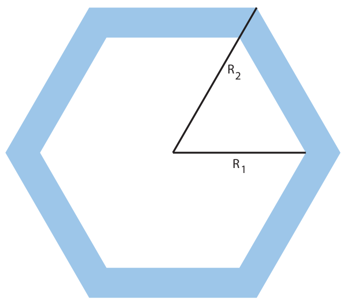

Figure 19: A hexagonal shell, simulating the superconducting wire presented in [3]. The inner radius is $R_1 = 10$ nm and the outer $R_2 = 14$ nm. The small system size is a consequence of the limitations of the numerical method and the computational power available. The energy gap is constant at Δ_0 throughout the region.

The 8 lowest positive energies of this system is given in Fig.(20), which shows energies on the order of 1 meV and with some energies above the gap. Thus not all the energies found are sub-gap states. In Fig.(21), the eigenfunctions corresponding to the first 4 positive eigenvalues are shown, and the presence of angular momentum is noted again. Contrary to the CdGM states, the higher energy states does not correspond to higher angular momentum. Furthermore, the v part of the wavefunction again exhibit higher angular momentum compared to that of the u part, exactly as was seen for the CdGM states. The opposite is true for eigenfunctions corresponding to the negative eigenvalues.

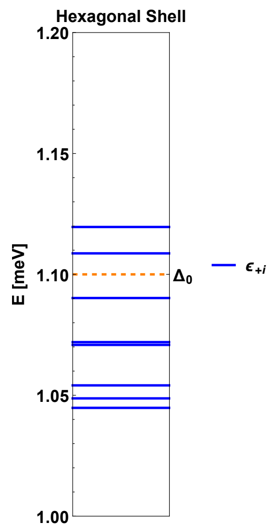

Figure 20: Energies of the 8 lowest positive eigenvalues for the hexagonal shell. The energies are of the order 1 meV, with some being above the energy gap.

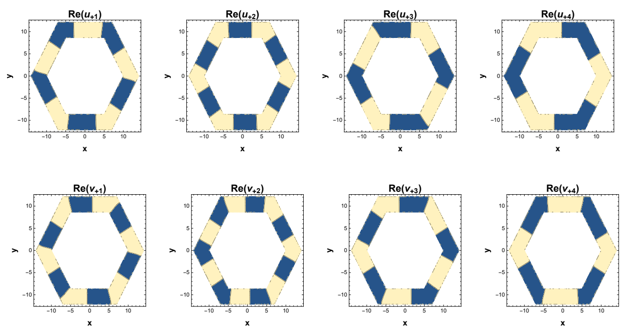

Figure 21: Eigenfunctions corresponding to the 4 lowest positive eigenvalues. As was the case for the CdGM states, the v part exhibits a higher angular momentum μ when compared with the corresponding u part. For the negative eigenvalues, this is reversed.

Finally, the supercurrent was determined once again and the first, third, fifth and seventh eigenfunction corresponding to negative eigenvalues is presented in Fig.(22). The number n present in the phase of the order parameter now plays an important role, as the winding of the system can change. The supercurrents behave very much like expected, exhibiting winding around the hexagonal shell. Once again, these current die out if the phase on the order parameter is removed, i.e $n = 0$.

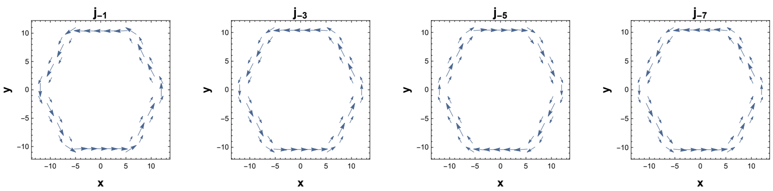

Figure 22: Supercurrents in the hexagonal shell. The first, third, fifth and seventh current is presented here. Again it is assumed these will sum to either a clockwise or anti-clockwise current, if all states were taken into account.

Noticeably, the supercurrent is expected to change direction if the winding is set as $n = -1$ instead of the usual $n = 1$. The resulting plot is shown in the Appendix (A.5), and the supercurrent is indeed observed to have changed direction, compared to Fig.(22).
The numerical method has now been applied to a hexagonal wire in the presence of a magnetic field. The material properties of $FeTe_{0.55}Se_{0.45}$ was used for easier computation and a 4 nm thick hexagonal hollow wire was investigated. The energies and eigenfunctions were shown, along with the supercurrents associated with some of the eigenfunctions corresponding to negative eigenvalues. Returning to the bound vortex states of Caroli et al., the inclusion of the magnetic field is studied next.

4 MAGNETIC FIELD EFFECTS

4.1 MAGNETIC FIELD EFFECTS

As a final examination of the energies of the CdGM states, one may take into consideration the effects of the magnetic field, which was neglected in [15]. The eigenvalues are determined analytically, followed by a comparison with the numerical work. This section will be based on the work of E. B. Hansen [16].

One can include magnetic field effects in the model by introducing the vector potential $\mathbf{A} = \frac{1}{2}B_0\left(-y, x, 0\right)$, where B_0 represents the magnetic field strength. This vector potential corresponds to a magnetic field pointing along the longitudinal direction, i.e. along the length of the cylinder. Converting this vector potential from Cartesian to cylindrical coordinates yields

$$\begin{aligned} A &= \frac{1}{2}B_0(-y\hat{x} + x\hat{y} + 0\hat{z}) \\ &= \frac{1}{2}B_0\left(-r\sin(\theta)\left[\cos(\theta)\hat{r} - \sin(\theta)\hat{\theta}\right] + r\cos(\theta)\left[\sin(\theta)\hat{r} + \cos(\theta)\hat{\theta}\right]\right) \\ &= \frac{1}{2}B_0 r\hat{\theta}. \end{aligned} \tag{4.1}$$

Note the vector potential only has a θ component, again corresponding to a magnetic field along the z-direction.

The Bogoliubov-de-Gennes equations, which take the form

$$-\frac{\hbar^2}{2m}\left(\boldsymbol{\nabla} - \frac{ie}{\hbar}\mathbf{A}\right)^2 u(r) - E_F u(r) + W(r)v(r) = \epsilon u(r), \tag{4.2a}$$

$$\frac{\hbar^2}{2m}\left(\boldsymbol{\nabla} + \frac{ie}{\hbar}\mathbf{A}\right)^2 v(r) + E_F v(r) + W^*(r)u(r) = \epsilon v(r), \tag{4.2b}$$

are now solved. Recall that the θ and z dependence in $u,\ v$ was suppressed for convenience. One can show explicitly how a new eigenvalue equation is obtained from Eq.(4.2a) when $\mathbf{A}$ is included. The first task is to determine $\left(\boldsymbol{\nabla} - \frac{ie}{\hbar}\mathbf{A}\right)^2 u(r)$, where the radial dependence is now suppressed as well. The squared term can be written out as

$$\begin{aligned} &\left(\boldsymbol{\nabla} - \frac{ie}{\hbar}\mathbf{A}\right) \cdot \left(\boldsymbol{\nabla} - \frac{ie}{\hbar}\mathbf{A}\right) u, \\ &\Updownarrow \\ &\nabla^2 u - \frac{ie}{\hbar}(\boldsymbol{\nabla}\cdot\mathbf{A})u - 2\frac{ie}{\hbar}(\mathbf{A}\cdot\boldsymbol{\nabla}u) - \frac{e^2}{\hbar^2}\left(\mathbf{A}\cdot\mathbf{A}\right)u. \end{aligned} \tag{4.3}$$

Show now that the divergence of $\mathbf{A}$ is zero, which is also evident from the form of the vector potential:

$$
\begin{aligned}
(\boldsymbol{\nabla} \cdot \mathbf{A})\, u &= \left(\frac{1}{r} \frac{\partial (r A_r)}{\partial r} + \frac{1}{r} \frac{\partial (A_\theta)}{\partial \theta} + \frac{\partial (A_z)}{\partial z} \right) u \\
&= \frac{1}{r} \frac{\partial}{\partial \theta} \left(\frac{1}{2} B_0 r \right) u = 0,
\end{aligned} \tag{4.4}
$$

where $\boldsymbol{\nabla}$ has been written in cylindrical coordinates. Thus the second term of Eq.(4.3) drops out. Continue with the first term by writing out the Laplacian in cylindrical coordinates:

$$
\nabla^2 u = \frac{\partial^2 u}{\partial r^2} + \frac{1}{r} \frac{\partial u}{\partial r} + \frac{1}{r^2} \frac{\partial^2 u}{\partial \theta^2} + \frac{\partial^2 u}{\partial z^2}. \tag{4.5}
$$

The last term of Eq.(4.3) is:

$$
\frac{e^2}{\hbar^2} (\mathbf{A} \cdot \mathbf{A})\, u = \left(\frac{e B_0 r}{2\hbar} \right)^2 u. \tag{4.6}
$$

Turning to the only remaining term of Eq.(4.3) one simply gets

$$
\begin{aligned}
\mathbf{A} \cdot (\boldsymbol{\nabla} u) &= \mathbf{A} \cdot \left(\frac{\partial u}{\partial r} \hat{r} + \frac{1}{r} \frac{\partial u}{\partial \theta} \hat{\theta} + \frac{\partial u}{\partial z} \hat{z} \right), \\
&= \frac{1}{2} B_0 r \hat{\theta} \left(\frac{1}{r} \frac{\partial u}{\partial \theta} \hat{\theta} \right), \\
&= \frac{1}{2} B_0 \frac{\partial u}{\partial \theta}.
\end{aligned} \tag{4.7}
$$

Thus the result of Eq.(4.3) becomes

$$
\frac{\partial^2 u}{\partial r^2} + \frac{1}{r} \frac{\partial u}{\partial r} + \frac{1}{r^2} \frac{\partial^2 u}{\partial \theta^2} + \frac{\partial^2 u}{\partial z^2} - 2 \frac{ie}{\hbar} \frac{1}{2} B_0 \frac{\partial u}{\partial \theta} - \left(\frac{e B_0 r}{2\hbar} \right)^2 u. \tag{4.8}
$$

The rest of the calculations follow closely those of Sec.(3.1), so the explanations will be brief. Writing again the definitions of u and v:

$$
\begin{aligned}
u &= e^{i k_F \cos(\alpha) z} e^{i\left(\mu - \frac{1}{2}\right)\theta} f_+(r), \\
v &= e^{i k_F \cos(\alpha) z} e^{i\left(\mu + \frac{1}{2}\right)\theta} f_-(r).
\end{aligned} \tag{4.9}
$$

Recall that one wants to obtain an expression for the eigenvalue equation with the applied magnetic field included. This is shown explicitly for the electron part only.

Let the derivative act on u, divide out the exponential functions and write out $W(r) = \Delta(r)\mathrm{e}^{-i\theta}$. Plugging the result back into the Bogoliubov Eq.(4.2a) yields:

$$-\frac{\hbar^2}{2m}\left[\frac{\partial^2 f_+}{\partial r^2} + \frac{1}{r}\frac{\partial f_+}{\partial r} - \frac{1}{r^2}\left(\mu - \frac{1}{2}\right)^2 f_+ - k_F^2\cos^2(\alpha) f_+ - \left(\frac{eB_0 r}{2\hbar}\right)^2 f_+ \right.$$
$$\left. + \frac{eB_0}{\hbar}\left(\mu - \frac{1}{2}\right) f_+\right] - E_F f_+ + \Delta f_- = \epsilon f_+, \tag{4.10}$$

where the radial dependence of $f_\pm$ and Δ has been suppressed. As in Sec.(3.1), the $e^{i\mu\theta}$ terms cancel, while the $e^{\pm i\frac{1}{2}\theta}$ terms combine to cancel the phase factor in W. One can again rewrite $-k_F^2\cos^2(\alpha) + \frac{2m}{\hbar^2}E_F = k_F^2\sin^2(\alpha)$. Split now the last term in the square bracket and pull these outside the parenthesis:

$$-\frac{\hbar^2}{2m}\left[\frac{\partial^2 f_+}{\partial r^2} + \frac{1}{r}\frac{\partial f_+}{\partial r} - \frac{1}{r^2}\left(\mu - \frac{1}{2}\right)^2 f_+ + k_F^2\sin^2(\alpha) f_+ - \left(\frac{eB_0 r}{2\hbar}\right)^2 f_+ \right.$$
$$\left. + \frac{eB_0}{\hbar}\mu f_+ - \frac{eB_0}{2\hbar} f_+\right] + \Delta f_- = \epsilon f_+$$
$$\Updownarrow$$
$$-\frac{\hbar^2}{2m}\left[\frac{\partial^2 f_+}{\partial r^2} + \frac{1}{r}\frac{\partial f_+}{\partial r} - \frac{1}{r^2}\left(\mu - \frac{1}{2}\right)^2 f_+ + k_F^2\sin^2(\alpha) f_+ - \left(\frac{eB_0 r}{2\hbar}\right)^2 f_+\right]$$
$$-\frac{\hbar^2}{2m}\mu\frac{eB_0}{\hbar} f_+ + \frac{\hbar^2}{2m}\frac{eB_0}{2\hbar} f_+ + \Delta f_- = \epsilon f_+. \tag{4.11}$$

Finally one can use the definition $\omega_L = -\frac{eB_0}{2m}$ from [16], thus obtaining the first eigenvalue equation for the vortex system with a non-zero magnetic field:

$$-\frac{\hbar^2}{2m}\left[\frac{\partial^2 f_+}{\partial r^2} + \frac{1}{r}\frac{\partial f_+}{\partial r} - \frac{1}{r^2}\left(\mu - \frac{1}{2}\right)^2 f_+ + k_F^2\sin^2(\alpha) f_+ - \left(\frac{eB_0 r}{2\hbar}\right)^2 f_+\right]$$
$$+ \mu\hbar\omega_L f_+ - \frac{1}{2}\hbar\omega_L f_+ + \Delta f_- = \epsilon f_+. \tag{4.12}$$

This can be rewritten to have the same structure as the regular case by introducing the notation:

$$-\frac{\hbar^2}{2m}\left[\frac{\partial^2 f_+}{\partial r^2} + \frac{1}{r}\frac{\partial f_+}{\partial r} - \frac{1}{r^2}\left(\mu - \frac{1}{2}\right)^2 f_+ + \Omega f_+ - \left(\frac{eB_0 r}{2\hbar}\right)^2 f_+\right]$$
$$+ \Delta f_- = \epsilon' f_+, \tag{4.13}$$

where $\Omega = k_F^2\sin^2(\alpha) + \frac{2m}{\hbar^2}\frac{1}{2}\hbar\omega_L$ and $\epsilon' = \epsilon - \mu\hbar\omega_L$, as also presented in [16]. Neglecting the term with B_0 to the second power is allowed, as this is small compared to $\hbar\omega_L$ in the core region [16]. Furthermore, if one assumes $\Omega \approx k_F^2 \sin^2(\alpha)$, i.e. that $\frac{2m}{\hbar^2}\frac{1}{2}\hbar\omega_L$ is small as well, then Eq.(4.13) reduces to the same form obtained in Sec.(3.1)! Specifically, Eq.(4.13) matches the form of the electronic part of Eq.(3.8). Thus the same procedure performed in Sec.(3.1) can be employed to obtain the eigenvalue ϵ'.

$$\epsilon' = \frac{\mu}{k_F \sin(\alpha)} \frac{d\Delta(r)}{dr}\bigg|_{r=0}. \tag{4.14}$$

The actual eigenenergies are found as $\epsilon = \epsilon' + \mu\hbar\omega_L$

$$\boxed{\epsilon = \frac{\mu}{k_F \sin(\alpha)} \frac{d\Delta(r)}{dr}\bigg|_{r=0} + \mu\hbar\omega_L. \tag{4.15}}$$

Thus the inclusion of the magnetic field leads to an increase in energy of $\mu\hbar\omega_L$, which depends on the magnetic field strength B_0. For positive energies (positive μ) the energy will increase, while for negative energies (negative μ) the energy should decrease further.
This also leads to an increased spacing between each energy, which in turn results in a lower density of states, as fewer states exist within the vortex. A caveat; I ignore the interaction between the magnetic field and the magnetic moment of the particles, which [16] states simply introduces a Zeeman splitting of the energies.
Returning to the numerical method, one can confirm the analytical result obtained in Eq.(4.15).

4.2 NUMERICAL APPROACH

The magnetic effects is now incorporated in the numerical work and one can investigate whether the energy spacing increases, as [16] and Eq.(4.15) predict.
The dimensionless equations with the addition of the magnetic field become

$$\begin{aligned}
&-\frac{d^2u(x,y)}{dx^2} - \frac{d^2u(x,y)}{dy^2} - i\frac{\hbar\omega_L}{E_F}\left(x\frac{du(x,y)}{dy} - y\frac{du(x,y)}{dx}\right) + \frac{m^2}{\hbar^2 k_F^4}\omega_L^2\left(x^2+y^2\right)u(x,y) \\
&-u(x,y) + \frac{\Delta(x,y)}{E_F}\mathrm{e}^{-in\arctan\left(\frac{y}{x}\right)}v(x,y) = \frac{\epsilon}{E_F}u(x,y), \qquad (4.16a)\\
&\frac{d^2v(x,y)}{dx^2} + \frac{d^2v(x,y)}{dy^2} - i\frac{\hbar\omega_L}{E_F}\left(x\frac{dv(x,y)}{dy} - y\frac{dv(x,y)}{dx}\right) - \frac{m^2}{\hbar^2 k_F^4}\omega_L^2\left(x^2+y^2\right)v(x,y) \\
&+v(x,y) + \frac{\Delta(x,y)}{E_F}\mathrm{e}^{in\arctan\left(\frac{y}{x}\right)}u(x,y) = \frac{\epsilon}{E_F}v(x,y), \qquad (4.16b)
\end{aligned}$$

once again written in Cartesian coordinates for the sake of the numerical method. Here x and y are dimensionless parameters, quite like in Eqs.(3.77 & 3.78), but where α and β were renamed back to x and y for notational clarity. Since $[\omega_L] = s^{-1}$, the third term is clearly dimensionless. The constant in front of the fourth term, however, warrants a closer inspection:

$$\left[\frac{m^2}{\hbar^2 k_F^4}\omega_L^2\right] = \frac{kg^2}{J^2 s^2 m^{-4}} s^{-2} = \frac{kg^2}{\frac{kg^2 m^4}{s^4} s^4 m^{-4}} = \frac{kg^2}{kg^2} = 1. \tag{4.17}$$

Thus Eqs.(4.16a) and (4.16b) are indeed dimensionless.
Now one can find the energy ϵ from the numerical method, exactly like in Sec.(3.2.2). The same values for the gap and the Fermi Energy as before are used, which came from the article [4]. Thus $\Delta_0 = 1.1$ meV and $E_F = 1.3$ meV. Furthermore, the radius for the vortex, the radius for the disk and other parameters of the model were kept the same. Inspired by an example given in [16], one may set $B_0 = 0.2$ T. Now, expecting ω_L to be positive, since it is a frequency, one must assume the electron charge is given by $e = -1.60 \cdot 10^{-19}$ C. Inserting this, along with the electron mass, yields

$$\hbar\omega_L \approx 1.16 \cdot 10^{-5}\text{eV} \tag{4.18}$$

This is in accordance with the analytical result in Eq.(4.15), so that the energy will increase for positive μ and decrease for negative μ. Like in [16] the term with ω_L to the second power is neglected, as this is small. The NDEigensystem method is used once more and the results are plotted in Fig.(23) along with the eigenvalues obtained in Sec.(3.2.2), where the magnetic field was neglected.

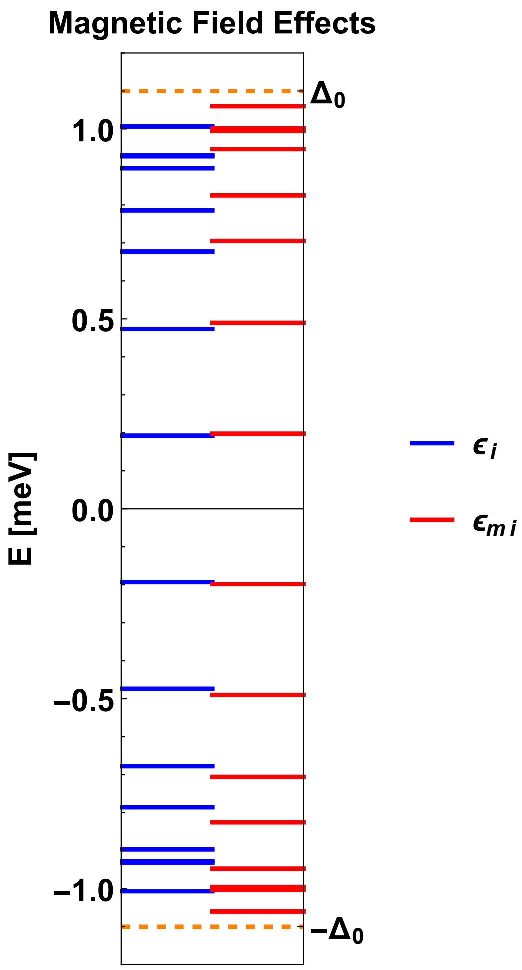

Figure 23: The 16 first eigenenergies (i ranges from -8 to $+8$) for the states in the vortex core system in meV in the case of neglecting the magnetic field (blue) and including it (red). The magnetic field is taken to be $B_0 = 0.2$ T following an example in [16]. The energy spacing is observed to increase, which was expected from Eq.(4.15), though only up until the states seem to join the continuum, as was the case in Sec.(3.2.2).

Fig.(23) presents the eigenvalues both with the magnetic field effects neglected (blue) and included (red). As expected from Eq.(4.15), one notes an increase in the energy spacing of the states when the magnetic field effects are included, labelled $\epsilon_{m\ i}$, compared to those of the original case, labelled ϵ_i. The energies of the low energy vortex states in a type-II superconductor have now been thoroughly analysed. The eigenenergies were found analytically and numerically, both with the magnetic field and without it. Turning to a more phenomenological study of the nature of CdGM states, the next section presents a suggestion on *how* these states might be bound in the vortex.

5 ANDREEV REFLECTION

Taking a closer look at the Caroli-de Gennes-Matricon (CdGM) states themselves, these were described as "Andreev states" in the notes by V.B. Eltsov [6], Fig.(4.11). Thus, in order to understand the more physical picture of what CdGM states actually are, one must understand Andreev states. This sparked my interest for Andreev reflections and will be the topic for the current section. Furthermore, one can imagine a cylinder with a normal core and a superconducting outer shell; another system which can exhibit Andreev reflections. This phenomenon is therefore an important one to understand.
The phenomenon was first discovered by A. F. Andreev in 1964 [19] and has been of great importance ever since. Before describing the nature of these Andreev reflections (AR) however, one must first describe the system in which they can occur. This section will follow the work of Blonder, Tinkham and Klapwijk [5], in which they study these ARs in a 1-dimensional system, which I will further extend to a 2-dimensional system. The system setup is as follows:

Consider a plane interface between 2 semi infinite regions; a superconductor (SC) and a normal conductor (N). Let the z-axis be normal to the interface, and define the regions as N for $z < 0$ and SC for $z > 0$, with the interface itself situated at $z = 0$. This system is shown in Fig.(24), along with the superconducting gap function, which for this case is set to be the simple Heaviside-theta function $\Delta(z) = \Delta_0\Theta(z)$. In making this assumption one essentially argues that the gap rises to its full value on a scale shorter than the coherence length ξ of the superconductor, i.e a particle will see the gap as immediately having risen to its full strength, Δ_0. Simultaneously, a possible phase on the gap function is neglected as well.

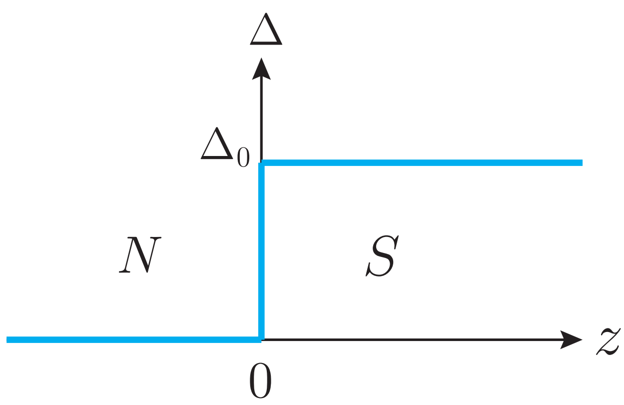

Figure 24: Sketch of the system. A normal metal is connected to a superconductor. It is assumed that the gap rises to its full strength Δ_0 immediately in the superconductor and remains constant throughout this region.

One may then investigate particles hitting the interface, coming from the normal metal towards the superconductor. Where [5] investigates particles hitting the interface perfectly perpendicular, an angle of incidence θ is introduced here. This angle is with respect to the direction of propagation, z, so that $\theta = 0$ corresponds to the particle moving perpendicular to the interface.

The goal is to find the probability for a particle to undergo Andreev reflection as a function of first this angle of incidence, θ and later as a function of the energy, ϵ, of the incident particle.

Often a potential barrier is introduced on the boundary as well, which will represent impurities and other similar effects situated on the interface between the two regions. This potential will be described with a delta function: $H(z) = H\delta(z)$, where H represents the strength of the barrier.

Andreev reflection itself is a process in which a particle hits an NS-interface and is reflected as the corresponding antiparticle with a different sign on all components of the velocity compared to the incident particle, as explained in for example the article [20] by R. Hoonsawat & I. M. Tang. The electron hitting the interface (from the normal region) will form a Cooper-pair in the superconductor by connecting with another electron of opposite momentum. The sudden absence of this second electron is exactly the hole, which will be filled by electrons from further away, essentially letting the hole move away from the interface. This in turn means AR is a charge transfer process of 2e across the interface. AR usually happens for particles with energy smaller than the gap (but not exclusively, as will be shown), meaning the process is generally sub-gap transport. Furthermore, the process is highly spin dependent; if the normal state material is fully spin polarized then AR cannot happen, as a pair of electrons of opposite spin cannot be formed in the superconductor. Finally, single particle transmission is of course impossible for particles with incident energy smaller than the gap, since there are no free states in the SC below the energy gap.

Moving on to the main part of the analysis; the scattering processes. As the particle hits the interface, 4 possible scattering events can occur: Andreev reflection, normal reflection, normal transmission and transmission with branch crossing. The latter of these means the particle is transmitted as the antiparticle into the superconductor, and will be referred to as "Andreev Transmission" going forward. Furthermore it is assumed that the incident particle is an electron, although the same procedure can be carried out for the hole.
The possible scattering events are presented in Fig.(25). The figure shows the group velocity in black and red for electrons and holes respectively. The wavevectors are shown in blue and one notes that the group velocity of holes are opposite their wavevector.

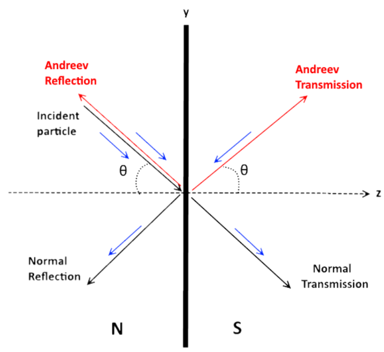

Figure 25: Normal reflection, Andreev reflection, normal transmission and transmission with branch crossing. All 3 components of the velocity will change sign if the particle undergoes Andreev reflection. The black arrows (electrons) and the red arrows (holes) on this figure represent group velocity, whereas the blue arrows are momenta. Notice that holes have group velocity opposite their momentum. The angle θ is with respect to the z-axis, so that $\theta = 0$ means moving completely perpendicular to the interface.

As mentioned earlier single particle transfer is not allowed, so if an electron has energy less than the gap Δ_0, only the two types of reflection can occur. Thus the most interesting case to investigate will be $E > \Delta_0$, where the subscript on Δ_0 is dropped subsequently. Furthermore, normal reflection can only occur if there exists a non-zero barrier strength at the interface, as will be seen later on. The main objective will be to find the probability for each of these processes to occur, both as a function of the incident energy and as a function of the angle with which the incident particle hits the interface. The results will be compared with those of [5]. The article [20] also investigates the effect of adding the angle of incidence θ on the probability of AR occurring; another result to compare with.

Describe first the wavefunction as a spinor of electrons and holes: $\Psi(\mathbf{r}) = \begin{pmatrix} u(\mathbf{r}) \\ v(\mathbf{r}) \end{pmatrix}$. Here u and v are as previously discussed the amplitudes for the Bogoliubov quasiparticles being superpositions of electrons and holes, with u denoting the electron part and v the hole part. In a normal metal $u = 1$ and $v = 0$ for an electron and vice versa for a hole.
In the normal region ($z < 0$) one observes an incident electron as well as the twofold types of reflections; Andreev reflected holes and normally reflected electrons. In the SC region there exists the two forms of transmission; normal transmission and Andreev transmission. As seen in Fig.(24), the gap function changes only in the z-direction. Furthermore, the angle of incidence is included as a method of changing the momentum perpendicular to the interface, so only the z-direction needs to be considered throughout this section.
The wavefunction in the normal region can be described by the following trial wavefunctions, written in spinor space of electrons and holes:

$$\psi_N = \begin{pmatrix} 1 \\ 0 \end{pmatrix} e^{ik_z^+ z} + a \begin{pmatrix} 0 \\ 1 \end{pmatrix} e^{ik_z^- z} + b \begin{pmatrix} 1 \\ 0 \end{pmatrix} e^{-ik_z^+ z}, \tag{5.1}$$

while for the superconducting region:

$$\psi_S = c \begin{pmatrix} u_0 \\ v_0 \end{pmatrix} e^{iq_z^+ z} + d \begin{pmatrix} v_0 \\ u_0 \end{pmatrix} e^{-iq_z^- z}. \tag{5.2}$$

Here $k^\pm$ represents electrons(+) and holes(-) in the normal metal, while $q^\pm$ represents the same in the superconductor. The letters a, b, c, d are the coefficients belonging to each type of scattering; Andreev reflection, normal reflection, normal transmission and Andreev transmission respectively. The actual probabilities (to be denoted with capital letters) can be found as the modulus squared of the coefficient times their group velocity [5]. This is also confirmed in the article [21] by Gifford et al., along with the definition of the group velocity $v_{gS} = |u_0|^2 - |v_0|^2$, which is also presented with the accompanying constants in [6], pages 103 and 104. Note here that u_0 and v_0, present also in Eqs.(5.1) and (5.2), represent the superconducting coherence factors, seen for example in [6], Eq.(2.82), and are given as

$$u_0 = \frac{1}{\sqrt{2}} \left(1 + \frac{\sqrt{\epsilon^2 - \Delta^2}}{\epsilon} \right)^{\frac{1}{2}} \qquad \text{and} \qquad v_0 = \frac{1}{\sqrt{2}} \left(1 - \frac{\sqrt{\epsilon^2 - \Delta^2}}{\epsilon} \right)^{\frac{1}{2}}, \tag{5.3}$$

which one notes depend on the energy ϵ.
Note also the signs in exponential functions of Eqs.(5.1) and (5.2); the reflected particle and the Andreev transmitted particle both have momentum in the $-z$ direction, the latter by virtue of holes having momentum in the opposite direction as that of their group velocity. Furthermore, as explained earlier, quasiparticles in the SC region are superpositions of u_0 and v_0.

Next, using the approximation $\mu \approx E_F$ one can write the wavenumber as $\hbar k^{\pm} = \sqrt{2m(\mu \pm \epsilon)} \approx \sqrt{2m(E_F \pm \epsilon)}$, as seen in [5] and with the inclusion of θ in [20]. Furthermore, one can write:

$$k_z^{\pm} = \sqrt{\frac{2mE_F}{\hbar^2} \pm \frac{2m\epsilon}{\hbar^2}} = \sqrt{k_F^2 \cos^2(\theta) \pm \frac{2m\epsilon}{\hbar^2}}, \tag{5.4}$$

for the normal metal, and likewise one gets $\hbar q^{\pm} = \sqrt{2m(\mu_S \pm \sqrt{\epsilon^2 - \Delta^2})}$ which can be rewritten to

$$q_z^{\pm} = \sqrt{k_F^2 \cos^2(\theta) \pm \frac{2m}{\hbar^2}\sqrt{\epsilon^2 - \Delta^2}}, \tag{5.5}$$

for the superconductor.
Assume now that $E_F \gg \epsilon$ (or Δ) so that Eqs.(5.4) and (5.5) reduce to yield $k_z^{\pm} = q_z^{\pm} = k_F \cos(\theta)$. This is called the Andreev approximation and essentially demands that the particle must have a large momenta perpendicular to the boundary. This is very often the case but one must be aware of the possible inaccuracy of this approximation, should the angle θ be too large. The article [22] by Mortensen et al. indeed explains that for incident angles near $\frac{\pi}{2}$ the approximation fails, but also that these particles of vanishing perpendicular momentum do not contribute significantly to the perpendicular current. This work however, is occupied with the probabilities for the different scattering events to occur, so this possible inaccuracy for large angles must be kept in mind.

One can now introduce the boundary conditions. First of all the wavefunctions must be continuous in the z-direction i.e. $\psi_N = \psi_S$ must hold at the interface. Furthermore, the first derivative of the wavefunctions must be continuous for a delta function potential. Examples of these are presented in [6], Eqs.(4.7) and (4.8). Thus:

$$\psi_N(0) - \psi_S(0) = 0 \quad \text{and} \quad \psi_S'(0) - \psi_N'(0) = \frac{2m}{\hbar^2} H \psi_S(0), \tag{5.6}$$

where H is the strength of the delta function potential at the interface. In the second equation above $\psi_S(0)$ is used since the wavefunction is continuous and thus can be either ψ_N or ψ_S at $z = 0$. Subjecting Eqs.(5.1) and (5.2) to these conditions, one finds the 4 equations

$$1 + b - c \cdot u_0 - d \cdot v_0 = 0, \tag{5.7}$$

$$a - c \cdot v_0 - d \cdot u_0 = 0, \tag{5.8}$$

$$\begin{aligned} &i(q_z^+ \hat{z}) c \cdot u_0 - i(q_z^- \hat{z}) d \cdot v_0 + (b - 1)\, i(k_z^+ \hat{z}) \\ &= \frac{2mH}{\hbar^2}(c \cdot u_0 + d \cdot v_0), \end{aligned} \tag{5.9}$$

$$\begin{aligned} &i(q_z^+ \hat{z}) c \cdot v_0 - i(q_z^- \hat{z}) d \cdot u_0 - a\ i(k_z^- \hat{z}) \\ &= \frac{2mH}{\hbar^2}(c \cdot v_0 + d \cdot u_0). \end{aligned} \tag{5.10}$$

Going forward, the subscript 0 on u_0 and v_0 is suppressed. The Eqs.(5.7) and (5.9) represent the electronic part, while Eqs.(5.8) and (5.10) consider the hole part.
One may now isolate the coefficients in above equations, starting with Eq.(5.9). Employ the Andreev approximation $k_z^{\pm} = q_z^{\pm} = k_F\cos(\theta)$, isolate b in Eq.(5.7) and plug this into Eq.(5.9) to get:

$$
\begin{aligned}
& k_F\cos(\theta) c\cdot u - k_F\cos(\theta) d\cdot v - k_F\cos(\theta) + b\ k_F\cos(\theta) \\
& = \frac{2mH}{i\hbar^2}(c\cdot u + d\cdot v) \\
\Updownarrow & \\
& k_F\cos(\theta) c\cdot u - k_F\cos(\theta) d\cdot v - k_F\cos(\theta) \\
& + (c\cdot u + d\cdot v - 1)k_F\cos(\theta) = \frac{2mH}{i\hbar^2}(c\cdot u + d\cdot v) \\
\Updownarrow & \\
& - 2k_F\cos(\theta) + 2k_F\cos(\theta) c\cdot u = -i\frac{2mH}{\hbar^2}(c\cdot u + d\cdot v) \\
\Updownarrow & \\
& \left(k_F\cos(\theta) + i\frac{mH}{\hbar^2}\right) c\cdot u + i\frac{mH}{\hbar^2} d\cdot v = k_F\cos(\theta).
\end{aligned}
\tag{5.11}
$$

The next step is to obtain an expression for d, by isolating a from Eq.(5.8) and plugging it into Eq.(5.10):

$$
\begin{aligned}
& k_F\cos(\theta) c\cdot v - k_F\cos(\theta) d\cdot u - a\ k_F\cos(\theta) \\
& = -i\frac{2mH}{\hbar^2}(c\cdot v + d\cdot u) \\
\Updownarrow & \\
& k_F\cos(\theta) c\cdot v - k_F\cos(\theta) d\cdot u - (c\cdot v + d\cdot u)k_F\cos(\theta) \\
& = -i\frac{2mH}{\hbar^2}(c\cdot v + d\cdot u) \\
\Updownarrow & \\
& - 2\left(k_F\cos(\theta) - i\frac{mH}{\hbar^2}\right) d\cdot u = -i\frac{2mH}{\hbar^2} c\cdot v \\
\Updownarrow & \\
& d = \frac{i\frac{mH}{\hbar^2}\cdot v}{u\left(k_F\cos(\theta) - i\frac{mH}{\hbar^2}\right)}\cdot c.
\end{aligned}
\tag{5.12}
$$

Insert this back into Eq.(5.11) to get

$$\left(k_F\cos(\theta)+i\frac{mH}{\hbar^2}\right)c\cdot u+i\frac{mH}{\hbar^2}\cdot\frac{i\frac{mH}{\hbar^2}\cdot v}{u\left(k_F\cos(\theta)-i\frac{mH}{\hbar^2}\right)}\cdot c\cdot v$$
$$=k_F\cos(\theta). \tag{5.13}$$

Defining the shorthand notation $\lambda_{\pm}=\left(k_F\cos(\theta)\pm i\frac{mH}{\hbar^2}\right)$ and rewrite Eq.(5.13) to

$$c\left(u\lambda_+-\frac{v^2\left(\frac{mH}{\hbar^2}\right)^2}{u\lambda_-}\right)=k_F\cos(\theta)$$
$$\Updownarrow$$
$$c=\frac{k_F\cos(\theta)}{\left(u\lambda_+-\frac{v^2\left(\frac{mH}{\hbar^2}\right)^2}{u\lambda_-}\right)}. \tag{5.14}$$

Plugging this back into the expression for d from Eq.(5.12) yields the first result:

$$d=\frac{i\frac{mH}{\hbar^2}\cdot v}{u\lambda_-}\cdot\frac{k_F\cos(\theta)}{\left(u\lambda_+-\frac{v^2\left(\frac{mH}{\hbar^2}\right)^2}{u\lambda_-}\right)} \tag{5.15}$$

$$d=\frac{i\frac{mH}{\hbar^2}\cdot v\ k_F\cos(\theta)}{u^2\lambda_-\lambda_+-v^2\left(\frac{mH}{\hbar^2}\right)^2} \tag{5.16}$$

$$d=\frac{i\frac{mH}{\hbar^2}\cdot v\ k_F\cos(\theta)}{u^2k_F^2\cos^2(\theta)+(u^2-v^2)\left(\frac{mH}{\hbar^2}\right)^2}=\frac{i\frac{mH}{k_F\hbar^2}\cdot v\cos(\theta)}{u^2\cos^2(\theta)+(u^2-v^2)\left(\frac{mH}{k_F\hbar^2}\right)^2}, \tag{5.17}$$

thus obtaining an expression for the first coefficient. Now yet another shorthand notation is introduced; $\Sigma=u^2\cos^2(\theta)+(u^2-v^2)\left(\frac{mH}{k_F\hbar^2}\right)^2$. Eq.(5.14) can be further reduced by inserting the newly found d (before dividing by k_F^2) back into Eq.(5.12):

$$\begin{aligned}c&=\frac{u\lambda_-}{i\left(\frac{mH}{\hbar^2}\right)v}\cdot\frac{i\frac{mH}{\hbar^2}\cdot vk_F\cos(\theta)}{u^2k_F^2\cos^2(\theta)+(u^2-v^2)\left(\frac{mH}{\hbar^2}\right)^2}\\&=\frac{u\lambda_-k_F\cos(\theta)}{u^2k_F^2\cos^2(\theta)+(u^2-v^2)\left(\frac{mH}{\hbar^2}\right)^2}=\frac{u\left(k_F\cos(\theta)-i\frac{mH}{\hbar^2}\right)k_F\cos(\theta)}{u^2k_F^2\cos^2(\theta)+(u^2-v^2)\left(\frac{mH}{\hbar^2}\right)^2}\\&=\frac{u\left(\cos^2(\theta)-i\left(\frac{mH}{k_F\hbar^2}\right)\cos(\theta)\right)}{\Sigma}.\end{aligned} \tag{5.18}$$

Now that c and d are found, one can quickly find the coefficients a and b from Eqs.(5.8) and (5.7) respectively:

$$a = c \cdot v + d \cdot u = \frac{u\ v \cos^2(\theta)}{\Sigma}, \tag{5.19}$$

$$b = c \cdot u + d \cdot v - 1 = \frac{u^2 \left(\cos^2(\theta) - i\left(\frac{mH}{k_F \hbar^2}\right)\cos(\theta)\right)}{\Sigma} + \frac{i\frac{mH}{k_F\hbar^2} \cdot v^2 \cos(\theta)}{\Sigma} - \frac{\Sigma}{\Sigma}. \tag{5.20}$$

The number 1 was rewritten so that everything will have the same numerator. One then gets

$$\begin{aligned} b =& \frac{\cancel{u^2 \cos^2(\theta)} - iu^2\left(\frac{mH}{k_F\hbar^2}\right)\cos(\theta) + iv^2\left(\frac{mH}{k_F\hbar^2}\right)\cos(\theta)}{\Sigma} \\ &- \frac{\cancel{u^2\cos^2(\theta)} + (u^2 - v^2)\left(\frac{mH}{k_F\hbar^2}\right)^2}{\Sigma} \\ b =& \frac{(v^2 - u^2)\left(\left(\frac{mH}{k_F\hbar^2}\right)^2 + i\left(\frac{mH}{k_F\hbar^2}\right)\cos(\theta)\right)}{\Sigma}. \end{aligned} \tag{5.21}$$

Thus all the coefficients are finally found! Writing them up once more for clarity:

$$\boxed{\begin{aligned} a &= \frac{u\ v\cos^2(\theta)}{\Sigma} & b &= \frac{(v^2 - u^2)\left(\left(\frac{mH}{k_F\hbar^2}\right)^2 + i\left(\frac{mH}{k_F\hbar^2}\right)\cos(\theta)\right)}{\Sigma} \\ c &= \frac{u\left(\cos^2(\theta) - i\left(\frac{mH}{k_F\hbar^2}\right)\cos(\theta)\right)}{\Sigma} & d &= \frac{iv\left(\frac{mH}{k_F\hbar^2}\right)\cos(\theta)}{\Sigma}, \end{aligned}} \tag{5.22}$$

where the shorthand notation for the numerator is $\Sigma = u^2\cos^2(\theta) + (u^2 - v^2)\left(\frac{mH}{k_F\hbar^2}\right)^2$. These exactly correspond to the findings of BTK. [5] page 4531 Eq.(A11a-d), with γ being our Σ and with their Z given by $\frac{mH}{k_F\hbar^2}$.
From these expressions one can already make an observation, namely how the different probabilities depend on the barrier potential H. One notices that for $H = 0$, both b and d will be zero, meaning only AR (a) and normal transmission (c) can occur. Specifically Eqs.(5.22) will reduce to:

$$a = \frac{v_0}{u_0}, \qquad b = 0, \qquad c = \frac{1}{u_0}, \qquad d = 0. \tag{5.23}$$

Thus for $H = 0$ there is no dependency on the angle of incidence and only AR and normal transmission can occur. Furthermore, in the case of a normal metal on both sides, i.e. $\Delta = 0$, one expects the probabilities for AR and Andreev transmission to go to zero. Recalling the coherence factors

$$u_0 = \frac{1}{\sqrt{2}}\left(1 + \frac{\sqrt{\epsilon^2 - \Delta^2}}{\epsilon}\right)^{\frac{1}{2}}, \qquad v_0 = \frac{1}{\sqrt{2}}\left(1 - \frac{\sqrt{\epsilon^2 - \Delta^2}}{\epsilon}\right)^{\frac{1}{2}}, \tag{5.24}$$

where the subscripts have been restored, one sees that v_0 becomes zero for $\Delta = 0$. Looking again at Eqs.(5.22), one immediately see that a and d becomes 0, as expected.

The dependence of the different probabilities on the angle θ and the energy ϵ is now studied. Starting with the former, the respective probabilities as functions of θ are plotted initially for some values of ϵ and Δ. To be completely clear the probabilities are given as:

$$A = aa^*, \qquad B = bb^*, \qquad C = cc^* v_{gS}, \qquad D = dd^* v_{gS}, \tag{5.25}$$

where $v_{gS} = |u_0|^2 - |v_0|^2$ as stated earlier. These probabilities are found using Mathematica and plotted for energies just above and below the gap, and for different strengths of the barrier potential as well. In Fig.(26) the probabilities are plotted as a function of the angle with energy larger than the gap. Specifically, $\epsilon = 1.1 \cdot \Delta$, inspired by [20].
Notice that as the angle of incidence increases, the normal reflection will dominate. This is in agreement with [22], who describes the increasing angle as effectively an increase to the barrier strength, thus reducing the likelihood of for example AR, as seen in Fig.(26). This is due to the fact that the perpendicular momentum of the incident particle becomes smaller, while the parallel momentum increases. The smaller momentum effectively corresponds to a stronger barrier potential. Finally, note that some AR still occur, even if the energy is large enough to allow single particle transmission.

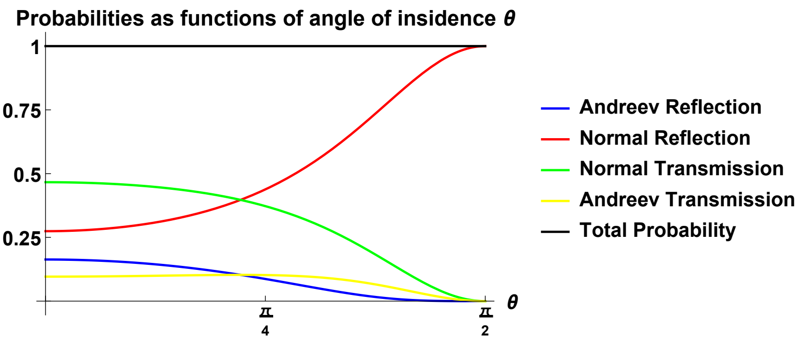

(a) $\epsilon = 1.1, \ \ \frac{mH}{k_F \hbar^2} = 1.$

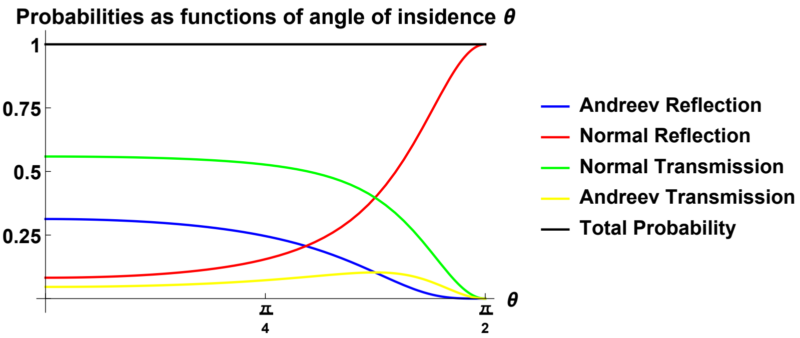

(b) $\epsilon = 1.1, \ \ \frac{mH}{k_F \hbar^2} = 0.5.$

Figure 26: Plots of the different probabilities, as well as the total probability, for $\Delta = 1$ with ϵ and the barrier strength written below each plot. *a)* As the angle of incidence increases, normal reflection becomes the dominant event, compared to the others. At $\theta = \frac{\pi}{2}$ only normal reflection is possible, but recall the possible inaccuracy of the Andreev approximation here. *b)* As the strength of the delta function barrier is reduced, both normal transmission and AR becomes more likely. This is in accordance with the expectation that normal reflection and Andreev transmission go to zero for $H = 0$.

In Fig.(27) the case of $\epsilon < \Delta$ is explored. As expected, there is no transmission possible for these energies. As in Fig.(27), note that normal reflection becomes less probable for a smaller barrier potential.

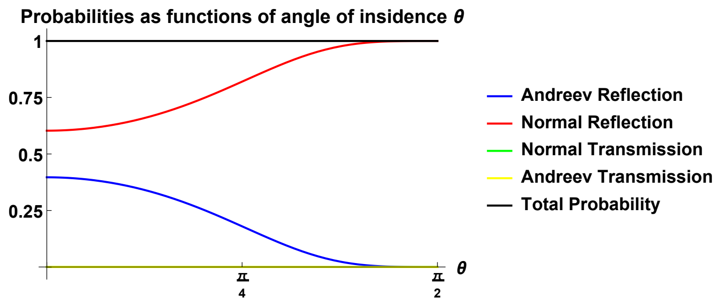

(a) $\epsilon = 0.9, \quad \frac{mH}{k_F \hbar^2} = 1.$

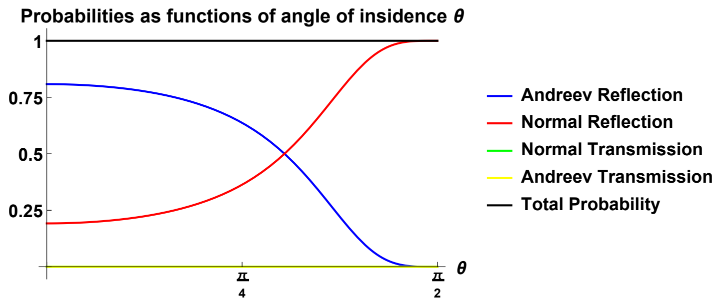

(b) $\epsilon = 0.9, \quad \frac{mH}{k_F \hbar^2} = 0.5.$

Figure 27: Plots of the different probabilities, for $\Delta = 1$ with ϵ and the barrier strength written below each plot. Since $\epsilon < \Delta$, single particle transmission is not allowed and thus only reflection is seen. *a)* The probability for AR is reduced with increasing angle, as the effective strength of the barrier increases with the angle. *b)* ARs are enhanced for a lower barrier strength. Note also that if $H = 0$, the only possible event to occur will be AR.

Next is the investigation of the different events' dependence on the energy of the incident particle and a comparison of the results with those of [5]. For this purpose, $\theta = 0$ is used in the following. Furthermore $\Delta = 1$ is used and shown in Fig.(28) are plots for different values of the barrier strength H.

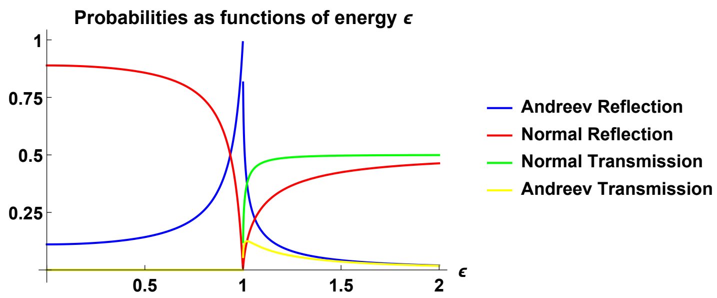

(a) $\frac{mH}{k_F\hbar^2} = 1$.

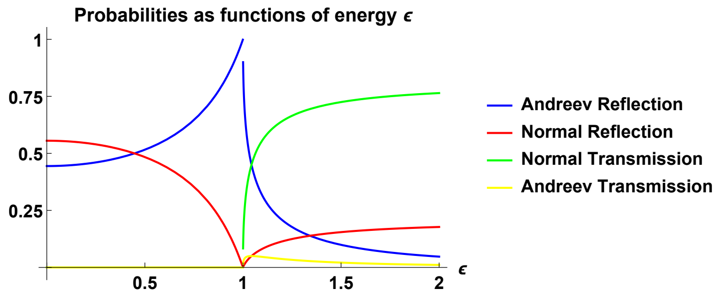

(b) $\frac{mH}{k_F\hbar^2} = 0.5$.

Figure 28: The probabilities as functions of energy ϵ. The total probability is no longer plotted. The values $\theta = 0$ and $\Delta = 1$ were used. Single particle transmission is not allowed for $\epsilon < \Delta$ as stated in the text. Further, AR tends to zero for energies larger than the gap. These results match those of [5], Fig.(5). *a)* Interestingly one sees that the probability for Andreev reflection grows significantly as ϵ approaches Δ and that it does not become zero immediately for $\epsilon > \Delta$. Further, normal reflection dominates for $\epsilon < \Delta$, while normal transmission dominates for $\epsilon > \Delta$. *b)* As the barrier strength is decreased, AR becomes more likely, while the probability for normal reflection drops for all energies.

It is seen that single particle transmission is indeed not allowed for energies below Δ, and also seen is an increased probability of AR for weaker barrier potentials, as was also the conclusion in Fig.(26) and Fig.(27). The likelihood of AR peaks near Δ and falls off as the energy grows beyond the gap. These figures are in agreement with the findings of [5], Fig.(5). For completeness, one may plot the probabilities as a function of the energy without a potential barrier, which is presented in Fig.(29). Again normal reflection and Andreev transmission cannot occur, as was the conclusion of Eq.(5.23).

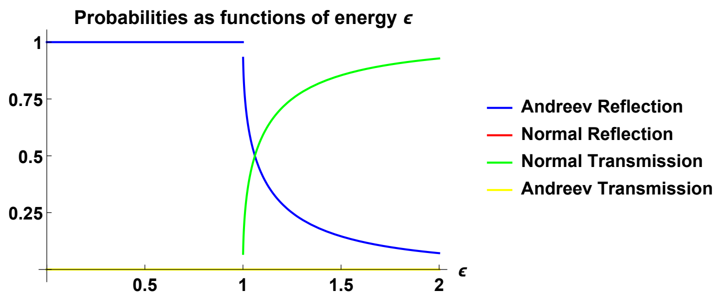

Figure 29: The probabilities as functions of energy. Here $H = 0$, showing that only AR can occur for energies smaller than the gap in this case and that both normal reflection and Andreev transmission is disallowed.

This I believe is simply due to the fact that there is nothing for the particle to scatter on; the surface is so perfectly smooth that the particle is completely unhindered. However, if the particle has energy lower than the gap, there are no states in the SC it can occupy and therefore it must undergo AR, creating a Cooper-pair that lives in the SC.

A few concluding remarks are in order.
First of all, the article [22] discusses a possible critical angle θ_c above which AR would no longer be possible. The authors show that this critical angle depends on the Fermi wavevector of both regions:

$$\theta_c = \arcsin\left(\frac{k_F^{(S)}}{k_F^{(N)}}\right). \tag{5.26}$$

Thus, if there is no Fermi wavevector mismatch, then the critical angle would be

$$\theta_c = \arcsin(1) = \frac{\pi}{2}, \tag{5.27}$$

which is the natural limit. If there were a mismatch however, then for any angle above the critical angle, the parallel momentum of the incident particle would exceed the Fermi momentum of the superconductor. This would lead to a breaking of the conservation of momentum, which is not allowed. Therefore AR is not allowed for $\theta > \theta_c$.
Another important observation concerns the wavevector of the Andreev reflected hole, in the case of an incident electron. As stated earlier, it was assumed the wavevectors were identical, but the fact remains; the trajectories of the incident electron and the outgoing hole are *not* completely identical, [6] Sec.(4.2). This will have consequences, which will be discussed in due time, along with the origin of this deviation. Finally, a brief comment on the barrier potential strength $\frac{mH}{k_F\hbar^2}$ follows. In a review on ARs by Yu. G. Naidyuk & K. Gloos [23] the physical meaning of the parameter is discussed. They report that the main contribution

to H, and therefore also normal reflection, is the disordered crystal lattice at the contact point. They state that even a few atomic layers are enough to produce the barrier strength, as used in this section. Furthermore they explain how a possible Fermi velocity mismatch does *not* contribute to this barrier strength at the interface.

This concludes the analysis of the different possible scattering events that can occur as a particle hits an interface between a normal metal and a superconductor. Having now understood the basics of Andreev reflections, one can suggest what is meant when the CdGM-states are called an Andreev state, named such by [6], Fig.(4.11). These are the Andreev Bound States (ABS), formed by the repeated process of Andreev reflection and are discussed in for example [6] and the article [24] by J. A. Sauls. The process is shown in Fig.(30), which represents a system consisting of a normal metal "sandwiched" between two superconducting metals. An incident electron undergoing AR on the interface between the normal metal and the right SC will create a Cooper-pair in the SC while expelling a hole moving to the left. The hole follows the same trajectory as the incident electron but in the opposite direction until it hits the interface between the metal and the left SC. Another AR happens in which this hole annihilates with an electron from a Cooper-pair in the SC, while the leftover electron is expelled into the normal metal, moving to the right. This electron follows exactly the path of the incident electron, and the process begins anew. The particles are thus localized in the normal metal and will have a discreet energy spectrum.

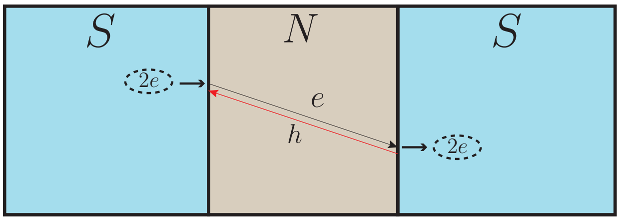

Figure 30: Sketch of an Andreev Bound State. A normal region is sandwiched between two superconducting regions. An incident electron hitting the interface to the right will create a Cooper-pair while expelling a hole that travels through the normal metal towards the other superconductor. This hole will annihilate a Cooper-pair in the left superconductor when hitting the interface and expel an electron, with which the process repeats.

The Abrikosov vortex from Sec.(3) can be seen as such an SNS system, even though there is only a single superconductor, completely surrounding the normal region. The particles will Andreev reflect off of the spatial variance of the gap function in the vortex, and thus one can expect the CdGM states to be at the very least analogue to ABS. This same description translates perfectly to a cylinder of a normal core and an superconducting outer shell; the particles traverse the normal core region and can Andreev reflect off of the superconductor at the interface.

Recalling the fact that an Andreev reflected hole will not be perfectly retro-reflected, but instead deviate slightly from the trajectory of the incident electron, one can imagine the ABS precess around in the vortex/cylinder core, as imagined in Fig.(31).

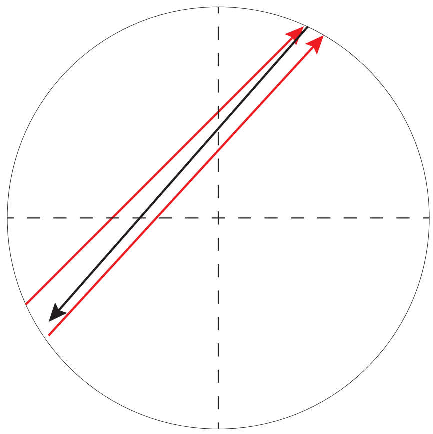

Figure 31: Rough sketch to show the idea behind the precession of the states. Each reflection has a small deviation from the incident particle/antiparticle and thus the ABS can precess around in the vortex. The red trajectories signify holes, while the black represents an electron. The particles are Andreev reflected off of the spatial variations of the order parameter. The above circle can also represent the normal core of a solid cylinder with an outer superconducting shell.

One could further imagine that as the states precess, at some point the angle of incidence would be almost parallel with the vortex edge, meaning normal reflection would become much more likely. Actual calculation of the precession would be necessary in order to understand exactly the underlying physics of the system.

Another very interesting article, this one by M. Stone [25], discusses the possible precession of the bound states, both due to the imperfect reflection but more importantly due to a possible supercurrent in the superconductor. The supercurrent circling the vortex core (generated to screen the magnetic field line in the center of the vortex from the rest of the SC) will let the bound states precess within the vortex, as shown in Fig.(5) of [25].

In the next section, I will be investigating exactly the force acting on the Andreev reflected particles as they hit the interface, in order to better understand this precession of the CdGM states within the vortex.

6 EHRENFEST DYNAMICS

Here I seek to describe the forces acting on a particle as it hits the NS-interface from the normal region. This section will go through the method of Ehrenfest dynamics in which one finds the time derivative of an expectation value of an operator. Thus one can find the total force acting on a particle as the time derivative of the expectation value of the momentum operator. I will specifically be interested in the off-diagonal forces, as these are the ones dealing with electron-hole transitions (and vice versa). These can describe what happens at the interface as a particle undergoes Andreev reflection. This one can use to better understand the CdGM states, behaving as Andreev states within the vortex, reflecting off of the spatially varying order parameter. As I discussed in the prior section, a supercurrent is circling the vortex line and may affect the states in such a way that a precession of the states is possible. Furthermore, returning to the superconducting cylinder with a normal core and a superconducting shell, I explained that a supercurrent can be induced in the superconductor due to a magnetic field, as was examined in the Little-Parks discussion. This supercurrent could possibly lead to a precession of the bound states within. The forces acting on a particle at the NS interface must therefore be investigated.
First, one can describe the quasiparticle excitation with the spinor wavefunction

$$\Psi(r) = \begin{pmatrix} u(r) \\ v(r) \end{pmatrix}, \tag{6.1}$$

where the functions u and v, quite familiar by now, are made time-dependent. This section follows the work of S. Hofmann and R. Kümmel [26].
Write first the time dependent BdG equations:

$$i\hbar \frac{\partial}{\partial t}\Psi(r,t) = \underline{\underline{\hat{\mathcal{H}}}}(r,t)\Psi(r,t), \tag{6.2}$$

where

$$\underline{\underline{\hat{\mathcal{H}}}}(r,t) = \begin{pmatrix} \hat{\mathcal{H}}_e(r,t) & \Delta(r,t) \\ \Delta^*(r,t) & -\hat{\mathcal{H}}_e^*(r,t) \end{pmatrix}, \tag{6.3}$$

is the Nambu (particle-hole) matrix Hamiltonian. Here $\hat{\mathcal{H}}_e(r,t) = \frac{(-i\hbar\boldsymbol{\nabla} - e\mathbf{A}(r,t))^2}{2m} + U(r,t) - \mu$, which is the Hamiltonian acting on single electrons and holes added to some external scalar potential U and the chemical potential μ. Finally e is the charge and $\mathbf{A}(r,t)$ is the vector potential. Going forward, the dependencies on r and t are suppressed. In the off-diagonal

of $\underline{\underline{\hat{\mathcal{H}}}}$ is the pair potential, or gap function, Δ.
The expectation value of some operator $\hat{\alpha}$ is defined to be

$$\begin{aligned}\langle\hat{\alpha}\rangle = \int dr\ \Psi^\dagger\hat{\alpha}\Psi = \int dr \begin{pmatrix} u \\ v \end{pmatrix}^\dagger \begin{pmatrix} \alpha_{11} & \alpha_{12} \\ \alpha_{21} & \alpha_{22} \end{pmatrix} \begin{pmatrix} u \\ v \end{pmatrix} \\ = \langle u|\alpha_{11}|u\rangle + \langle u|\alpha_{12}|v\rangle + \langle v|\alpha_{21}|u\rangle + \langle v|\alpha_{22}|v\rangle,\end{aligned} \tag{6.4}$$

inspired by Eq.(6) of [26] and using Eq.(6.1). The † represents the adjoint of a matrix operator.
The Ehrenfest theorem, stated by P. Ehrenfest, gives an expression for the time derivative of an operator, see Eq.(7) of [26].

$$\frac{\partial}{\partial t}\langle\hat{\alpha}\rangle = \int dr \left[\left(\frac{\partial\Psi^\dagger}{\partial t}\right)\hat{\alpha}\Psi + \Psi^\dagger\left(\frac{\partial\hat{\alpha}}{\partial t}\right)\Psi + \Psi^\dagger\hat{\alpha}\left(\frac{\partial\Psi}{\partial t}\right)\right] \tag{6.5}$$

One may find the time derivatives of the wavefunctions from the Eqs.(6.2): $\left(\frac{\partial\Psi}{\partial t}\right) = \frac{-i}{\hbar}\underline{\underline{\hat{\mathcal{H}}}}\Psi$ and $\left(\frac{\partial\Psi^\dagger}{\partial t}\right) = \frac{+i}{\hbar}\left(\underline{\underline{\hat{\mathcal{H}}}}\Psi\right)^\dagger = \frac{+i}{\hbar}\Psi^\dagger\underline{\underline{\hat{\mathcal{H}}}}^\dagger$.
If there is no explicit time dependence on the operator $\hat{\alpha}$, then the second term in Eq.(6.5) is zero and one can write

$$\frac{\partial}{\partial t}\langle\hat{\alpha}\rangle = \int dr \left[\frac{i}{\hbar}\Psi^\dagger\left(\underline{\underline{\hat{\mathcal{H}}}}^\dagger\hat{\alpha} - \hat{\alpha}\underline{\underline{\hat{\mathcal{H}}}}\right)\Psi\right] \tag{6.6}$$

Using Eq.(6.6) to find an expression for the velocity, given as the time derivative of the expectation value of the position operator $\hat{\mathbf{q}}(r)$, one finds:

$$\mathbf{v} = \frac{\partial}{\partial t}\langle\hat{\mathbf{q}}\rangle = \int d\mathbf{q}\frac{i}{\hbar}\left[\begin{pmatrix} u \\ v \end{pmatrix}^\dagger \left[\begin{pmatrix} \hat{\mathcal{H}}_e & \Delta \\ \Delta^* & -\hat{\mathcal{H}}_e^* \end{pmatrix}^\dagger \hat{\mathbf{q}} - \hat{\mathbf{q}}\begin{pmatrix} \hat{\mathcal{H}}_e & \Delta \\ \Delta^* & -\hat{\mathcal{H}}_e^* \end{pmatrix}\right]\begin{pmatrix} u \\ v \end{pmatrix}\right], \tag{6.7}$$

where $\hat{\mathbf{q}}$ is proportional to the identity matrix in the Nambu space and contains no explicit time dependence. Perform the dot products to get

$$\begin{aligned}\mathbf{v} = \int d\mathbf{q}\frac{i}{\hbar}\Big[&\langle u|\hat{\mathcal{H}}_e\hat{\mathbf{q}}|u\rangle + \langle u|\Delta\hat{\mathbf{q}}|v\rangle + \langle v|\Delta^*\hat{\mathbf{q}}|u\rangle + \langle v|\left(-\hat{\mathcal{H}}_e^*\right)\hat{\mathbf{q}}|v\rangle \\ &-\left(\langle u|\hat{\mathbf{q}}\hat{\mathcal{H}}_e|u\rangle + \langle u|\hat{\mathbf{q}}\Delta|v\rangle + \langle v|\hat{\mathbf{q}}\Delta^*|u\rangle + \langle v|\hat{\mathbf{q}}(-\hat{\mathcal{H}}_e^*)|v\rangle\right)\Big].\end{aligned} \tag{6.8}$$

Here the fact that $\hat{\mathcal{H}}_e$ is hermitian was used, by virtue of the momentum operator, $\hat{\mathbf{p}} = -i\hbar\boldsymbol{\nabla}$, being formally self-adjoint (= hermitian), i.e. $\hat{\mathbf{p}}^\dagger = \hat{\mathbf{p}}$. That the momentum operator is indeed hermitian is shown in Appendix (A.6).

This, alongside the fact that $\hat{\mathbf{q}}$ commutes with Δ, which allows one to cancel all $\Delta^{(*)}\mathbf{q}$ terms, allows Eq.(6.8) to be rewritten as

$$\mathbf{v} = \int d\mathbf{q} \frac{i}{\hbar}\Big[- \langle u| \left[\hat{\mathbf{q}}, \hat{\mathcal{H}}_e\right] |u\rangle + \langle v| \left[\hat{\mathbf{q}}, \hat{\mathcal{H}}_e^*\right] |v\rangle \Big]. \tag{6.9}$$

Now one can write out $\hat{\mathcal{H}}_e$ again using the definition $\hat{\mathbf{p}} = -i\hbar\boldsymbol{\nabla}$, and since $\hat{\mathbf{q}}$ also commutes with U and μ, one finds

$$\mathbf{v} = \int d\mathbf{q} \frac{i}{\hbar}\left[- \left\langle u \middle| \left[\hat{\mathbf{q}}, \frac{(\hat{\mathbf{p}} - e\mathbf{A})^2}{2m}\right] \middle| u \right\rangle + \left\langle v \middle| \left[\hat{\mathbf{q}}, \frac{(-\hat{\mathbf{p}} - e\mathbf{A})^2}{2m}\right] \middle| v \right\rangle \right]. \tag{6.10}$$

Note the sign change on $\hat{\mathbf{p}}$ in the last term from the complex conjugate of $\hat{\mathcal{H}}_e$. The relevant commutation relations between position and momentum is $\quad [\hat{\mathbf{q}}, \hat{\mathbf{p}}] = i\hbar \quad$ and $\quad [\hat{\mathbf{q}}, \hat{\mathbf{p}}^2] = 2i\hbar\hat{\mathbf{p}} \quad$ and using these one gets

$$\begin{aligned}
\mathbf{v} &= \int d\mathbf{q} \frac{i}{\hbar 2m}\Big[- \langle u| \left(2i\hbar\hat{\mathbf{p}} - 2i\hbar e\mathbf{A}\right) |u\rangle + \langle v| \left(2i\hbar\hat{\mathbf{p}} + 2i\hbar e\mathbf{A}\right) |v\rangle \Big] \\
&= \int d\mathbf{q} \frac{1}{m}\Big[\langle u| \left(\hat{\mathbf{p}} - e\mathbf{A}\right) |u\rangle - \langle v| \left(\hat{\mathbf{p}} + e\mathbf{A}\right) |v\rangle \Big] \\
&= \int d\mathbf{q} \frac{1}{m}\Big[\langle u|\hat{\mathbf{p}}_e|u\rangle - \langle v|\hat{\mathbf{p}}_h|v\rangle \Big],
\end{aligned} \tag{6.11}$$

where $\hat{\mathbf{p}}_e = -i\hbar\boldsymbol{\nabla} - e\mathbf{A} \quad$ and $\quad \hat{\mathbf{p}}_h = -i\hbar\boldsymbol{\nabla} + e\mathbf{A}$. The velocity can now be written in its Nambu matrix form, from which one also obtains the momentum operator:

$$\mathbf{v} = \frac{1}{m}\left\langle \begin{pmatrix} \mathbf{p}_e & 0 \\ 0 & -\mathbf{p}_h \end{pmatrix} \right\rangle, \qquad \hat{\mathbf{p}} = \begin{pmatrix} \mathbf{p}_e & 0 \\ 0 & \mathbf{p}_h \end{pmatrix}. \tag{6.12}$$

Note here that holes have momentum with opposite direction from their group velocity, as explained in Sec.(5).

Next, using this same technique once again, one can calculate the time derivative of the new-found momentum operator. This will of course give the total force acting on the quasi-particles, which one can split into diagonal and off-diagonal parts. Therefore

$$\frac{\partial}{\partial t}\langle \hat{\mathbf{p}} \rangle = \int d\mathbf{q} \left[\Psi^\dagger \left(\frac{\partial \hat{\mathbf{p}}}{\partial t}\right) \Psi + \frac{i}{\hbar} \Psi^\dagger \left(\underline{\underline{\hat{\mathcal{H}}}}^\dagger \hat{\mathbf{p}} - \hat{\mathbf{p}} \underline{\underline{\hat{\mathcal{H}}}} \right) \Psi \right]. \tag{6.13}$$

Notice that the first term is not neglected due to the vector potential $\mathbf{A}$ possibly having an explicit time dependence. Eq.(6.13) is written out:

$$\begin{aligned}\frac{\partial}{\partial t}\langle\hat{\mathbf{p}}\rangle &= \int d\mathbf{q}\left[\Psi^\dagger\left(\frac{\partial\hat{\mathbf{p}}}{\partial t}\right)\Psi + \frac{i}{\hbar}\Psi^\dagger\left[\begin{pmatrix}\hat{\mathcal{H}}_e & \Delta\\ \Delta^* & -\hat{\mathcal{H}}_e^*\end{pmatrix}^\dagger\begin{pmatrix}\hat{\mathbf{p}}_e & 0\\ 0 & \hat{\mathbf{p}}_h\end{pmatrix} - \begin{pmatrix}\hat{\mathbf{p}}_e & 0\\ 0 & \hat{\mathbf{p}}_h\end{pmatrix}\begin{pmatrix}\hat{\mathcal{H}}_e & \Delta\\ \Delta^* & -\hat{\mathcal{H}}_e^*\end{pmatrix}\right]\Psi\right]\\ &= \int d\mathbf{q}\left[\Psi^\dagger\begin{pmatrix}\frac{\partial}{\partial t}\hat{\mathbf{p}}_e & 0\\ 0 & \frac{\partial}{\partial t}\hat{\mathbf{p}}_h\end{pmatrix}\Psi + \frac{i}{\hbar}\Psi^\dagger\left[\begin{pmatrix}\hat{\mathcal{H}}_e\hat{\mathbf{p}}_e & \Delta\hat{\mathbf{p}}_h\\ \Delta^*\hat{\mathbf{p}}_e & -\hat{\mathcal{H}}_e^*\hat{\mathbf{p}}_h\end{pmatrix} - \begin{pmatrix}\hat{\mathbf{p}}_e\hat{\mathcal{H}}_e & \hat{\mathbf{p}}_e\Delta\\ \hat{\mathbf{p}}_h\Delta^* & -\hat{\mathbf{p}}_h\hat{\mathcal{H}}_e^*\end{pmatrix}\right]\Psi\right].\end{aligned} \tag{6.14}$$

Write out the wavefunctions and take the dot product:

$$\begin{aligned}\frac{\partial}{\partial t}\langle\hat{\mathbf{p}}\rangle = \frac{i}{\hbar}\Big[&\langle u|\hat{\mathcal{H}}_e\hat{\mathbf{p}}_e|u\rangle + \langle u|\Delta\hat{\mathbf{p}}_h|v\rangle + \langle v|\Delta^*\hat{\mathbf{p}}_e|u\rangle + \langle v| - \hat{\mathcal{H}}_e^*\hat{\mathbf{p}}_h|v\rangle,\\ &-\left(\langle u|\hat{\mathbf{p}}_e\hat{\mathcal{H}}_e|u\rangle + \langle u|\hat{\mathbf{p}}_e\Delta|v\rangle + \langle v|\hat{\mathbf{p}}_h\Delta^*|u\rangle + \langle v| - \hat{\mathbf{p}}_h\hat{\mathcal{H}}_e^*|v\rangle\right),\\ &+\langle u|\frac{\hbar}{i}\frac{\partial\hat{\mathbf{p}}_e}{\partial t}|u\rangle + \langle v|\frac{\hbar}{i}\frac{\partial\hat{\mathbf{p}}_h}{\partial t}|v\rangle\Big].\end{aligned} \tag{6.15}$$

The time derivative of $\hat{\mathbf{p}}_e$ and $\hat{\mathbf{p}}_h$ can be written out as

$$\frac{\partial\hat{\mathbf{p}}_e}{\partial t} = \frac{\partial}{\partial t}\left(-i\hbar\boldsymbol{\nabla} - e\mathbf{A}\right) = -e\frac{\partial\mathbf{A}}{\partial t}, \qquad \frac{\partial\hat{\mathbf{p}}_h}{\partial t} = \frac{\partial}{\partial t}\left(-i\hbar\boldsymbol{\nabla} + e\mathbf{A}\right) = e\frac{\partial\mathbf{A}}{\partial t}. \tag{6.16}$$

Collecting the terms in Eq.(6.15) yields

$$\begin{aligned}\frac{\partial}{\partial t}\langle\hat{\mathbf{p}}\rangle = \frac{i}{\hbar}\Big[&-\langle u|\left[\hat{\mathbf{p}}_e, \hat{\mathcal{H}}_e\right] + \frac{e\hbar}{i}\frac{\partial\mathbf{A}}{\partial t}|u\rangle - \langle u|\left(\hat{\mathbf{p}}_e\Delta - \Delta\hat{\mathbf{p}}_h\right)|v\rangle\\ &-\langle v|\left(\hat{\mathbf{p}}_h\Delta^* - \Delta^*\hat{\mathbf{p}}_e\right)|u\rangle + \langle v|\left[\hat{\mathbf{p}}_h, \hat{\mathcal{H}}_e^*\right] + \frac{e\hbar}{i}\frac{\partial\mathbf{A}}{\partial t}|v\rangle\Big]\\ = \frac{i}{\hbar}\Big[&\langle u|\hat{\mathbf{f}}_{11}|u\rangle + \langle u|\hat{\mathbf{f}}_{12}|v\rangle + \langle v|\hat{\mathbf{f}}_{21}|u\rangle + \langle v|\hat{\mathbf{f}}_{22}|v\rangle\Big],\end{aligned} \tag{6.17}$$

where the force operator $\hat{\mathbf{f}}$ was introduced, given by the time derivative of the momentum; $\langle\hat{\mathbf{f}}\rangle = \left\langle\begin{pmatrix}\hat{\mathbf{f}}_{11} & \hat{\mathbf{f}}_{12}\\ \hat{\mathbf{f}}_{21} & \hat{\mathbf{f}}_{22}\end{pmatrix}\right\rangle = \frac{\partial}{\partial t}\langle\hat{\mathbf{p}}\rangle$. The off-diagonal forces $\hat{\mathbf{f}}_{12}$ and $\hat{\mathbf{f}}_{21}$ which are the ones relating u and v, are the ones of interest to this section and are written below

$$\langle u|\mathbf{f}_{12}|v\rangle = -\frac{i}{\hbar}\langle u|\left(\mathbf{p}_e\Delta - \Delta\mathbf{p}_h\right)|v\rangle \tag{6.18}$$

$$\langle v|\mathbf{f}_{21}|u\rangle = -\frac{i}{\hbar}\langle v|\left(\mathbf{p}_h\Delta^* - \Delta^*\mathbf{p}_e\right)|u\rangle. \tag{6.19}$$

One notes that these forces deal with events that scatter electrons into holes and vice-versa. Write out $\hat{\mathbf{p}}_e$ and $\hat{\mathbf{p}}_h$ in Eq.(6.18) to get

$$\begin{aligned}
\langle u|\hat{\mathbf{f}}_{12}|v\rangle &= -\frac{i}{\hbar}\langle u|\big(\left(-i\hbar\boldsymbol{\nabla} - e\mathbf{A}\right)\Delta - \Delta\left(-i\hbar\boldsymbol{\nabla} + e\mathbf{A}\right)\big)|v\rangle, \\
&= \int d\mathbf{q}u^*\frac{-i}{\hbar}\Big[-i\hbar\left(\boldsymbol{\nabla}\Delta\right)v - \cancel{i\hbar\left(\boldsymbol{\nabla}v\right)\Delta} + \cancel{i\hbar\Delta\left(\boldsymbol{\nabla}v\right)} - 2e\mathbf{A}\Delta v\Big], \\
&= \int d\mathbf{q}u^*\frac{-i}{\hbar}\Big[-i\hbar\left(\boldsymbol{\nabla}\Delta\right)v - 2e\mathbf{A}\Delta v\Big] = -\frac{i}{\hbar}\langle u|\left(-i\hbar\boldsymbol{\nabla} - 2e\mathbf{A}\right)\Delta|v\rangle. \qquad (6.20)
\end{aligned}$$

In the last equality the derivative acts only on the gap function, Δ, and not on the state $|v\rangle$. The same is done for $\hat{\mathbf{f}}_{21}$ and one finds these off-diagonal forces to be

$$\begin{aligned}
\langle u|\hat{\mathbf{f}}_{12}|v\rangle &= \langle u|\frac{-i}{\hbar}\left(-i\hbar\boldsymbol{\nabla} - 2e\mathbf{A}\right)\Delta|v\rangle, \\
\langle v|\hat{\mathbf{f}}_{21}|u\rangle &= \langle v|\frac{-i}{\hbar}\left(-i\hbar\boldsymbol{\nabla} + 2e\mathbf{A}\right)\Delta^*|u\rangle. \qquad (6.21)
\end{aligned}$$

These forces are non-zero when Δ is non-zero, which is true only in the SC region. One can add the two contributions and define the sum as $\hat{\mathbf{f}}_\Delta$:

$$\begin{aligned}
\hat{\mathbf{f}}_\Delta &= \langle u|\hat{\mathbf{f}}_{12}|v\rangle + \langle v|\hat{\mathbf{f}}_{21}|u\rangle \\
&= \int d\mathbf{q}\left[u^*\left(-\boldsymbol{\nabla}\Delta + \frac{i}{\hbar}2e\mathbf{A}\Delta\right)v + v^*\left(-\boldsymbol{\nabla}\Delta^* - \frac{i}{\hbar}2e\mathbf{A}\Delta^*\right)u\right]. \qquad (6.22)
\end{aligned}$$

Notice that these are each others complex conjugate and thus the addition of the two terms will equal twice the real part of either one:

$$\hat{\mathbf{f}}_\Delta = 2\mathrm{Re}\int d\mathbf{q}\left[u^*v\left(-\boldsymbol{\nabla}\Delta + \frac{i}{\hbar}2e\mathbf{A}\Delta\right)\right]. \qquad (6.23)$$

Now one may write out the pair potential as $\Delta = |\Delta|\exp(i\phi)$ and let $\boldsymbol{\nabla}$ act on each component

$$\hat{\mathbf{f}}_\Delta = 2\mathrm{Re}\int d\mathbf{q}\left[u^*ve^{i\phi}\left(-(\boldsymbol{\nabla}|\Delta|) - i|\Delta|(\boldsymbol{\nabla}\phi) + \frac{i}{\hbar}2e\mathbf{A}|\Delta|\right)\right]. \qquad (6.24)$$

Split first this into the following two terms

$$\hat{\mathbf{f}}_\Delta = -2\mathrm{Re}\int d\mathbf{q}\left[u^*v(\boldsymbol{\nabla}|\Delta|)e^{i\phi}\right] - 2\mathrm{Re}\int d\mathbf{q}\left[u^*v\cdot i\left((\boldsymbol{\nabla}\phi) - \frac{2e\mathbf{A}}{\hbar}\right)|\Delta|e^{i\phi}\right]. \qquad (6.25)$$

Use now that the real part of a complex number times i is given by minus the imaginary part, i.e. $Re(i \cdot z) = Re(i \cdot a - b) = -b = -Im(z)$, where $z = a + i \cdot b$ is a complex number. Thus one can write

$$\hat{\mathbf{f}}_\Delta = 2\mathrm{Re} \int d\mathbf{q} \left[u^* v \left(-\boldsymbol{\nabla} |\Delta| \right) e^{i\phi} \right] + 2\mathrm{Im} \int d\mathbf{q} \left[u^* v (\boldsymbol{\nabla} \phi - \frac{2e\mathbf{A}}{\hbar}) \Delta \right] \tag{6.26}$$

$$= \hat{\mathbf{f}}_{\Delta 1} + \hat{\mathbf{f}}_{\Delta 2}. \tag{6.27}$$

Here $\hat{\mathbf{f}}_{\Delta 1}$ corresponds to a radial part, dependent on the gradient of the gap, and $\hat{\mathbf{f}}_{\Delta 2}$ to a "convective" part dependent on the gradient of the phase of the order parameter. The first force is the one responsible for the AR process and is thus a force that acts perpendicular to the interface, as also explained in [26]. One can further rewrite the latter of the forces by introducing the Cooper-pair velocity $\mathbf{v}_s = \frac{\hbar}{2m} \left(\boldsymbol{\nabla} \phi - \frac{2e}{\hbar} \mathbf{A} \right)$, which was also presented in Sec.(2), Eq.(2.11). Thus

$$\boxed{\hat{\mathbf{f}}_{\Delta 2} = \frac{4m}{\hbar} \mathrm{Im} \int d\mathbf{q} \left[u^* v \ \mathbf{v}_s \Delta \right]. \tag{6.28}}$$

It is this convective contribution from the off-diagonal force which are of greatest interest. One can see that this force is dependent on the supercurrent velocity of the Cooper-pairs. The article [27] (again by S. Hofmann and R. Kümmel) confirms this; the force $\hat{\mathbf{f}}_{\Delta 2}$ is exerted on the Andreev reflected quasiparticles by the supercurrent. They elaborate further; electron-to-hole scattering takes momentum from the quasiparticle in order to provide the created Cooper-pair enough momentum to join the moving condensate. Oppositely, in the hole-to-electron case, a Cooper-pair is broken apart and the momentum of the pair is transferred to the outgoing quasiparticle. The momentum gained or lost is in the direction of the supercurrent, i.e. parallel to the interface. It is this transfer of momenta that is the origin of the "convective" nickname given to the force $\hat{\mathbf{f}}_{\Delta 2}$. The authors of [27] also show that $\hat{\mathbf{f}}_{\Delta 2}$ indeed acts parallel to the interface. Finally they claim that their results, obtained for a plane NS interface, is valid for the vortex line as well (page 1321).
Lastly I introduce the article by B. Götzelmann, S. Hofmann and R. Kümmel [28], in which they discuss these off-diagonal forces further. First of all, the force acting parallel to the interface, $\hat{\mathbf{f}}_{\Delta 1}$, is finite if u and v belong to quasiparticles with energy less than the maximum value of the gap. This is normally what one would expect, although Sec.(5) did show some AR for energies just above the gap.

More interesting, however, is their investigation of $\hat{\mathbf{f}}_{\Delta 2}$. They explain how the force, present when one has a non-zero supercurrent in the SC region, will change the trajectories of the Andreev reflected particles compared to the case of $v_s = 0$. This is seen clearly in their Fig.(2a), presented in our Fig.(32). An incoming electron undergoes AR, creating a Cooper-pair in the superconductor while expelling a hole back into the normal region.

Since the created Cooper-pair must have momentum equal to the moving condensate, this momentum is transferred from the incoming particle. The result is the changed trajectory of the outgoing hole. The trajectory deviation has been exaggerated a lot for clarity.

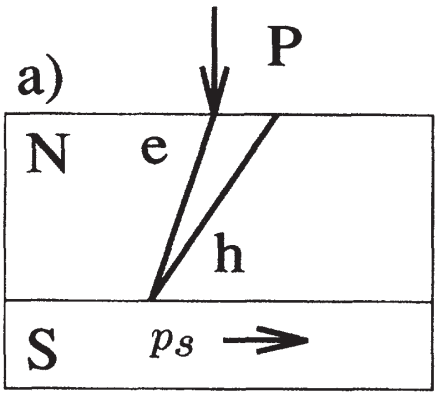

Figure 32: Figure taken from [28], Fig.(2a). Changed trajectory of an Andreev reflected particle, due to the force $\hat{\mathbf{f}}_{\Delta 2}$ acting parallel to the interface. P labels the point contact from which the electron (e) is emitted, while p_s labels the supercurrent. The electron undergoes AR at the NS interface and is repelled as a hole, h. The deviation (grossly exaggerated for clarity) is due to a momentum transfer from the quasiparticle to the created Cooper-pair, which must have momentum enough to join the moving condensate.

This confirms the suspicion that the supercurrent circling the vortex core indeed can lead to a precession of the bound CdGM states, as I hypothesized, inspired by the article [25]! The vortex states are Andreev states, moving back and forth inside the vortex by scattering off the spatial variance of the gap, and in the presence of a supercurrent in the superconductor, these states are affected by the force $\hat{\mathbf{f}}_{\Delta 2}$. This force acts parallel to the interface and can change the trajectory of the outgoing particle, compared to that of the ingoing, effectively leading to the precession of these bound states. This is imagined to translate well to the solid cylinder with a supercurrent. I would expect the precession of states in a normal core of a cylinder with a superconducting shell, due to the circulating supercurrent, from the force $\hat{\mathbf{f}}_{\Delta 2}$.

7 CONCLUSION

I have in this thesis studied the different sub-gap states of a superconducting cylinder (or hexagonal shell), focusing mostly on the Caroli-de Gennes-Matricon states existing in vortices in a type-II superconductor. The energy spectrum of these states was studied, followed by an analysis of their nature, i.e. how these are bound in the system.

I presented first a study on the LP effects on superconducting cylinders in the presence of an axial magnetic field and derived the dependence of the critical temperature and the supercurrent velocity as a function of the applied magnetic field.

An analytical study of the vortex states following the work of Caroli et al.[15] was presented. A rather involved calculation was performed to obtain the energy spectrum of the states through the use of the Bogoliubov-de Gennes equation. Then, constructing a method using the NDEigensystem function in Mathematica, the energies were found numerically. Inspired by the work in [4], I successfully found credible results for the energy spectrum of the CdGM states in a vortex system based on the experiment presented in [4]. The energies were shown to each have a partner of opposite sign, due to the particle-hole symmetry. It was shown how the energy-spacing decreased as the states condensed close to the continuum at Δ_0. Furthermore, I presented the eigenfunctions of the CdGM states and these were found to resemble Bessel functions in the radial direction, while the angular momentum μ determined the order of the excitations. Further, the supercurrents were plotted and, as a sanity check, shown to disappear in the case of no phase on the superconducting order parameter. Finally, I briefly investigated the small value of the Fermi energy, showing how this corresponded to a very small carrier density compared to other often used superconducting compounds.

An example of a hollow hexagonal wire system was studied for the same material as used for the solid superconductor housing the CdGM states, $FeTe_{0.55}Se_{0.45}$. The energies of a very small nanowire system was determined to showcase the numerical method, along with both the eigenfunctions and the supercurrents in the hexagonal shell. For such a system the supercurrent was found to depend on the winding number n presented in the LP section.

Thereafter I included the effects of an applied magnetic field. Analytically, the energy spacing between states was found to increase due to the magnetic field. This was also verified numerically.

The concept of Andreev reflection was investigated, in order to describe the vortex states as Andreev states, bound in the vortex due to the spatial variance of the order parameter Δ. Furthermore, this description applies just as well to a solid cylinder with a normal metal core and a superconducting outer shell. I investigated thoroughly how AR depends both on the energy and the angle of incidence for the incoming particle as it hits an interface, inspired by the work of [5]. AR was found to occur usually for incident particles with energy below the gap, although it was seen to occur for energies above the gap as well. It was understood that as the barrier strength increased, the probability for all scattering events except normal reflection decreased. Since an increase to the angle of incidence effectively increases the barrier strength, the same conclusion was drawn for the probabilities as a function of θ. Furthermore, I showed that for energies below the gap, only AR and normal reflection is allowed, since no single particle transmission is allowed. I suggested further how the states in either the vortex or a normal core of a cylinder with a superconducting shell might be bound in the form of multiple Andreev reflections.

Lastly I discussed the forces acting on Andreev reflected particles as they come into contact with the interface between a normal metal and a superconductor. The force responsible for Andreev scattering, which acts perpendicular to the interface, was identified, alongside another force that acts parallel to the interface on a particle undergoing Andreev reflection. This latter force depends on the supercurrent in the SC and will change the path of the outgoing particles, compared to the case of $v_s = 0$. I hypothesized that this deviation in trajectory can lead to precession of the states in either a vortex or the aforementioned cylinder, as the scattering is no longer perfectly retro-reflective.

APPENDIX

A

A.1 $\psi(r)$ AND $K(r)$

It is trivial to show that Eq.(3.35) satisfies Eq.(3.33) using $\cos(\psi(r)) \approx 1$, since $\psi(r)$ is small:

$$\frac{d}{dr}\left(a^{-1}\int_0^r \Delta(r')dr'\right) = a^{-1}\Delta(r). \tag{A.1}$$

The anti-derivative evaluated in zero vanishes since there is no r-dependence.
Next, taking the derivative of Eq.(3.36) yields:

$$\begin{aligned}\frac{d\psi(r)}{dr} &= 2\frac{dK(r)}{dr}\cdot\psi(r) - e^{2K(r)}\cdot\left(0 - e^{-2K(r)}\left(2q + \frac{\mu}{k_F\sin(\alpha)r^2}\right)\right)\\ &= 2(a)^{-1}\Delta(r)\psi(r) + 2q + \frac{\mu}{k_F\sin(\alpha)r'^2}.\end{aligned} \tag{A.2}$$

In the above, it was used that the product rule when taking the derivative of $\psi(r)$ and that $\frac{dF(\infty)}{dr}$ (where F represents the anti-derivative of $\psi(r)$) is zero since it has no r dependence. Pull now $\frac{2}{a}$ outside a parenthesis on the RHS:

$$\begin{aligned}&\frac{d\psi(r)}{dr} = 2a^{-1}\left[\left(\epsilon + a\frac{\mu}{2k_F\sin(\alpha)r'^2}\right) + \Delta(r)\psi(r)\right]\\ &\Updownarrow\\ &\frac{d\psi(r)}{dr} = 2a^{-1}\left[\left(\epsilon + \frac{\hbar^2\mu}{2mr^2}\right) + \Delta(r)\psi(r)\right]\end{aligned} \tag{A.3}$$

Using that $\psi(r)$ is small one can let $\sin(\psi(r)) \approx \psi(r)$ in Eq. (3.34) and thus it is shown that Eq.(3.36) indeed satisfies Eq. (3.34)

A.2 SHOWING $\hat{g}$, EQ.(3.26), IS A SOLUTION TO EQ.(3.25)

It is shown here how Eq.(3.26) is a solution to the differential equation Eq.(3.25), if one neglects the second order derivative.
Look first at the g_+ equation of Eq.(3.26):

$$\begin{aligned}
&-ia\left[e^{-K(r)}\left(\frac{d}{dr}e^{\frac{i}{2}\psi(r)}\right)+e^{\frac{i}{2}\psi(r)}\left(\frac{d}{dr}e^{-K(r)}\right)\right]-i\Delta(r)e^{-\frac{i}{2}\psi(r)}e^{-K(r)}\\
&=\left(\epsilon+\frac{\hbar^2\mu}{2mr^2}\right)e^{\frac{i}{2}\psi(r)}e^{-K(r)}\\
&\Updownarrow\\
&-ia\left[e^{-K(r)}\frac{i}{2}\left(\frac{d\psi(r)}{dr}\right)e^{\frac{i}{2}\psi(r)}+e^{\frac{i}{2}\psi(r)}\left(-\frac{dK(r)}{dr}\right)e^{-K(r)}\right]-i\Delta(r)e^{-\frac{i}{2}\psi(r)}e^{-K(r)}\\
&=\left(\epsilon+\frac{\hbar^2\mu}{2mr^2}\right)e^{\frac{i}{2}\psi(r)}e^{-K(r)}
\end{aligned}\tag{A.4}$$

Use now Eqs.(3.33) and (3.34) with the small angle approximation on the cosine and sine, while also dividing $e^{-K(r)}$ from all terms:

$$\begin{aligned}
&-ia\left[\frac{i}{2}2(a)^{-1}\left[\left(\epsilon+\frac{\hbar^2\mu}{2mr^2}\right)+\Delta(r)\psi(r)\right]e^{\frac{i}{2}\psi(r)}+e^{\frac{i}{2}\psi(r)}\left(-a^{-1}\Delta(r)\right)\right]\\
&-i\Delta(r)e^{-\frac{i}{2}\psi(r)}=\left(\epsilon+\frac{\hbar^2\mu}{2mr^2}\right)e^{\frac{i}{2}\psi(r)}.
\end{aligned}\tag{A.5}$$

Multiply by $e^{\frac{-i}{2}\psi(r)}$ and reduce:

$$\begin{aligned}
&\left(\epsilon+\frac{\hbar^2\mu}{2mr^2}\right)+\Delta(r)\psi(r)+i\Delta(r)-i\Delta(r)e^{-i\psi(r)}=\left(\epsilon+\frac{\hbar^2\mu}{2mr^2}\right)\\
&\Updownarrow\\
&\Delta(r)\psi(r)+i\Delta(r)-i\Delta(r)e^{-i\psi(r)}=0.
\end{aligned}\tag{A.6}$$

Finally one can divide $\Delta(r)$ out, write the exponential function in terms of cosine and sine and once again use the small angle approximation:

$$\begin{aligned}
&\psi(r)+i-i(\cos(\psi(r))-i\sin(\psi(r)))=0\\
&\Updownarrow\\
&\psi(r)+i-i+i^2\psi(r)\\
&\Updownarrow\\
&\psi(r)-\psi(r)=0,
\end{aligned}\tag{A.7}$$

and it is shown!

Showing g_- also satisfies Eq. (3.25):

$$
\begin{aligned}
&ia\left[-ie^{-K(r)}\left(\frac{d}{dr}e^{\frac{-i}{2}\psi(r)}\right)-ie^{\frac{-i}{2}\psi(r)}\left(\frac{d}{dr}e^{-K(r)}\right)\right]+\Delta(r)e^{\frac{i}{2}\psi(r)}e^{-K(r)}\\
&=-\left(\epsilon+\frac{\hbar^2\mu}{2mr^2}\right)ie^{\frac{-i}{2}\psi(r)}e^{-K(r)}\\
&\Updownarrow\\
&ia\left[e^{-K(r)}\frac{-1}{2}\left(\frac{d\psi(r)}{dr}\right)e^{\frac{-i}{2}\psi(r)}-ie^{\frac{-i}{2}\psi(r)}\left(-\frac{dK(r)}{dr}\right)e^{-K(r)}\right]+\Delta(r)e^{\frac{i}{2}\psi(r)}e^{-K(r)}\\
&=-\left(\epsilon+\frac{\hbar^2\mu}{2mr^2}\right)ie^{\frac{-i}{2}\psi(r)}e^{-K(r)}.
\end{aligned}
\tag{A.8}
$$

Use again Eqs.(3.33) and (3.34) and divide by $e^{-K(r)}$:

$$
\begin{aligned}
&ia\left[\frac{-1}{2}2(a)^{-1}\left[\left(\epsilon+\frac{\hbar^2\mu}{2mr^2}\right)+\Delta(r)\psi(r)\right]e^{\frac{-i}{2}\psi(r)}+ie^{\frac{-i}{2}\psi(r)}\left(a^{-1}\Delta(r)\right)\right]\\
&+\Delta(r)e^{\frac{i}{2}\psi(r)}=-\left(\epsilon+\frac{\hbar^2\mu}{2mr^2}\right)ie^{\frac{-i}{2}\psi(r)}.
\end{aligned}
\tag{A.9}
$$

Multiply by $e^{\frac{i}{2}\psi(r)}$ and reduce further:

$$
\begin{aligned}
&-i\left[\left(\epsilon+\frac{\hbar^2\mu}{2mr^2}\right)+\Delta(r)\psi(r)\right]-\Delta(r)+\Delta(r)e^{i\psi(r)}=-\left(\epsilon+\frac{\hbar^2\mu}{2mr^2}\right)i\\
&\Updownarrow\\
&-i\Delta(r)\psi(r)-\Delta(r)+\Delta(r)e^{i\psi(r)}=0.
\end{aligned}
\tag{A.10}
$$

Finally write out the exponential function and reduce:

$$
\begin{aligned}
&-i\psi(r)-1+\cos(psi(r))+i\sin(\psi(r))=0\\
&\Updownarrow\\
&-i\psi(r)-1+1+i\psi(r)=0,
\end{aligned}
\tag{A.11}
$$

and it is shown.

A.3 FINDING $\psi(r_c)$ FOR $g_-(r_c)$

It is shown how to obtain $\psi(r_c)$ using the hole part $(g_-(r_c))$ of Eq.(3.44):

$$\begin{aligned}
&A_-\sqrt{\frac{2}{\pi}}\,(\gamma - qr_c)^{-\frac{1}{2}}\cos\left[\gamma - qr_c + \frac{(\mu+\frac{1}{2})^2}{2\,(\gamma - qr_c)} - \frac{\pi}{2}\left(\mu+\frac{1}{2}\right) - \frac{\pi}{4}\right]\\
&= \sqrt{\frac{2}{\pi}}\,\gamma^{-\frac{1}{2}}\Bigg(g_-(r_c)\exp\left[i\left(\gamma + \frac{n^2}{2\gamma} - \frac{\pi}{2}n - \frac{\pi}{4}\right)\right]\\
&+ g_-^*(r_c)\exp\left[-i\left(\gamma + \frac{n^2}{2\gamma} - \frac{\pi}{2}n - \frac{\pi}{4}\right)\right]\Bigg).
\end{aligned} \tag{A.12}$$

Now use the definition of g_- from Eq.(3.26), which one can write as $g_- = -ie^{-\frac{i}{2}\psi(r_c)+i\frac{\pi}{4}}$, again having neglected $e^{K(r_c)}$ and the constant c. Reduce now the RHS as follows:

$$\begin{aligned}
RHS &= \sqrt{\frac{2}{\pi}}\,\gamma^{-\frac{1}{2}}\Bigg(-i\exp\left[i\left(\gamma + \frac{n^2}{2\gamma} - \frac{\pi}{2}n - \frac{\pi}{4} - \frac{\psi(r_c)}{2} + \frac{\pi}{4}\right)\right]\\
&+ i\exp\left[-i\left(\gamma + \frac{n^2}{2\gamma} - \frac{\pi}{2}n - \frac{\pi}{4} - \frac{\psi(r_c)}{2} + \frac{\pi}{4}\right)\right]\Bigg)\\
&= 2\sqrt{\frac{2}{\pi}}\,\gamma^{-\frac{1}{2}}\sin\left[\gamma + \frac{n^2}{2\gamma} - \frac{\pi}{2}n - \cancel{\frac{\pi}{4}} - \frac{\psi(r_c)}{2} + \cancel{\frac{\pi}{4}}\right].
\end{aligned} \tag{A.13}$$

Eq.(A.12) becomes:

$$\begin{aligned}
(\gamma + qr_c)^{-\frac{1}{2}}\cos&\left[\gamma - qr_c + \frac{(\mu+\frac{1}{2})^2}{2\,(\gamma - qr_c)} - \frac{\pi}{2}\left(\mu+\frac{1}{2}\right) - \frac{\pi}{4}\right]\\
&= \gamma^{-\frac{1}{2}}\sin\left(\gamma + \frac{n^2}{2\gamma} - \frac{\pi}{2}n - \frac{\psi(r_c)}{2}\right)
\end{aligned} \tag{A.14}$$

Using again $\gamma >> qr_c$ and making the same approximations as in the main text, while also rewriting the sine function to a cosine function on the RHS, yields:

$$\gamma^{-\frac{1}{2}}\cos\left[\gamma - qr_c + \frac{(\mu+\frac{1}{2})^2}{2\gamma} - \frac{\pi}{2}\left(\mu+\frac{1}{2}\right) - \frac{\pi}{4}\right] = \gamma^{-\frac{1}{2}}\cos\left[\gamma + \frac{n^2}{2\gamma} - \frac{\pi}{2}n - \frac{\psi(r_c)}{2} - \frac{\pi}{2}\right]. \tag{A.15}$$

Matching the arguments and writing out $n = \sqrt{\mu^2 + \frac{1}{4}}$ yields

$$\gamma - qr_c + \frac{(\mu + \frac{1}{2})^2}{2\gamma} - \frac{\pi}{2}\left(\mu + \frac{1}{2}\right) - \frac{\pi}{4} = \gamma + \frac{\mu^2 + \frac{1}{4}}{2\gamma} - \frac{\pi}{2}\sqrt{\mu^2 + \frac{1}{4}} - \frac{\psi(r_c)}{2} - \frac{\pi}{2}$$
$$\Updownarrow$$
$$-qr_c + \frac{\mu}{2\gamma} - \frac{\pi}{2}\mu - \cancel{\frac{\pi}{2}} = -\frac{\pi}{2}\sqrt{\mu^2 + \frac{1}{4}} - \frac{\psi(r_c)}{2} - \cancel{\frac{\pi}{2}}. \tag{A.16}$$

Finally approximate $\sqrt{\mu^2 + \frac{1}{4}} \approx \mu$ for large μ, and one obtains the expression

$$\boxed{\psi(r_c) = 2qr_c - \frac{\mu}{k_F \sin(\alpha) r_c},} \tag{A.17}$$

which indeed matches Eq.(3.51), as one would expect.

A.4 ORDER OF TERMS IN EQ.(3.23)

A brief discussion on the size of the different terms is presented, as to investigate whether the terms $\frac{1}{r} H_n \frac{d\hat{g}}{dr}$ and $-\sigma_z \frac{\hbar^2}{2m} \frac{d^2\hat{g}}{dr^2}$ are small and if neglecting these can indeed be justified. One can write up the different terms from the LHS of Eq.(3.23) and compare them using the superconducting coherence length ξ. Note that the Hankel functions are divided out later and are therefore not included. The coherence length is:

$$\xi \approx \frac{\hbar v_f}{\Delta_0}. \tag{A.18}$$

From Eq.(3.23), the terms to compare are the following:

$$k_F \frac{d\hat{g}}{dr}, \qquad \frac{d^2\hat{g}}{dr^2}, \qquad \frac{1}{r}\frac{d\hat{g}}{dr}, \qquad \frac{2m}{\hbar^2}\Delta(r)\hat{g}. \tag{A.19}$$

Here $k_F \frac{d\hat{g}}{dr}$ came from the derivative of the Hankel functions in Eq.(3.23). One can now investigate the size of the first term. The derivative of g_+ is once more:

$$\frac{dg_+(r)}{dr} = \frac{d}{dr}\left(e^{\frac{i}{2}\psi(r)} e^{-K(r)} e^{i\frac{\pi}{4}}\right) = g_+\left(\frac{i}{2}\frac{d\psi(r)}{dr} - \frac{dK(r)}{dr}\right), \tag{A.20}$$

where the derivatives of $K(r)$ and $\psi(r)$ are given by Eqs.(3.33) and (3.34). The $e^{i\frac{\pi}{4}}$ term was ignored here. Focus now on the terms $\frac{\Delta}{a}$ and $\frac{\Delta}{a}\psi(r)$ from Eqs.(3.33) and (3.34) respectively, where in the latter it was argued that the $\epsilon + \frac{\hbar^2 \mu}{2mr^2}$ bracket is small. Recall the argumentation of [15] that $\epsilon \ll \Delta_0$ and that $\mu \ll k_F r$. One can then write

$$\frac{\Delta}{\hbar v_F \sin(\alpha)} \approx \frac{1}{\xi \sin(\alpha)}, \tag{A.21}$$

by using $a = \hbar v_F \sin(\alpha)$, so that

$$k_F \frac{d\hat{g}}{dr} \propto \frac{k_F}{\xi} \hat{g}. \tag{A.22}$$

Looking at the second derivative one finds

$$\frac{d^2\hat{g}}{dr^2} \propto \frac{1}{\xi^2}\hat{g} = \frac{1}{\xi k_F} \frac{k_F}{\xi} \hat{g}. \tag{A.23}$$

Thus the second order derivative is a factor $\frac{1}{\xi k_F}$ smaller than the first derivative, allowing us to safely neglect this second order derivative of $\hat{g}(r)$.
Looking at the term

$$\frac{1}{r}\frac{d\hat{g}}{dr} \propto \frac{1}{r\xi}\hat{g} = \frac{1}{rk_F} \frac{k_F}{\xi} \hat{g}, \tag{A.24}$$

one notes this term is also small compared to $k_F \frac{d\hat{g}}{dr}$, by virtue of r being large. Finally the last term can be rewritten as follows (where $\Delta(r) = \Delta_0$ for large r):

$$\frac{2m}{\hbar^2}\Delta_0 \hat{g} = \frac{2k_F}{\hbar v_F}\Delta_0 \hat{g} \approx \frac{2k_F}{\hbar v_F} \frac{\hbar v_F}{\xi} \hat{g} = \frac{2}{\pi} \frac{k_F}{\xi} \hat{g}. \tag{A.25}$$

This is seen to be on the same order of magnitude as the term $k_F \frac{d\hat{g}}{dr}$ and is therefore not neglectable.

A.5 SUPERCURRENTS IN THE HEXAGONAL SHELL FOR $n = -1$

The supercurrents of the hexagonal shell is found for $n = -1$. The currents are seen to have changed direction as the sign on n changed, compared to Fig.(22).

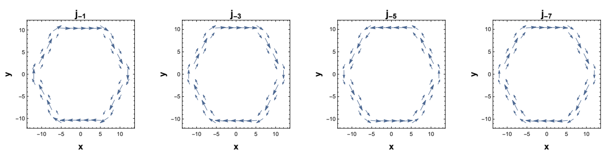

Figure 33: Supercurrents in a hexagonal shell for $n = -1$. The currents have shifted directions as the sign on the phase of the order parameter changed.

A.6 SHOWING THE MOMENTUM OPERATOR IS HERMITIAN

This can be shown as follows:

$$\int d\mathbf{x}\ (\hat{\mathbf{p}}\psi)^*\psi = \int d\mathbf{x}\,(-i\hbar\boldsymbol{\nabla}\psi)^*\,\psi = \int d\mathbf{x}\ i\hbar\,(\boldsymbol{\nabla}\psi^*)\,\psi = 0 - \int d\mathbf{x}\ i\hbar\psi^*\,(\boldsymbol{\nabla}\psi) =$$
$$\int d\mathbf{x}\ \psi^*\,(\hat{\mathbf{p}}\psi)\,,$$

and thus $\hat{\mathbf{p}}$ is hermitian. To get the third equality one uses that the total derivative is zero, since the wavefunctions ψ are assumed to vanish at infinity.

BIBLIOGRAPHY

[1] J Bardeen, L N Cooper, and J R Schrieffer. Theory of Superconductivity. *Physics Review*, 108(5):1175–1204, 1957. (Cited on page 1.)

[2] Roman M Lutchyn, Georg W Winkler, Bernard Van Heck, Torsten Karzig, Karsten Flensberg, Leonid I Glazman, and Chetan Nayak. Topological superconductivity in full shell proximitized nanowires. *arXiv:1809.05512v1*, 2018. (Cited on page 1.)

[3] S. Vaitiekenas, M. T. Deng, P. Krogstrup, and C. M. Marcus. Flux-induced Majorana modes in full-shell nanowires. *arXiv:1809.05513*, 2018. (Cited on pages 1, 4, 9, 10, 11, and 40.)

[4] Mingyang Chen, Xiaoyu Chen, Huan Yang, Zengyi Du, Xiyu Zhu, Enyu Wang, and Hai Hu Wen. Discrete energy levels of Caroli-de Gennes-Matricon states in quantum limit in FeTe0.55Se0.45. *Nature Communications*, 9(1):1–7, 2018. (Cited on pages 1, 11, 13, 25, 32, 33, 35, 38, 39, 47, and 71.)

[5] G. E. Blonder, M Tinkham, and T. M. Klapwijk. Transition from metallic to tunneling regimes in superconducting microconstrictions: Excess current, charge imbalance, and supercurrent conversion. *Physical Review B*, 25(7):4515–4532, 1981. (Cited on pages 1, 49, 50, 51, 52, 53, 56, 59, 60, and 71.)

[6] V.B. Eltsov. Theory of Superconductivity. *Notes*, 2017. (Cited on pages 2, 11, 12, 13, 16, 21, 34, 35, 39, 49, 52, 53, 61, and 62.)

[7] A A Abrikosov. The Magnetic Properties of Superconducting Alloys. *Journal of Physics and Chemistry of Solids*, 2(3):199–208, 1957. (Cited on page 2.)

[8] J. F. Annett. *Superconductivity, Superfluids and Condensates.* Oxford University Press, 2003. (Cited on page 3.)

[9] A. A. Abrikosov. *Fundamentals of the Theory of Metals.* Elsevier Science Publishers B.V, 1988. (Cited on pages 3, 5, and 8.)

[10] W. A. Little and R. D. Parks. Observation of quantum periodicity in the transition temperature of a superconducting cylinder. *Physical Review Letters*, 9(1):9–12, 1962. (Cited on pages 4, 5, and 8.)

[11] P. G. de Gennes. *Superconductivity of Metals and Alloys.* Westview Press, Advanced Book Classics, 1999. (Cited on pages 5 and 11.)

[12] M. Tinkham. *Introduction to superconductivity.* Keyword Publishing Services, 1996. (Cited on pages 7 and 8.)

[13] I. Sternfeld, E. Levy, M. Eshkol, A. Tsukernik, M. Karpovski, Hadas Shtrikman, A. Kretinin, and A. Palevski. Magnetoresistance oscillations of superconducting al-film cylinders covering InAs nanowires below the quantum critical point. *Physical Review Letters*, 107(3), 2011. ISSN 00319007. (Cited on page 9.)

[14] Georg Schwiete and Yuval Oreg. Persistent Current in Small Superconducting Rings. *Physical Review Letters*, 103(037001):1–4, 2009. (Cited on page 9.)

[15] C. Caroli, P.G. De Gennes, and J. Matricon. Bound Fermion States on a Vortex Line in a Type II Superconductor. *Phys. Lett.*, 9(4):307, 1964. (Cited on pages 11, 12, 13, 15, 16, 18, 21, 23, 25, 43, 71, and 78.)

[16] E Brun Hansen. The bound excitations of a single vortex in a pure type II superconductor. *Phys. Lett.*, 27A(8):576–577, 1968. (Cited on pages 11, 13, 43, 45, 46, 47, and 48.)

[17] K. F. Riley and M. P. Hobson. *Essential Mathematical Methods*. Cambridge University Press, 2011. (Cited on pages 15 and 26.)

[18] Yuan Cao, Valla Fatemi, Shiang Fang, Kenji Watanabe, Takashi Taniguchi, Efthimios Kaxiras, and Pablo Jarillo-Herrero. Unconventional superconductivity in magic-angle graphene superlattices. *Nature*, 556(7699):43–50, 2018. (Cited on pages 38 and 39.)

[19] A F Andreev. The Thermal Conductivity of the Intermediate State in Superconductors. *Soviet Physics Jetp*, 19(5):1228–1231, 1964. (Cited on page 49.)

[20] R. Hoonsawat and I. M. Tang. Andreev reflection at a NS interface for non-normal angle of incidence. *Physics Letters A*, 127(8-9):441–443, 1988. (Cited on pages 50, 51, 53, and 57.)

[21] J. A. Gifford, C. N. Snider, J. Martinez, and T. Y. Chen. Effect of three dimensional interface in determination of spin polarization using Andreev reflection spectroscopy. *Journal of Applied Physics*, 113(17):1–4, 2013. (Cited on page 52.)

[22] Niels Asger Mortensen, Karsten Flensberg, and Antti-Pekka Jauho. Angle dependence of Andreev scattering at semiconductor–superconductor interfaces. *Physical Review B*, 59(15):10176–10182, 1999. (Cited on pages 53, 57, and 61.)

[23] Yu G Naidyuk and K Gloos. Anatomy of point-contact Andreev reflection spectroscopy from the experimental point of view (review). *Low Temperature Physics*, 44(257):1–20, 2018. (Cited on page 61.)

[24] J. A. Sauls. Andreev Bound States and Their Signatures. *Philosophical Transactions A*, 376(2125):1–21, 2018. (Cited on page 62.)

[25] Michael Stone. Spectral Flow, Magnus Force and Mutual Friction via the Geometric Optics Limit of Andreev Reflection. *Physical Review B*, 54(18), 1996. (Cited on pages 63 and 70.)

[26] Reiner Kümmel and Stephan Hoffman. Ehrenfest theorem for inhomogeneous superconductors and supercurrent force on Andreev reflected quasiparticles. *Z. Phys. B - Condensed matter*, 84(2):237–241, 1991. (Cited on pages 64, 65, and 69.)

[27] Stephan Hofmann and Reiner Kümmel. Off-Diagonal Pair Potential Forces and Vortex Dynamics in High-k Superconductors. *Physical Review Letters*, 70(9):1319–1322, 1993. (Cited on page 69.)

[28] B Götzelmann, S Hofmann, and R Kümmel. Supercurrent force on Andreev-reflected quasiparticles and excess currents. *Physical Review B*, 52(6):3848–3851, 1995. (Cited on pages 69 and 70.)